Sand Waves, Bars, and Wind-Blown Sands of the Río Orinoco, Venezuela and Colombia

United States Geological Survey Water-Supply Paper 2326–A

Prepared in cooperation with the Venezuelan Ministerio del Ambiente y de los Recursos Naturales Renovables

AVAILABILITY OF BOOKS AND MAPS OF THE U.S. GEOLOGICAL SURVEY

Instructions on ordering publications of the U.S. Geological Survey, along with prices of the last offerings, are given in the current-year issues of the monthly catalog "New Publications of the U.S. Geological Survey." Prices of available U.S. Geological Survey publications released prior to the current year are listed in the most recent annual "Price and Availability List." Publications that are listed in various U.S. Geological Survey catalogs (**see back inside cover**) but not listed in the most recent annual "Price and Availability List" are no longer available.

Prices of reports released to the open files are given in the listing "U.S. Geological Survey Open-File Reports," updated monthly, which is for sale in microfiche from the U.S. Geological Survey, Books and Open-File Reports Section, Federal Center, Box 25425, Denver, CO 80225. Reports released through the NTIS may be obtained by writing to the National Technical Information Service, U.S. Department of Commerce, Springfield, VA 22161; please include NTIS report number with inquiry.

Order U.S. Geological Survey publications **by mail** or **over the counter** from the offices given below.

BY MAIL

Books

Professional Papers, Bulletins, Water-Supply Papers, Techniques of Water-Resources Investigations, Circulars, publications of general interest (such as leaflets, pamphlets, booklets), single copies of Earthquakes & Volcanoes, Preliminary Determination of Epicenters, and some miscellaneous reports, including some of the foregoing series that have gone out of print at the Superintendent of Documents, are obtainable by mail from

U.S. Geological Survey, Books and Open-File Reports
Federal Center, Box 25425
Denver, CO 80225

Subscriptions to periodicals (Earthquakes & Volcanoes and Preliminary Determination of Epicenters) can be obtained ONLY from the

Superintendent of Documents
Government Printing Office
Washington, D.C. 20402

(Check or money order must be payable to Superintendent of Documents.)

Maps

For maps, address mail orders to

U.S. Geological Survey, Map Distribution
Federal Center, Box 25286
Denver, CO 80225

Residents of Alaska may order maps from

Alaska Distribution Section, U.S. Geological Survey,
New Federal Building - Box 12
101 Twelfth Ave., Fairbanks, AK 99701

OVER THE COUNTER

Books

Books of the U.S. Geological Survey are available over the counter at the following Geological Survey Public Inquiries Offices, all of which are authorized agents of the Superintendent of Documents:

- **WASHINGTON, D.C.**--Main Interior Bldg., 2600 corridor, 18th and C Sts., NW.
- **DENVER, Colorado**--Federal Bldg., Rm. 169, 1961 Stout St.
- **LOS ANGELES, California**--Federal Bldg., Rm. 7638, 300 N. Los Angeles St.
- **MENLO PARK, California**--Bldg. 3 (Stop 533), Rm. 3128, 345 Middlefield Rd.
- **RESTON, Virginia**--503 National Center, Rm. 1C402, 12201 Sunrise Valley Dr.
- **SALT LAKE CITY, Utah**--Federal Bldg., Rm. 8105, 125 South State St.
- **SAN FRANCISCO, California**--Customhouse, Rm. 504, 555 Battery St.
- **SPOKANE, Washington**--U.S. Courthouse, Rm. 678, West 920 Riverside Ave..
- **ANCHORAGE, Alaska**--Rm. 101, 4230 University Dr.
- **ANCHORAGE, Alaska**--Federal Bldg, Rm. E-146, 701 C St.

Maps

Maps may be purchased over the counter at the U.S. Geological Survey offices where books are sold (all addresses in above list) and at the following Geological Survey offices:

- **ROLLA, Missouri**--1400 Independence Rd.
- **DENVER, Colorado**--Map Distribution, Bldg. 810, Federal Center
- **FAIRBANKS, Alaska**--New Federal Bldg., 101 Twelfth Ave.

Chapter A

Sand Waves, Bars, and Wind-Blown Sands of the Río Orinoco, Venezuela and Colombia

By CARL F. NORDIN, JR., and DAVID PEREZ-HERNANDEZ

Prepared in cooperation with the Venezuelan Ministerio del Ambiente y de los Recursos Naturales Renovables

U.S. GEOLOGICAL SURVEY WATER-SUPPLY PAPER 2326

THE WATERS AND SEDIMENTS OF THE RIO ORINOCO AND ITS MAJOR TRIBUTARIES, VENEZUELA AND COLOMBIA

DEPARTMENT OF THE INTERIOR
DONALD PAUL HODEL, Secretary

U.S. GEOLOGICAL SURVEY
Dallas L. Peck, Director

UNITED STATES GOVERNMENT PRINTING OFFICE: 1989

For sale by the
Books and Open-File Reports Section
U.S. Geological Survey
Federal Center
Box 25425
Denver, CO 80225

Library of Congress Cataloging-in-Publication Data

Nordin, Carl F.
Sand waves, bars, and wind-blown sands of the Río Orinoco, Venezuela and Colombia / by Carl F. Nordin, Jr. and David Pérez-Hernández.
p. cm. — (The Waters and sediments of the Río Orinoco and its major tributaries, Venezuela and Colombia ; ch. A) (United States Geological Survey water-supply paper ; 2326-A)
"Prepared in cooperation with the Venezuelan Ministerio del Ambiente y de los Recursos Naturales Renovables."
Bibliography: p.
Supt. of Docs. no.: I 19.13:2326-A
1. Sand waves—Venezuela—Orinoco River Watershed. 2. Sand waves-Colombia. 3. Sand-bars. 4. Sand—Venezuela—Orinoco River Watershed. 5. Sand—Colombia. I. Pérez-Hernández, David. II. Venezuela. Ministerio del Ambiente y de los Recursos Naturales Renovables. III. Title. IV. Series. V. Series: U.S. Geological Survey water-supply paper ; 2326.
GB719.V4W37 ch. A
[GB649.S3]
551.48'3'0987 s—dc19 88-607947
[551.3.'55] CIP

FOREWORD

The Río Orinoco is one of the great rivers of the world. It drains about 900,000 square kilometers and discharges to the ocean an average flow in excess of 36,000 cubic meters per second and an average sediment load of about 7,600 kilograms per second (240 million tonnes per year), ranking it third largest in the world in terms of flow to the oceans and sixth largest in terms of sediment loads. It is an international river, draining parts of Colombia and Venezuela, and forming the boundary between these two nations along some 300 kilometers of its course.

The basin is rich in natural resources, containing extensive fields of petroleum and natural gas, including the largest proven reserve of heavy crude oil in the world, and rich deposits of bauxite, iron ore, gold, diamonds, and other mineral wealth. Its renewable resources include its forests, fish and wildlife, agriculture and grazing lands, and most important, its waters. The basin is not developed to any great extent; large parts of the watershed still are undisturbed. Although it accounts for 70 percent of the nation's land, it supports only 5 percent of the population. This situation, though, is likely to change in the near future. The development of the Río Orinoco's natural resources is the key to Venezuela's future.

In 1981, Project Orinoco-Apure was organized under the auspices of the Venezuelan Ministerio del Ambiente y de los Recursos Naturales Renovables to serve as the focal point and coordinating body for scientific studies of the resources of the basin and for feasibility studies and preliminary planning of its development. An important part of the project effort was directed to investigations of the basin's water resources. In 1982, the United States Geological Survey and the Venezuelan Ministerio del Ambiente y de los Recursos Naturales Renovables agreed to collaborate in a series of scientific studies of the Río Orinoco and its major tributaries. A strong foundation already had been laid for the hydrology of the basin with the establishment of a gaging and sediment sampling program in 1965, but by 1980, the program had been substantially reduced. Data on the bed sediments of the rivers and on the sediment transport were especially sparse. The main emphasis of the collaboration therefore was directed toward sediment studies. The studies had three principal objectives: (1) to develop and test new technology for measuring the water and sediment discharge of large tropical rivers, (2) to determine the characteristics of the bed material and suspended sediment of the major rivers of the basin, and (3) to provide measurements and samples that along with the existing hydrologic information would provide a set of baseline scientific data against which future changes in the basin could be measured. Between March 1982, and June 1985, seven major campaigns to collect data along the river and in the major tributaries were completed, and the collaboration expanded considerably to include participation of engineers, scientists, and consultants from universities, private enterprises, and other government agencies of Venezuela, Colombia, and the United States.

At the beginning of the collaboration, it was agreed that the results of these studies would be made available to the scientific community. A few short papers have been published in symposium proceedings and in technical journals, but the main results and all the basic data are contained in this series of reports. Each chapter is self-contained; taken together, they provide comprehensive data and analyses of the waters and sediments of the Río Orinoco and its major tributaries in Venezuela and Colombia. The results of these studies should be of interest and value to anyone who is concerned with large tropical rivers.

Dallas L. Peck
Director
United States Geological Survey

Guillermo Colmenares F.
Minister
Ministerio del Ambiente y de los Recursos Naturales Renovables
Republica de Venezuela

CONTENTS

FRONTISPIECE

FIGURES

TABLES

SYMBOLS AND UNITS

		Unit
A	A coefficient.	
A_e	Area of an ellipsoid	m^2
A_p	Area of a particle projected on the bed	m^2
A_s	Area of the bed sheltered by a particle	m^2
B	Length of a sand-wave crest	m
C	Concentration	mg/L
D	Depth	m
d	Particle diameter	mm
d_a	Diameter of armor particle	mm
d_m	Effective particle diameter	mm
d_s	Sieve diameter	mm
f	Friction factor.	
f	Fraction of the bed sheltered by a particle.	
f_i	Fraction of the bed material of size d_i.	
g	Acceleration due to gravity	m/s^2
H	Sand-wave height	m
K	A coefficient.	
K_s	A roughness length	m
L	Sand-wave length	m
Q	Water discharge	m^3/s
Q_s	Sediment discharge	kg/s
q_s	Mass sediment discharge per unit width	kg/s/m
q_T	Volume sediment discharge per unit width	m^2/s
r	Radius	m
R	Reynolds number.	
r	Radius, equal to ½ d_a	mm
S	Slope.	
U	Mean velocity	m/s
U_z	Velocity at the distance z from the bed	m/s
U_*	Shear velocity	m/s
U_{*c}	Critical shear velocity	m/s
u	Horizontal velocity fluctuation	m/s
V	Wind velocity	m/s
V_c	Critical velocity	m/s
v	Vertical velocity fluctuation	m/s
W	Width	m
x	Major axis of ellipse in figure 57	mm
z	Distance from the bed	m
α	Impact angle of saltating particle	degrees
Θ	Dimensionless shear stress.	
Θ_c	Critical dimensionless shear stress.	

SYMBOLS AND UNITS—Continued

		Unit
κ	von Karman's coefficient.	
ν	Kinematic viscosity	m^2/s
ρ	Density of water	kg/m^3
ρ_a	Density of air	kg/m^3
ρ_s	Density of sediment	kg/m^3
σ	Sorting coefficient.	
σ_v	Standard deviation of vertical velocity fluctuations.	m/s
τ	Shearing stress	$g/cm/s^2$
τ_c	Critical shearing stress	$g/cm/s^2$
ϕ	Dimensionless transport function.	
Ψ	Dimensionless parameter.	
ω	Particle fall velocity	m/s

Sand Waves, Bars, and Wind-Blown Sands of the Río Orinoco, Venezuela and Colombia

By Carl F. Nordin, Jr., *and* David Pérez-Hernández[1]

Abstract

During March 1982, a reconnaissance study was carried out along a reach of the Río Orinoco between Puerto Ayacucho and Ciudad Bolívar. This was the low-flow season. Samples of bed material and suspended sediments were collected, sonic records of the bed were obtained at several locations, and the exposed bars and sand waves were studied at four locations. Sounding records were obtained at two of these locations during June and November when flow covered the bars, and additional studies were made on the ground at some of these same sites during March 1983.

The bed of the river is mostly sand with small quantities, about 5 percent by weight on average, of gravel. Suspended-sediment concentrations were low, ranging between 20 milligrams per liter above Río Apure to almost 40 milligrams per liter below its confluence with the Río Orinoco. The annual sediment load is estimated to be 240×10^6 megagrams per year.

During the dry season, 35 percent or more of the bed is exposed in the form of large bars composed of many sand waves. Trade winds blow upriver and there is substantial upriver transport of river sediments by the wind. If the bars contain very coarse sands and fine gravel, deflation forms a lag deposit that armors the bar surface and prevents further erosion. Theoretical calculations show that the lower limit for the fraction of the bed that needs to be covered with nonmoving particles to prevent further erosion and the smallest size of the armor particles depend only on wind speed.

Calculations of bed-material transport were made for a typical wide and narrow section of the river; the annual load, excluding the wash load, is about 30×10^6 megagrams per year. A new definition for wash load is proposed; it is material that can be suspended as soon as its motion is initiated. For the Río Orinoco, this is material finer than 0.1 millimeters.

INTRODUCTION

In 1982, the U.S. Geological Survey and the Venezuelan Ministerio del Ambiente y de los Recursos Naturales Renovables agreed to cooperate in a series of investigations of the waters and sediments of the Río Orinoco and its major tributaries. This is the first of several reports presenting the results of these investigations.

During low flow of March 1982, a reconnaissance study was undertaken along a reach of the Río Orinoco in Venezuela between Ciudad Bolívar and Puerto Ayacucho (fig. 1). The purposes of the study were to collect samples of bed material at various locations along the river, to document some of the properties of the exposed channel bed configurations, the ripples, sand waves, bars, and other features formed of the bed sediments by the flowing water, and to locate cross sections and short reaches along the river that might be suitable for further detailed studies. Size distributions of bed material were needed in order to compute the sediment discharge of the river, and some examples of these computations are given in this report. The dimensions of the sand waves and other bed configurations were needed to determine the channel roughness and to estimate resistance coefficients for flood routing and other hydraulic

[1]Ministerio del Ambiente y de los Recursos Naturales Renovables, Caracas, Venezuela.

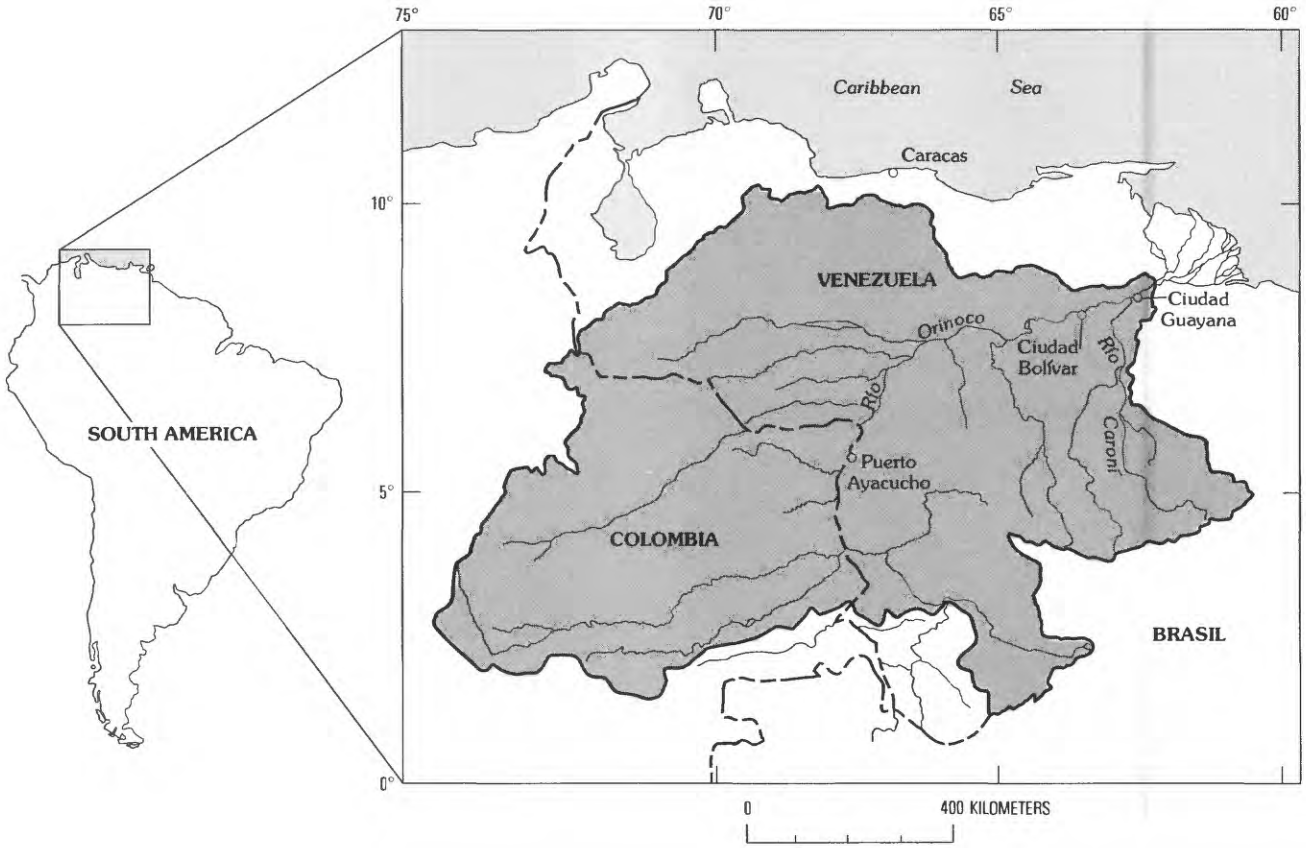

Figure 1. Location of the Río Orinoco drainage area (stippled, bounded by solid line).

calculations. The detailed hydraulic calcuations are given in a later chapter of this series.

Additional field studies were undertaken during the higher flows of June, August, and November, 1982, and again during low flow of March 1983. During the June and November 1982 studies, longitudinal profiles of the river bed were collected with an echo-sounder at the same locations where the sand waves and bars had been exposed and had been observed on the ground during March 1982. Some of these same sites were exposed again during March 1983, and additional measurements and field maps were made at that time to document the length and heights of sand waves and the cross-channel lengths of their crests. Data also were collected on the internal structure and cross stratification of the bars and sand waves; those data are reported by McKee (1989) in another paper of this series.

The purposes of this report are: (1) to describe the particle-size distributions of the bed samples and the concentrations of the suspended-sediment samples that were collected during March 1982, (2) to summarize observations on the characteristics of the sedimentary features of the channel exposed during low flows, and (3) to present some approximate relations for estimating transport of sediment by wind and water.

ACKNOWLEDGMENTS

The writers are indebted to many persons who helped with these studies. Herman Roo G. and Abel Mejía B., Proyecto Orinoco-Apure, were instrumental in initiating and organizing these investigations and took part in many of the field studies. We appreciate their assistance and support. W. F. Curtis, consultant, and C. C. Cranston, E. D. McKee, and R. H. Meade, U.S. Geological Survey, assisted in many aspects of the investigations. Others who had a major role in the field studies include Alain Deredec and Sarkis Farchakh, Proyecto Orinoco-Apure, and Omar Alvarado, Luis Bravo, and Lois and Omar Hernandez, Ministerio del Ambiente y de los Recursos Naturales Renovables.

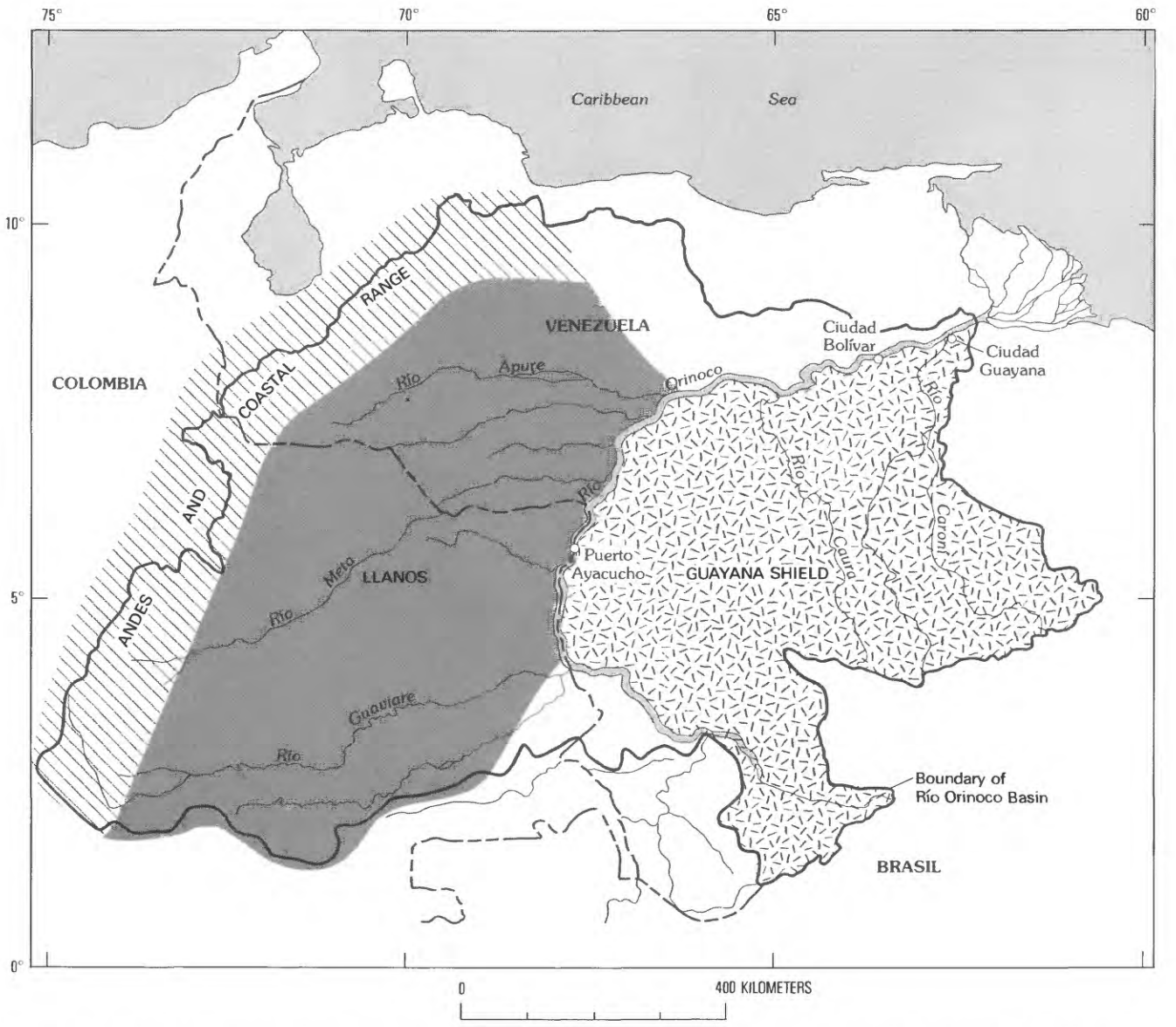

Figure 2. The Río Orinoco basin. The three main sediment-contributing tributaries are the Río Guaviare, Río Meta, and Río Apure. Solid line encloses drainage area (fig. 1).

GENERAL HYDROLOGY OF THE RIO ORINOCO

The Río Orinoco drains an area of about 830,000 km² (square kilometers) in Venezuela and Colombia (fig. 1). Of this total, 640,000 km², or about 77 percent, are in Venezuela. The average water discharge to the delta, just below the Río Caroní at Ciudad Guayana, is about 36,000 m³/s (cubic meters per second) and its average suspended sediment discharge to the delta is in excess of 200×10^6 Mg/yr (megagrams per year). The Río Orinoco is third largest in flow among the world's rivers discharging to the ocean and eighth largest in sediment discharge (Meade and others, 1983).

The main sediment-contributing tributaries to the Río Orinoco enter along the left bank and drain the east slope of the Andes and the dry llanos. The three most important tributaries are the Río Guaviare, Río Meta, and Río Apure (fig. 2). Of these, only the Río Meta and

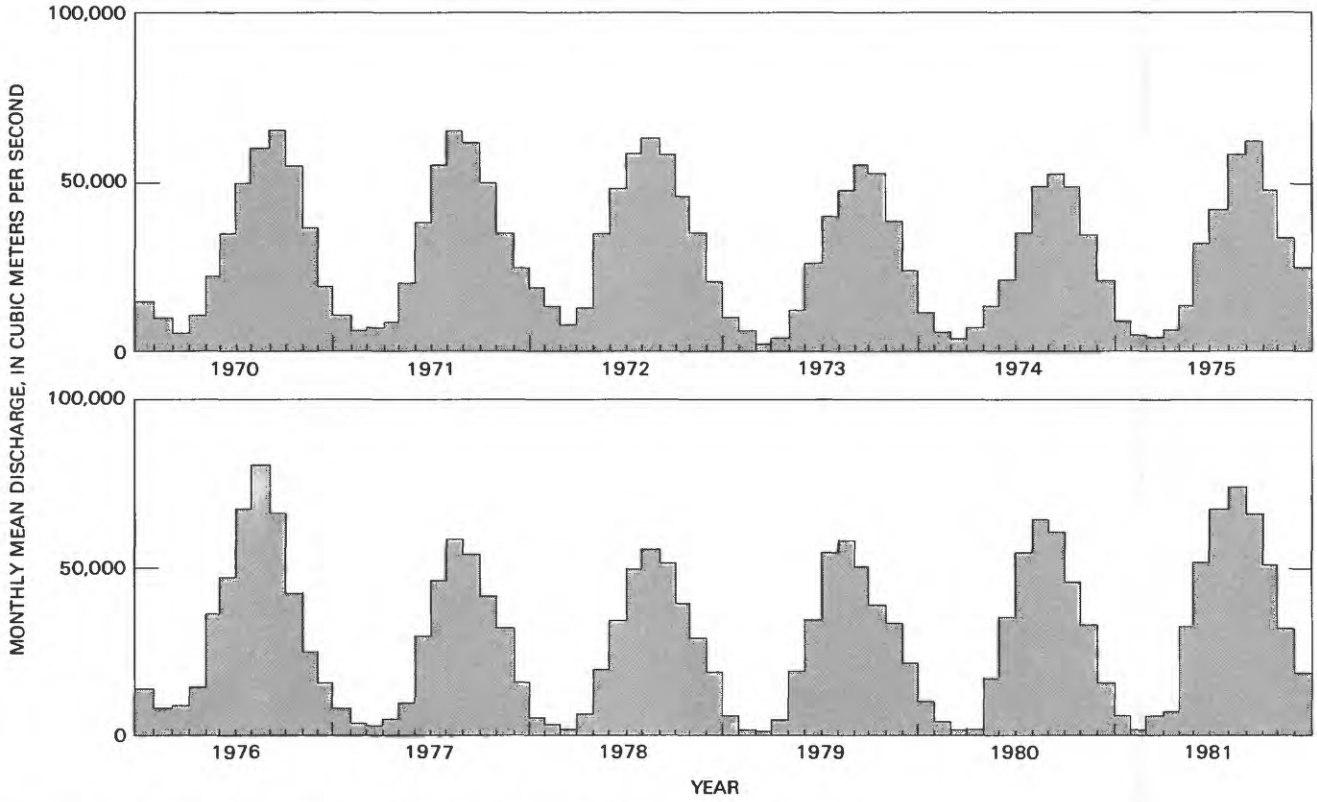

Figure 3. Monthly mean discharge for Río Orinoco at Musinacio, 1970–1981.

Río Apure enter the study reach. Alluvial fans constructed by the Andean tributaries force the Río Orinoco against the Guayana Shield along much of its length, and the river is characterized by a series of rapids and bed-rock controls. Between controls, the river flows in alluvial channels whose wide flood plains are inundated during high flows. During low flows, large areas of the bed are exposed in these alluvial reaches, and the sand waves, bars, and other bed features formed during higher flows are preserved, although they usually are modified somewhat by wind action, as will be shown in a later section.

Streams draining the Guayana Shield have small suspended-sediment concentrations, but contribute large flows and substantial amounts of bed load. The two most important streams draining the Shield are the Río Caroní and Río Caura (fig. 2).

An important characteristic of the Río Orinoco that makes it possible to undertake detailed studies of its bed forms is the wide range of both stage and discharge between high and low flow. During the period of record, 1970 through 1981, the monthly mean discharges for the

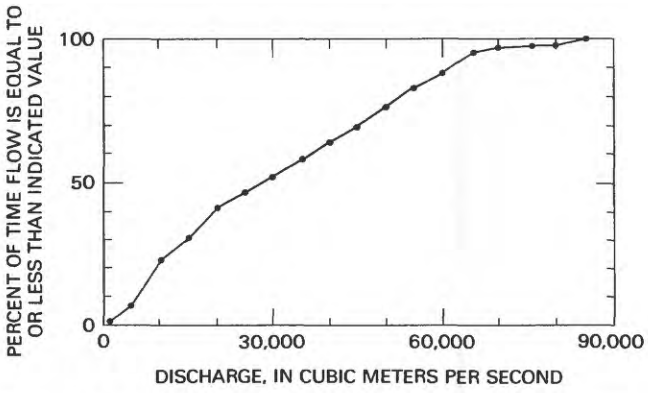

Figure 4. Flow-duration curve for Río Orinoco at Musinacio, 1970–1976 (from Meade and others, 1983).

Río Orinoco at Musinacio (fig. 3) varied from 1,330 m^3/s to 81,100 m^3/s. The flow-duration curve for this station (fig. 4) shows that about one percent of the time, flows are greater than 80,000 m^3/s or less than 2,000 m^3/s (Meade and others, 1983). The daily mean discharges

Table 1. Annual maximum and minimum daily mean discharge, Río Orinoco at Musinacio, 1970–1981

[m^3/s, cubic meters per second]

Year	Maximum		Minimum		
	Date	Discharge (m^3/s)	Date	Discharge (m^3/s)	Ratio
1970	Sept. 11	66,500	Mar. 28	5,410	12.3
1971	Aug. 20	66,100	Feb. 28	6,020	11.0
1972	Aug. 15	64,800	March 27	7,960	8.11
1973	Sept. 26	58,000	March 15	2,930	19.8
1974	Sept. 3,4	53,700	March 29,30	3,790	14.2
1975	Sept. 1	62,000	March 4	3,420	18.2
1976	Aug. 5	82,100	March 2	5,640	14.6
1977	Aug. 26	61,400	March 17–19	3,420	18.0
1978	Sept. 2	59,300	March 30,31	1,100	53.8
1979	Aug. 19	60,500	March 8	1,220	49.7
1980	Sept. 3	65,600	March 23	1,050	62.2
1981	Aug. 5	75,800	Feb. 19–21	2,810	27.0
Average	.....	64,600	Average	3,730	25.7

varied from a low of 1,050 m^3/s on March 23, 1980, to a high of 82,100 m^3/s on August 5, 1976. The annual maximum and minimum flows and the ratio of maximum to minimum flows are shown in table 1. The ratios vary from a high of 54 in 1978 to a low of 8.1 in 1972 and average about 26. This high ratio between maximum and minimum flow is characteristic of tropical or subtropical rivers that drain areas with a wet-dry climate, such as the Orinoco and Yangtze, but it is not typical of the two other large tropical rivers, the Amazon and Zaire (Congo) that flow along the equator and drain areas in both Northern and Southern Hemispheres. The ratio of maximum to minimum flow for these rivers is on the order of 3 (Nordin and Meade, 1985).

The range in stage also is large on the Río Orinoco. The stage-discharge relation for the Río Orinoco at Musinacio (fig. 5), defined from streamflow measurements made from 1969 through 1975, shows that the difference in water-surface elevation between high and low flow is about 17 m (meters). A similar range in stage is recorded from the gage readings at Ciudad Bolívar. Table 2 lists maximum and minimum stages for each year of record, 1923–1982, for the station of Ciudad Bolívar. The station has not been rated with discharge measurements, except for a few measurements made during low flows during the period 1943–1962. No major tributaries enter the Río Orinoco between Musinacio and Ciudad Bolívar, however, so the range of flows should be about the same.

The long-term suspended-sediment discharge of the Río Orinoco at Musinacio can be estimated approximately using an instantaneous sediment rating curve (fig. 6) and the flow-duration curve of figure 4. These data are from Pérez-Godoy (1982) and Meade

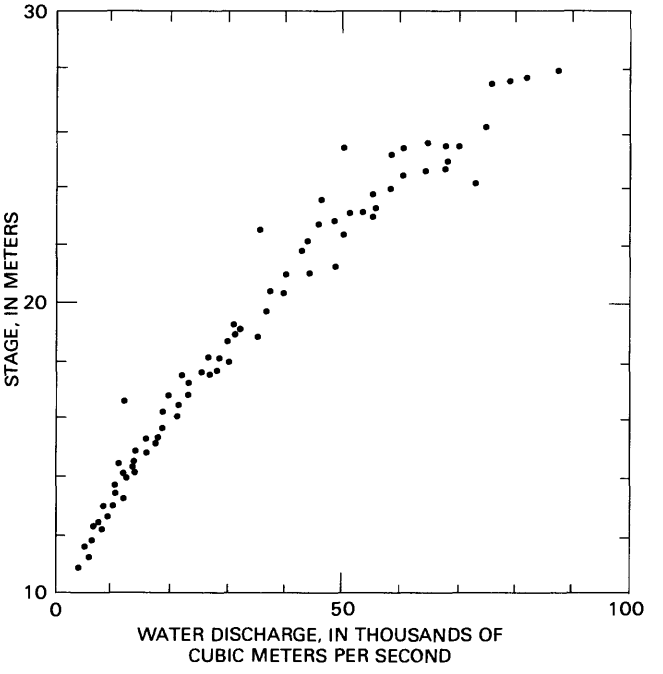

Figure 5. Stage-discharge relation, Río Orinoco at Musinacio.

Table 2. Annual highest and lowest stages, Río Orinoco at Ciudad Bolívar, 1923–1982
[Measurements in meters (m)]

Year	Lowest		Highest		Year	Lowest		Highest	
	Date	Stage (m)	Date	Stage (m)		Date	Stage (m)	Date	Stage (m)
1923	May 1	5.68	Sept. 16–17	16.12	1954	Feb. 28, Mar. 1–2.	3.08	Aug. 26	17.35
1924	April 15–18	2.03	Aug. 18	16.33	1955	Mar. 19–20	3.51	Aug. 10–12	15.20
1925	Mar, 27	2.06	Sept. 9–10	16.00	1956	April 14–15	4.22	Aug. 27–30	16.61
1926	Mar. 19,20,21	[1]1.62	Sept. 14	14.16	1957	Mar. 27–31	2.23	Sept 4,5	15.65
1927	Mar. 14,15	1.84	Aug. 10	17.21					
1928	Mar. 13	2.33	Aug. 30	15.86	1958	Mar. 1–6	2.41	Sept. 1–3	15.12
1929	Mar. 23,24,25	2.48	Aug. 12	16.70	1959	Mar. 17,18	2.58	Aug. 23–25	15.99
1930	Mar. 9–11	2.48	Aug. 22,23	15.53	1960	April 18–20	2.15	Aug. 22–23	16.15
1931	Mar. 26	2.16	Aug. 18	16.86	1961	Mar. 25–29	1.73	Sept. 20–22	15.67
1932	Feb. 29	2.52	Aug. 29	16.12	1962	Mar. 12	2.34	Aug. 26	17.29
1933	Mar. 8–10	3.13	Aug. 12	15.42	1963	April 5–7	2.78	Aug. 12–14	16.65
1934	Mar. 31–Feb. 3	2.63	Sept. 9,10	15.32	1964	Missing.			
1935	Mar. 27,28	2.33	Aug. 30	16.00	1965	April 10–11	2.30	Sept. 4–5	15.17
1936	Mar. 13	2.06	Aug. 18	15.20	1966	Mar. 22–28	2.21	Aug. 20	15.36
1937	April 7	3.14	Aug. 17,18	15.43	1967	April 4,7,8	2.56	Aug. 22,27,28	17.30
1938	Feb. 12	3.12	Aug. 16	16.95	1968	Mar. 10–11	2.25	Aug. 25	16.17
1939	April 2	2.70	Aug. 24	14.30	1969	April 8	2.98	Sept. 3	15.55
1940	Mar. 31–April 1	1.83	Sept. 11	14.58	1970	Mar. 30	3.15	Sept. 13	16.19
1941	Mar. 29–31	2.21	Aug. 30	15.13	1971	Mar. 3	3.37	Sept. 3–4	16.16
1942	Mar. 26	1.74	Aug. 26–28	16.12	1972	Mar. 11	4.11	Aug. 17	15.90
1943	Mar. 24,25	3.48	Aug. 18	[2]18.03	1973	Mar. 19	1.82	Sept. 29	15.00
1944	Mar. 7	2.67	Sept. 10	16.37	1974	April 6–8	2.25	Sept. 12–13	14.22
1945	April 3,4	2.48	Aug. 24	17.07	1975	Mar. 4–5	2.25	Sept. 7–8	15.56
1946	Mar. 13–15	2.28	Sept. 2–5	17.50	1976	Mar. 4–5	3.23	Sept. 4–6	18.00
1947	Mar. 31	2.14	Aug. 27	16.08	1977	Mar. 17	2.30	Aug. 23	16.34
1948	April 3	1.84	Aug. 14–16	16.20	1978	Mar. 31	1.97	Aug. 3	16.06
1949	Mar. 26–27	2.19	Sept. 15	16.43	1979	Mar. 8–12	2.05	Aug. 19	16.10
1950	April 10–13	3.02	Aug. 20–22	16.66	1980	Mar. 31–April 1	1.84	Sept. 4–5	16.91
1951	April 7	4.01	Aug. 20	17.73	1981	Feb. 25–28, Mar. 1–4.	2.85	Aug. 18–19	17.33
1952	April 4–5	2.24	Sept. 2	16.67					
1953	Mar. 24	3.68	Aug. 16–26	16.96	1982	Mar. 21	3.09	Aug. 23	16.68

[1]Lowest stage of record.
[2]Highest stage of record.

and others (1983). The computations tabulated in table 3 show the average suspended-sediment discharge for this period to be about 190×10^6 Mg/yr.

THE STUDY REACH AND TYPES OF SAMPLING

The data collection began on March 9, 1982, from Cabruta (fig. 7). The first leg of the cruise, from March 9 to March 12, was from Cabruta at river kilometer (km) 856 upstream to Puerto Ayacucho, at river km 1,176. On March 10, a few observations were made on a large exposed sandbar about 10 km downstream of the mouth of the Río Suapure (fig. 7, site A). Twenty-four samples of bed material were collected between Cabruta and Puerto Ayacucho, including samples on two tributaries, the Río Meta and Río Parguaza.

The second leg of the cruise ran from March 12 through March 15, and covered the same reach from Puerto Ayacucho back to Cabruta. On the downriver leg of the cruise, flow velocities were measured and a few depth-integrated suspended-sediment samples were collected with a large-volume collapsible bag sampler

Table 3. Computation of average suspended-sediment discharge for Río Orinoco at Musinacio
[m^3/s, cubic meters per second; Mg/d, megagrams per day]

Water discharge (from fig. 4)			Sediment discharge (from fig. 6)	
Range (m^3/s)	Mean (m^3/s)	Frequency (f)	Q_s (Mg/d)	fQ_s (Mg/d)
0–5,000	2,500	0.0621	7,500	466
5,000–10,000	7,500	.1654	43,800	7,245
10,000–15,000	12,500	.0821	99,000	8,128
15,000–20,000	17,500	.1005	169,500	17,035
20,000–25,000	22,500	.0551	250,000	13,775
25,000–30,000	27,500	.0567	345,000	19,562
30,000–35,000	32,500	.0583	500,000	29,150
35,000–40,000	37,500	.0602	559,500	33,682
40,000–45,000	42,500	.0504	720,000	36,288
45,000–50,000	47,500	.0739	830,000	61,337
50,000–55,000	52,500	.0661	990,000	65,439
55,000–60,000	57,500	.0528	1,120,000	59,136
60,000–65,000	62,500	.0731	1,300,000	95,030
65,000–70,000	67,500	.0211	1,470,000	31,017
70,000–75,000	72,500	.0051	1,650,000	8,415
75,000–80,000	77,500	.0063	1,820,000	11,466
80,000–85,000	82,500	.0106	2,020,000	21,417

$\Sigma fQ_s = 519{,}000$ Mg/d
Average suspended-sediment discharge $= 365 \times 519{,}000$
$= 190 \times 10^6$ megagrams per year

(Nordin, Cranston, and Mejía, 1983). Bed samples and a few suspended-sediment samples also were collected at intermediate points between the stations occupied on the upriver leg of the cruise. A series of sand waves exposed along the right bank downstream of the rapids "Raudal San Borja" (fig. 7, site B) was investigated in some detail.

On March 16th, studies were made of the wind-blown deposits along the right bank at Capuchinos a few kilometers upstream of Curiquima (site C) and of sand waves along the left bank commencing at Cabruta and running downstream about 2 km (site D on fig. 7).

The cruise continued downstream from Cabruta on March 17 and ended in Ciudad Bolívar March 20. Through this reach, bed-material samples were collected at 38 sites, spaced about every 10 or 15 km along the reach, and suspended-sediment samples were collected at three locations.

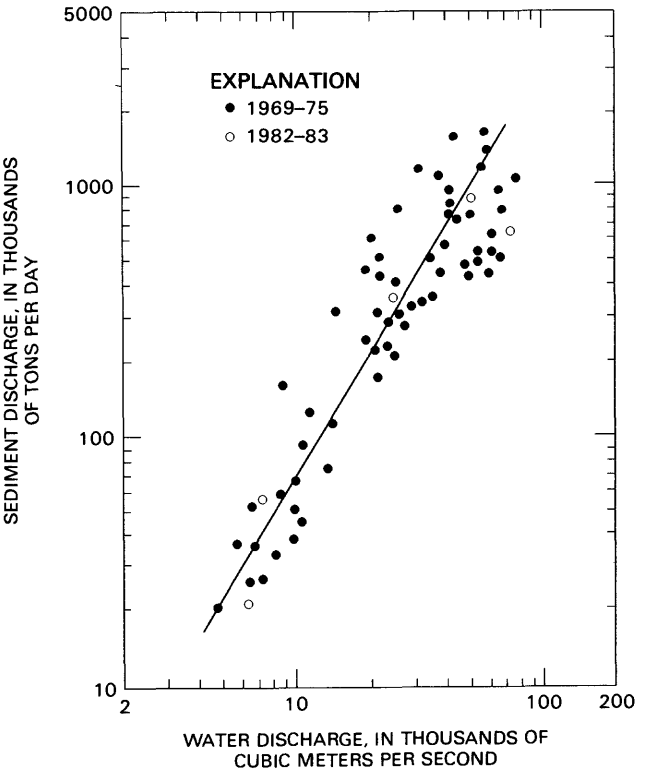

Figure 6. Relation between sediment discharge and water discharge, Río Orinoco at Musinacio.

BED MATERIAL

Methods

Bed-material samples were collected with the USBM–54 bed-material sampler at most locations, and with a small drag sampler where the bed contained

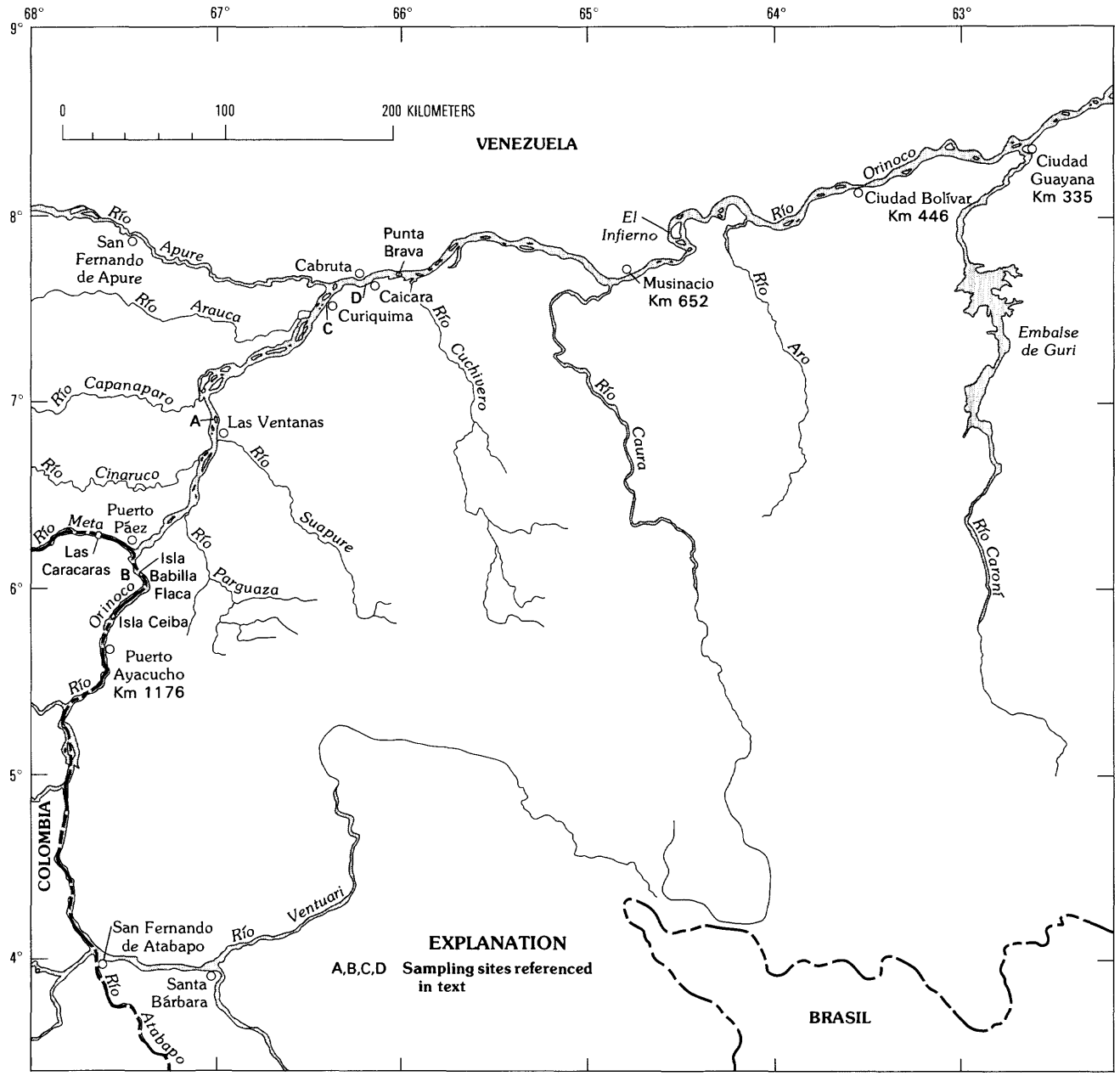

Figure 7. Location of the study reach.

appreciable amounts of gravel. The BM–54 sampler is described in Report 14 by Federal Inter-Agency Sedimentation Project (1963); it collects a sample of 1–2 kg from the top 5 cm (centimeter) of the bed. If the bed contains gravel, the sampler commonly will jam partly closed against a gravel particle allowing the fine material to be washed from the sample. When this happened, the sample was discarded and a second sample was collected. If, after several tries, an unbiased sample could not be collected with the BM–54, the bed was sampled with a small drag sampler.

The drag sampler was constructed from a piece of thick-wall steel pipe 10 cm inside diameter and about 40 cm long. One end was welded shut and the other end was beveled from the inside to a cutting edge. A loop of chain three or four times the length of the sampler was

attached to two holes drilled near the cutting edge. A shackle was mounted at the center of the chain to attach the sampler to a rope or cable for sampling.

When sampling with the BM–54, the vessel is held stationary. With the drag sampler, however, the vessel is allowed to drift with the current while the sampler is lowered, dragged along the bed, and retrieved. Usually, a length of line two or three times the depth is played out so the sampler drags almost horizontally along the bed well upstream from the sampling vessel. The sampler is retrieved slowly so the open end is not exposed to high velocities, which would wash out some of the finer material. The top 10 cm or so of the sample is discarded to ensure that the finer sediments were not lost due to action of the flow.

Each sample was split into two parts, sealed in plastic bags, and labeled. One part was shipped to the U.S. Geological Survey in Denver, Colorado; the other part was shipped to Ministerio del Ambiente y de los Recursos Naturales Renovables in Caracas.

Samples consisting of sand and gravel were oven-dried and sieved for particle-size analysis. A few samples were collected where low velocities or backwater effects had caused depositions of mud consisting of silt- and clay-size particles. A few of these samples were analyzed using the pipet and visual accumulation tube method (Guy, 1969).

Sampling sites were identified by stations along the river numbered 1 through 75. Each station was located where possible by latitude and longitude, by river kilometer, and by proximity to identifiable landmarks such as mouths of tributaries, villages and towns, or islands. River kilometers are those established by Instituto National de Canalizaciones giving distance upstream from the river's mouth. Under this system, a few reference points along the river are as follows:

Location	River kilometer
Ciudad Guayana	335
Ciudad Bolívar	446
Musinacio	652
Caicara	848
Puerto Ayacucho	1176

The station locations, date of sampling, number and kind of samples collected, type of sampler used, and a few remarks about the samples are given in table 4. The particle-size distributions of bed samples are listed by station and date in table 5.

At many locations, only a single sample of bed material was collected near the centerline of the channel. At a few stations, three samples were collected across the section at approximately equal centroids of flow. At these stations, sample A was collected in the left one-third of the channel (looking downstream), sample B was collected in the center one-third of the flow near the channel centerline, and sample C was collected in the right one-third of the channel.

A few miscellaneous samples were collected and are noted in table 4 and listed in table 5. A sample of the bank material was collected at station 8 about 6 m below the flood-plain surface at El Burro, a small community along the right bank of the Río Orinoco just across from the mouth of the Río Meta. A sample of gravel was collected at station 75 along the right bank about 3 km upstream of the bridge at Ciudad Bolívar.

Bed-material samples were collected from three tributaries—the Río Parguaza at station 11, the Río Meta at station 18, and the Río Cinaruco at station 32.

Results

There are considerable differences in the size distributions and mineralogical characteristics of sediments from the tributaries draining the Andes and llanos (plains), such as the Río Meta and Río Cinaruco, and from streams draining the Precambrian rocks of the Guayana Shield, characterized by the Río Parguaza. The size distributions of bed samples from these three streams are plotted in figure 8. The samples from Río Meta and Río Cinaruco consist mostly of sand-size material that has median diameters of 0.26 mm (millimeters); 98 percent of the material is between 0.125 and 1.0 mm. Both samples contain less than one percent gravel (>2 mm in diameter). The sample of bed sediment from Río Parguaza is considerably coarser; has a median diameter of 1.5 mm; only 2 percent is finer than 0.5 mm, compared with 90 percent finer for Río Meta and 96 percent finer for Río Cinaruco; and 24 percent of the material is gravel. The Río Parguaza bed sample also shows the properties of a nearly logarithmic-normal distribution of particle sizes, characterized by the straight line part of the curve for sizes coarser than about 0.5 mm. The dashed line on figure 8 would be a log-normal distribution encompassing 99 percent of the sample. Whether the log-normal distribution is characteristic of the sediments derived from the shield or whether this is simply fortuitous remains to be determined. Sediments from the shield are not transported great distances from

Table 4. Station numbers, locations, and information about the samples

[°, degrees; ′, minutes; ″, seconds; °C, degrees Celsius; QW, quality of water sample for chemical analysis collected—locations for station 10–30 are from Mapa de Suelos, Puerto Ayacucho, 1:100,000; all others are from Mapa Base Río Orinoco, 1:50,000, Oficina Técnica Del Monte Y Assoc. C.A., 1981]

Station No.	March 1982	Time (hour)	River kilometer	Location		Type of sample			Depth (meters)	Water temperature (°C)	Remarks
				Latitude	Longitude	Bed	Suspended	Other			
1	9	1425	882	07°35′30″	66°26′10″	x			2.4	28	
2	9	1530	905	07°25′15″	66°29′05″	x			1.2	28	
3	9	1735	920	07°19′40″	66°35′10″	x			1.2	28	Silt and clay.
4	9	1830	933	07°17′45″	66°41′45″	x			1.8	28	
5	10	0805	942	07°16′40″	66°45′50″	x			7.3	28	
6	10	1010	959	07°10′45″	66°52′40″	x			1.2	28	
7	10	1140	971	07°11′05″	66°59′45″	x			4.6	28	
8	10	1525	1,009	06°54′40″	67°00′30″	x			3.8	29	
9	10	1725	1,020	06°48′30″	67°01′45″	x			7.5	30	
10	11	0625		06°30′10″	67°00′05″	x			4.1	30	
11	11	1015		06°25′00″	67°10′00″	x		x	0.9	30	Río Parguaza, QW sample.
12	11	1055		06°26′00″	67°11′00″	x		x	14.0	30	QW sample.
13	11	1320		06°15′50″	67°19′45″	x			9.4	30	
14	11	1445	1,102	06°10′15″	67°24′10″			x		31	Bank sample at El Burro.
15	11	1510		06°09′50″	67°27′40″	x			9.4	31	Small sample, repeat.
16	11	1515		06°09′50″	67°27′40″	x			10.3	31	Combined with station 15.
17	11	1520		06°09′50″	67°27′40″	x			11.0	31	Duplicate of station 15.
18	11	1630		06°10′10″	67°28′00″	x	x	x	1.2	31	Río Meta, QW sample.
19	11	1755		06°07′40″	67°28′10″	x		x	3.4	31	Above Río Meta, QW sample.
20	12	0700		06°05′00″	67°27′50″	x			3.8	30	
21A	12	0915		05°55′20″	67°30′00″	x			3.7	30	
21B	12	0925		05°55′15″	67°30′05″	x			3.5	30	
21C	12	0930		05°55′13″	67°30′08″	x			3.6	30	
22	12	1115		05°47′50″	67°36′40″	x		x	5.1	30	QW sample.
23	12	1315		05°42′00″	67°38′40″	x			20.3	31	
24	12	1730	1,176	05°38′40″	67°36′35″	x			39.3	31	Puerto Ayacucho, QW sample.
25A	13	0810		05°58′10″	67°27′00″	x			3.0	29	
25B	13	0815		05°58′00″	67°26′40″	x			4.1	29	
25C	13	0820		05°57′40″	67°26′30″	x			6.8	29	
26A	13	1410		06°04′45″	67°29′25″	x	x		19.8	30	
26B	13	1415		06°04′50″	67°29′10″	x	x		7.0	30	Above Río Meta.
26C	13	1435		06°05′00″	67°28′55″	x	x		5.1	30	
27A	13	1800		06°16′50″	67°21′25″	x	x		6.9	30	
27B	13	1815		06°16′30″	67°20′55″	x	x		9.0	30	Below Río Meta.
27C	13	1830		06°16′10″	67°20′40″	x	x		9.7	30	
28A	14	0735				x			7.3	28	
28B	14	0740		06°24′20″	67°13′20″	x			5.2	28	
28C	14	0745				x			3.5	28	
29A	14	1035				x			6.5	28	
29B	14	1040		06°35′00″	67°08′00″	x			11.4	28	
29C	14	1045				x			4.3	29	
30	14	1150		06°40′00″	67°05′00″	x			1.2	29	
31A	14	1245				x			5.8	30	
31B	14	1250	1,026	06°45′00″	67°02′30″	x			5.8	30	
31C	14	1255				x			5.3	30	
32	14	1230		06°36′30″	67°08′00″	x		x	0.7	31	Río Cinaruco, QW sample.
33A	14	1720		07°00′45″	67°04′35″	x			5.1	30	
33B	14	1725	995	07°00′55″	67°04′10″	x			7.7	30	
33C	14	1730		07°01′05″	67°03′50″	x			3.8	30	
34A	15	0840		07°11′45″	66°51′50″	x			11.6	28	
34B	15	0845	956	07°11′45″	66°51′45″	x			11.9	28	
34C	15	0850		07°11′35″	66°51′40″	x			10.6	28	
35	15	1340	910	07°22′40″	66°31′10″	x			6.1	30	
36A	15	1510		07°27′45″	66°30′28″	x	x		6.7	30	
36B	15	1520	900	07°27′45″	66°30′08″	x	x	x	9.1	30	Above Río Apure, QW sample.
36C	15	1530		07°27′45″	66°29′48″	x	x		5.4	30	

Table 4. Station numbers, locations, and information about the samples—Continued

Station No.	March 1982	Time (hour)	River kilometer	Location		Type of sample			Depth (meters)	Water temperature (°C)	Remarks
				Latitude	Longitude	Bed	Suspended	Other			
37A	15	1810		07°39'00"	66°19'30"	x	x		10.8	30	
37B	15	1805	866	07°38'30"	66°19'18"	x	x	x	12.8	30	Below Río Apure, QW sample.
37C	15	1800		07°38'20"	66°19'10"	x	x		12.2	30	
38A	17	0910					x		13.7	28	
38B	17	0925					x		6.4	28	
38C	17	0937	859	07°38'20"	66°15'45"		x		7.0	28	At Cabruta, below Río Apure.
38D	17	0953					x		7.6	28	
38E	17	1005					x		4.6	28	
39	17	1110	847	07°39'45"	66°10'45"	x			21.6	29	
40A	17	1150				x			3.7	29	
40B	17	1155	838	07°40'15"	66°06'00"	x			3.5	29	
40C	17	1200				x			5.2	29	
41A	17	1240				x			3.8	29	
41B	17	1245	828	07°41'15"	66°00'45"	x			5.6	29	Above Río Cuchivero.
41C	17	1250				x			5.3	29	
42A	17	1350				x			3.8	30	
42B	17	1345	800	07°42'50"	65°49'50"	x			6.1	30	
42C	17	1340				x			11.9	30	
43	17	1420	799	07°45'25"	65°48'00"	x			13.6	30	
44	17	1440		No sample					No sample		
45	17	1545	788	07°50'25"	65°44'15"	x			6.8	30	
46A	17	1635				x	x		11.6	30	
46B	17	1630	782	07°51'55"	65°41'50"	x	x	x	10.0	30	Above Las Bonitas, QW sample.
46C	17	1625				x	x		6.4	30	
47	17	1825	767	07°55'00"	65°35'30"	x			11.5	30	
48	18	0710	750	07°51'10"	65°28'10"	x			7.3	28	
49	18	0810	738	07°52'30"	65°21'18"	x			5.6	28	
50A	18	0910	721	07°50'20"	65°12'45"	x			5.5	28	
50B	18	0915	721	07°50'20"	65°12'45"	x			6.4	28	
51	18	1010	706	07°47'20"	65°06'10"	x			6.9	28	
52	18	1050	696	07°46'10"	65°01'35"	x			5.5	28	
53	18	1125	686	07°42'20"	64°58'20"	x			8.1	29	
54	18	1215	676	07°40'45"	64°54'35"	x			4.8	29	
55	18	1310	665	07°39'45"	64°49'10"	x			3.7	29	
56A	18	1510				x	x		11.9	30	
56B	18	1505	657	07°41'30"	64°45'30"	x	x		10.0	30	Musinacio section.
56C	18	1500				x	x		9.8	30	
57	18	1700	638	07°46'00"	64°37'00"	x			13.1	30	
58	18	1745	629	07°45'00"	64°32'35"	x			7.3	30	
59	19	0745		07°49'45"	64°27'30"	x			12.2	28	Below El Infierno, silt and clay.
60	19	0755	611	07°50'45"	64°28'15"	x			3.0	28	
61	19	0850	600	07°54'00"	64°33'15"	x			5.7	28	
62	19	0935	590	07°57'00"	64°34'25"	x			19.7	28	
63	19	1025	580	07°50'40"	64°30'25"	x			6.7	28	
64	19	1125	570	08°00'10"	64°25'10"	x			14.2	29	
65	19	1220	559	08°02'05"	64°20'25"	x			6.9	29	
66	19	1310	550	08°05'30"	64°17'25"	x			9.6	30	
67	19	1415	535	08°02'00"	64°11'00"	x			5.0	30	
68	19	1505	523	07°59'20"	64°06'30"	x			11.4	30	
69A	19	1611	514	07°56'50"	64°01'40"	x			11.4	30	
69B	19	1617	514	07°56'50"	64°01'40"	x			23.6	30	
70A	19	1702				x			15.4	30	
70B	19	1656	513	07°56'50"	64°01'25"	x			14.9	30	
70C	19	1653				x			10.4	30	
71	19	1830	499	07°58'50"	63°54'40"	x			4.3	30	
72A	20	0740				x	x		11.3	28	
72B	20	0735	487	08°04'45"	63°51'30"	x	x		11.3	28	El Almacén.
72C	20	0730				x	x		11.2	28	
73	20	0920	476	08°08'45"	63°48'00"	x			4.7	28	
74	20	1010	463	08°08'15"	63°41'00"	x			7.6	28	
75	20	1145	459	08°06'45"	63°39'00"			x	—	—	

Table 5. Particle-size distributions of bed-material samples, Río Orinoco and tributaries, March 1982
Leaders (---) indicate zero or 100 percent

Station No.	Date Year-Month-Day	Percent by weight finer than sieve size (millimeters) indicated																	
		0.062	0.088	0.125	0.177	0.250	0.353	0.500	0.707	1.00	1.41	2.00	2.83	4.00	5.66	8.00	11.3	16.0	22.6
1	82-03-09	---	---	0.0	0.7	2.9	24.6	68.4	85.1	92.1	95.6	97.4	98.5	99.6	99.8	100	---	---	---
2	82-03-09	---	---	0.0	2.9	26.6	81.2	94.9	97.9	98.9	99.5	99.5	100	---	---	---	---	---	---
4	82-03-09	---	---	0.0	2.1	26.7	82.4	97.7	99.5	100	---	---	---	---	---	---	---	---	---
5	82-03-10	---	0.0	0.7	14.4	37.2	78.9	91.6	95.3	97.4	98.5	98.5	98.5	100	---	---	---	---	---
6	82-03-10	0.0	0.7	3.8	33.5	74.2	97.6	99.3	99.3	99.3	99.3	100	---	---	---	---	---	---	---
7	82-03-10	---	---	0.0	1.6	14.3	51.2	75.6	85.7	90.4	92.8	95.5	96.4	98.7	99.1	99.6	100	---	---
8	82-03-10	---	---	0.0	4.2	19.9	44.1	66.5	80.1	87.9	93.1	96.1	97.5	99.2	100	---	---	---	---
9	82-03-10	1.4	2.0	4.3	8.5	30.8	69.4	88.1	94.4	97.3	99.1	100	---	---	---	---	---	---	---
10	82-03-11	---	---	---	0.0	1.1	23.8	80.5	95.7	98.0	98.3	98.9	99.8	99.8	100	---	---	---	---
11	82-03-11	0.0	0.2	0.2	0.2	0.3	0.6	2.0	7.2	21.5	48.0	76.6	93.6	98.5	99.7	100	---	---	---
12	82-03-11	0.5	0.5	0.7	1.4	3.0	17.2	82.6	97.9	98.6	99.1	99.1	99.1	100	---	---	---	---	---
13	82-03-11	0.4	0.4	0.6	2.3	5.8	40.3	74.6	91.2	95.4	96.9	97.8	98.1	99.8	99.8	100	---	---	---
14	82-03-11	31.9	51.8	72.4	91.9	94.8	96.5	98.0	98.5	99.3	99.3	99.3	100	---	---	---	---	---	---
15	82-03-11	0.0	0.4	1.4	4.7	6.8	14.1	35.6	60.0	76.7	84.7	86.8	92.0	94.4	95.6	99.2	100	---	---
17	82-03-11	0.0	0.7	2.0	5.9	8.7	13.5	27.1	47.6	64.2	76.2	84.1	89.3	91.9	95.6	99.1	100	---	---
18	82-03-11	---	0.0	0.2	12.2	46.8	74.9	90.0	96.7	98.2	99.0	99.6	100	---	---	---	---	---	---
19	82-03-11	---	---	0.0	1.3	12.6	48.3	70.7	80.3	85.5	90.5	93.4	96.4	98.6	99.6	100	---	---	---
20	82-03-12	---	---	---	0.0	2.7	24.1	59.7	84.2	93.9	97.8	100	---	---	---	---	---	---	---
21A	82-03-12	---	---	0.0	16.9	54.8	75.1	82.4	87.4	91.3	94.9	97.3	100	---	---	---	---	---	---
21B	82-03-12	---	---	0.0	2.2	14.0	39.3	56.3	68.3	76.2	83.4	88.9	94.1	100	---	---	---	---	---
21C	82-03-12	---	---	0.0	2.7	10.2	38.4	64.5	78.9	87.8	93.6	96.3	97.1	100	---	---	---	---	---
22	82-03-12	---	---	0.0	0.4	4.0	24.6	58.2	77.9	88.0	94.9	97.2	99.1	100	---	---	---	---	---
23	82-03-12	---	0.0	0.5	6.7	16.1	26.3	36.4	49.2	63.9	76.5	85.8	91.9	100	---	---	---	---	---
24	82-03-12	7.0	18.1	34.2	67.8	87.2	95.0	97.0	97.7	98.3	98.3	99.7	100	---	---	---	---	---	---
25A	82-03-13	0.0	0.2	0.2	1.2	8.0	31.6	50.1	61.6	73.0	82.8	93.4	96.3	98.8	100	---	---	---	---
25B	82-03-13	---	0.0	0.2	5.3	23.6	60.6	75.8	81.3	85.4	89.3	92.0	92.6	93.8	94.7	100	---	---	---
25C	82-03-13	0.0	0.2	0.2	6.4	34.7	67.4	84.0	91.4	95.0	96.5	97.1	97.6	98.0	98.5	100	---	---	---
26A	82-03-13	0.0	0.8	1.6	6.8	31.7	74.2	82.7	86.2	89.1	94.2	97.7	100	---	---	---	---	---	---
26B	82-03-13	---	0.0	0.2	1.5	3.6	8.0	16.8	30.9	45.9	65.3	82.3	93.5	99.0	100	---	---	---	---
26C	82-03-13	---	0.2	0.4	1.3	5.3	19.8	50.8	78.1	93.0	97.7	99.1	99.6	100	---	---	---	---	---
27A	82-03-13	0.0	0.1	0.2	2.2	13.7	64.2	89.7	95.9	97.6	98.3	99.0	99.1	100	---	---	---	---	---
27B	82-03-13	---	---	---	0.0	7.6	51.3	82.4	93.4	96.5	97.4	98.6	99.2	99.5	100	---	---	---	---
27C	82-03-13	---	---	0.0	0.9	2.1	8.0	29.6	61.6	85.1	96.8	99.9	99.9	99.9	100	---	---	---	---
28A	82-03-14	---	---	0.0	1.9	3.8	29.5	53.1	68.6	77.8	85.8	92.1	96.9	99.0	99.6	100	---	---	---
28B	82-03-14	---	---	0.0	2.9	17.0	44.9	71.8	88.6	94.8	97.6	98.6	98.8	99.9	100	---	---	---	---

28C	82-03-14	1.2	1.4	2.6	5.8	12.3	25.1	44.1	65.7	79.8	89.1	94.0	97.2	97.7	98.6	98.8	100		
29A	82-03-14	3.7	4.6	5.6	9.8	15.8	48.9	94.3	97.7	98.2	99.1	99.5	99.6	100	---	---	---	---	---
29B	82-03-14	0.4	1.4	1.8	2.0	3.0	5.7	18.1	43.9	72.5	87.9	94.1	97.0	100	---	---	---	---	---
29C	82-03-14	0.8	1.0	1.2	1.6	3.2	11.3	28.3	54.9	73.1	85.5	92.8	97.8	100	---	---	---	---	---
30	82-03-14	---	---	0.0	0.4	1.4	8.9	47.2	81.9	93.8	97.7	99.0	99.4	100	---	---	---	---	---
31A	82-03-14	1.2	3.7	7.6	13.8	16.5	29.0	58.4	82.9	94.2	98.4	99.2	100	---	---	---	---	---	---
31B	82-03-14	0.0	0.7	3.8	14.0	20.8	31.4	56.2	81.3	88.9	91.9	93.2	95.0	95.3	95.5	97.5	98.6	100	---
31C	82-03-14	---	0.9	6.0	21.6	32.8	45.1	64.4	78.1	85.1	90.7	94.9	97.4	97.9	98.3	99.1	100	---	---
32	82-03-14	---	0.0	0.6	11.0	45.2	76.5	96.6	98.3	98.9	99.1	99.3	99.4	100	---	---	---	---	---
33A	82-03-14	3.2	4.7	7.1	19.1	44.9	85.0	95.3	96.9	100	---	---	---	---	---	---	---	---	---
33B	82-03-14	0.7	1.9	2.9	11.4	31.2	44.8	52.3	60.0	67.3	76.5	86.4	92.3	95.3	99.9	100	---	---	---
33C	82-03-14	1.6	3.5	3.9	4.3	6.0	16.9	45.6	69.6	84.2	92.0	95.3	97.5	99.4	99.8	100	---	---	---
34A	82-03-15	0.0	3.5	15.5	29.5	42.4	61.6	74.2	80.3	84.3	89.0	93.0	96.6	98.4	99.3	100	---	---	---
34B	82-03-15	0.0	0.3	1.1	2.8	9.0	31.5	67.5	88.8	95.6	98.3	99.5	99.7	99.7	100	---	---	---	---
34C	82-03-15	0.0	1.2	2.6	7.8	21.5	50.9	82.3	95.2	97.6	98.0	98.4	98.4	98.4	99.0	100	---	---	---
35	82-03-15	---	---	0.0	0.3	2.6	24.3	58.3	83.1	92.2	96.7	97.7	98.7	100	---	---	---	---	---
36A	82-03-15	---	---	0.0	2.1	13.5	47.5	69.5	83.3	91.2	96.1	98.4	100	---	---	---	---	---	---
36B	82-03-15	---	---	0.0	0.5	2.1	20.0	69.9	84.9	91.3	95.8	97.6	98.8	100	---	---	---	---	---
36C	82-03-15	1.3	1.8	2.2	4.4	13.1	34.4	66.5	91.4	95.4	96.4	97.8	99.1	100	---	---	---	---	---
37A	82-03-15	---	0.2	1.2	6.8	11.8	39.8	66.3	77.5	83.1	87.4	91.3	96.0	100	---	---	---	---	---
37B	82-03-15	0.2	1.8	7.4	31.4	36.4	39.8	46.7	52.1	57.7	65.9	75.7	86.5	100	---	---	---	---	---
39	82-03-17	1.5	3.8	14.1	49.5	75.8	97.8	99.9	99.9	99.9	100	---	---	---	---	---	---	---	---
40A	82-03-17	---	---	---	0.5	3.5	28.5	55.1	74.0	84.7	92.3	96.6	98.7	100	---	---	---	---	---
40B	82-03-17	---	---	---	0.8	7.5	39.7	65.2	78.3	88.6	95.1	98.0	99.4	99.9	99.9	100	---	---	---
40C	82-03-17	---	---	0.0	2.1	19.1	80.9	93.6	95.6	97.7	98.8	99.4	99.9	100	---	---	---	---	---
41A	82-03-17	---	0.3	1.9	7.0	16.0	47.2	74.0	85.9	92.4	95.9	98.4	99.5	100	---	---	---	---	---
41B	82-03-17	---	---	---	0.7	5.0	29.9	60.7	79.4	89.7	95.2	98.0	99.6	99.8	100	---	---	---	---
41C	82-03-17	---	---	---	0.6	3.2	16.8	43.4	64.6	78.0	88.1	93.5	98.3	100	---	---	---	---	---
42A	82-03-17	0.2	0.6	1.2	3.6	11.3	28.5	44.8	59.0	70.1	80.6	90.9	96.8	100	---	---	---	---	---
42B	82-03-17	---	---	0.0	1.2	6.1	35.7	72.4	87.4	93.8	97.4	99.2	100	---	---	---	---	---	---
42C	82-03-17	0.0	0.2	0.2	1.1	13.0	58.2	85.1	93.0	96.0	98.1	99.2	100	---	---	---	---	---	---
43	82-03-17	0.4	0.5	0.7	3.0	9.2	46.4	82.3	92.7	95.3	97.2	98.6	99.7	100	---	---	---	---	---
45	82-03-17	---	---	0.0	0.2	3.1	29.5	72.6	89.2	94.6	96.5	98.1	99.5	100	---	---	---	---	---
46A	82-03-17	---	0.7	2.8	6.9	17.6	86.9	92.1	97.5	99.1	100	---	---	---	---	---	---	---	---
46B	82-03-17	4.4	7.5	9.7	11.9	16.9	26.2	61.3	79.8	88.4	95.0	98.4	100	---	---	---	---	---	---
46C	82-03-17	5.3	6.8	8.2	16.7	43.0	96.0	98.2	98.6	98.8	99.5	99.7	100	---	---	---	---	---	---
47	82-03-17	0.0	0.7	3.9	13.4	36.2	82.7	96.7	99.4	99.7	99.7	99.7	100	---	---	---	---	---	---
48	82-03-18	0.2	0.2	0.6	7.5	30.0	65.8	86.7	94.4	96.2	98.7	99.4	100	---	---	---	---	---	---
49	82-03-18	---	---	---	0.0	1.0	18.3	74.4	91.9	96.4	98.2	99.0	99.4	100	---	---	---	---	---
50A	82-03-18	---	---	---	0.0	4.4	25.1	31.3	35.0	38.9	43.1	47.8	56.5	66.7	79.8	93.6	100		

Table 5. Particle-size distributions of bed-material samples, Río Orinoco and tributaries, March 1982—Continued

Station No.	Date Year-Month-Day	Percent by weight finer than sieve size (millimeters) indicated																	
		0.062	0.088	0.125	0.177	0.250	0.353	0.500	0.707	1.00	1.41	2.00	2.83	4.00	5.66	8.00	11.3	16.0	22.6
50B	82-03-18	0.0	0.5	1.0	3.0	4.7	13.7	45.9	78.2	91.9	96.4	97.1	97.6	97.6	98.4	100	---	---	---
51	82-03-18	0.0	0.2	0.9	24.1	51.9	58.1	76.2	89.1	95.4	99.1	99.9	100	---	---	---	---	---	---
52	82-03-18	---	---	---	0.0	0.8	26.2	41.9	78.9	91.3	94.9	96.2	97.0	97.8	98.9	99.3	100	---	---
53	82-03-18	0.0	0.2	0.7	2.2	12.1	36.8	55.9	68.9	80.1	91.9	98.2	99.8	100	---	---	---	---	---
54	82-03-18	0.2	0.2	1.1	12.9	28.2	59.4	84.0	91.7	96.2	98.4	99.5	99.8	100	---	---	---	---	---
55	82-03-18	49.3	72.7	85.2	91.1	93.8	98.6	99.8	100	---	---	---	---	---	---	---	---	---	---
56A	82-03-18	---	0.0	1.4	3.2	11.9	29.7	48.4	64.3	77.3	87.7	93.6	97.7	100	---	---	---	---	---
56B	82-03-18	0.2	0.4	0.8	1.7	3.1	18.5	54.3	77.6	86.9	92.5	96.3	99.4	100	---	---	---	---	---
56C	82-03-18	0.1	0.4	0.4	0.7	6.6	70.8	97.4	99.5	99.7	99.7	100	---	---	---	---	---	---	---
57	82-03-18	0.4	1.5	6.9	19.5	23.2	38.5	59.1	83.1	94.6	98.9	99.8	100	---	---	---	---	---	---
58	82-03-18	0.0	0.2	0.4	1.3	4.1	21.3	62.3	81.8	88.9	93.3	95.3	97.1	99.1	100	---	---	---	---
60	82-03-19	---	---	0.0	0.2	5.5	35.3	74.5	92.7	99.0	99.3	99.8	100	---	---	---	---	---	---
61	82-03-19	---	---	0.0	0.2	3.2	14.9	39.4	65.5	80.9	91.7	95.8	98.3	100	---	---	---	---	---
62	82-03-19	1.4	7.9	17.6	22.0	34.4	75.9	93.5	97.8	98.6	99.5	100	---	---	---	---	---	---	---
63	82-03-19	---	0.0	1.7	9.3	18.3	58.8	88.7	95.2	96.7	97.1	97.7	97.9	98.2	98.3	98.7	100	---	---
64	82-03-19	2.3	7.4	14.3	28.2	39.3	60.3	80.1	93.1	96.1	98.6	99.8	100	---	---	---	---	---	---
65	82-03-19	---	0.0	0.4	3.1	16.6	70.2	96.0	98.2	98.9	99.6	99.8	100	---	---	---	---	---	---
66	82-03-19	0.1	0.2	1.0	18.1	46.8	75.5	93.9	98.3	99.1	99.3	99.5	100	---	---	---	---	---	---
67	82-03-19	3.8	19.6	67.0	94.9	95.8	96.7	98.1	98.5	99.6	99.9	99.9	100	---	---	---	---	---	---
68	82-03-19	---	0.0	0.2	3.3	14.9	44.6	71.5	87.8	95.7	98.3	99.0	99.3	99.3	100	---	---	---	---
69A	82-03-19	5.2	11.9	26.2	40.9	42.8	45.0	48.2	56.1	67.5	82.5	91.6	96.4	100	---	---	---	---	---
69B	82-03-19	21.1	34.6	52.4	68.8	72.3	75.4	80.2	87.1	93.4	97.2	99.1	99.8	100	---	---	---	---	---
70A	82-03-19	1.2	3.1	4.7	6.6	8.2	15.1	33.6	59.4	77.3	88.9	93.8	96.5	99.4	100	---	---	---	---
70B	82-03-19	8.1	13.8	17.4	24.4	32.0	41.3	57.6	81.8	93.0	97.4	98.8	99.0	100	---	---	---	---	---
70C	82-03-19	4.6	7.2	7.7	10.1	10.4	10.6	10.7	13.0	20.0	36.7	57.5	75.2	90.3	100	---	---	---	---
71	82-03-20	---	---	0.0	0.2	0.7	15.3	40.7	60.2	74.0	83.6	90.3	94.0	95.3	95.3	96.6	96.6	100	---
72A	82-03-20	2.6	5.2	9.1	18.5	46.9	56.5	66.2	69.8	72.4	74.0	76.3	78.6	83.2	86.8	88.5	92.7	100	---
72B	82-03-20	0.2	0.4	0.4	0.6	5.7	28.0	46.1	60.4	75.0	87.6	95.3	98.8	100	---	---	---	---	---
72C	82-03-20	0.2	1.0	2.4	4.0	12.2	47.4	68.5	80.1	87.5	92.8	97.2	99.2	100	---	---	---	---	---
73	82-03-20	---	---	0.0	0.5	2.0	8.5	39.2	69.4	87.1	95.4	99.0	99.8	100	---	---	---	---	---
74	82-03-20	---	---	0.0	0.8	7.1	19.4	45.7	66.3	82.4	90.9	95.7	98.6	100	---	---	---	---	---
75	82-03-20	---	---	---	---	---	0.0	1.0	1.2	1.4	2.0	3.0	7.3	20.5	45.9	82.7	97.7	100	---

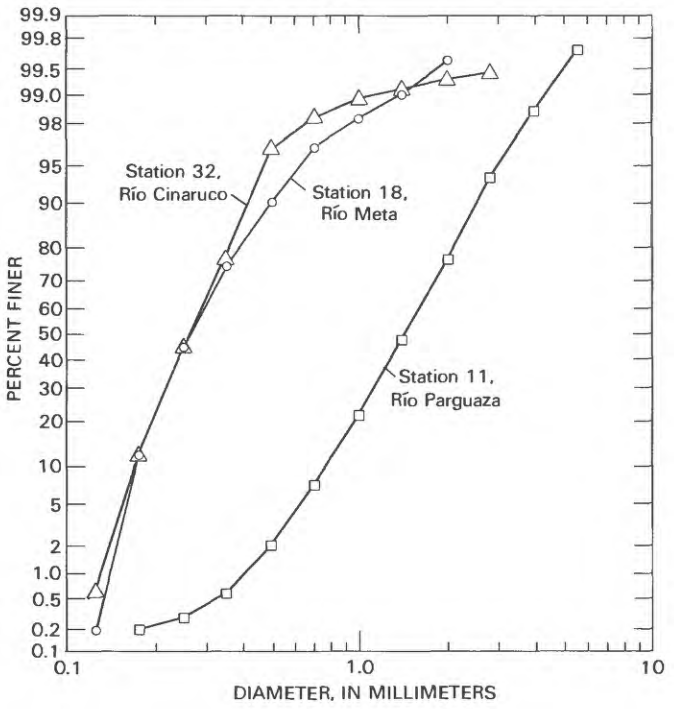

Figure 8. Size distributions of bed-material samples from Río Cinaruco, Río Parguaza, and Río Meta.

their sources, so their size distributions probably reflect more the weathering process and the granitic texture of the crystalline rocks from which they derive than any hydraulic sorting associated with their transport.

Striking differences in the mineralogical compositions of the samples are apparent from visual inspection. A photograph of the three samples (fig. 9) shows clearly the well-rounded predominantly quartz grains of the Río Cinaruco (A), the coarse, angular, iron-stained grains derived from the Guayana Shield (B), and the mixture of quartz and dark-grained aggregates of the Río Meta (C) that are characteristic of many streams draining the Eastern slopes of the Andes. The differences between Río Meta and Río Cinaruco sediments are attributed to two characteristics of the Río Cinaruco: First, our field measurements of pH showed the waters of the Río Cinaruco to be more acid than the waters of the Río Meta, so the stable quartz grains are more prevalent in the Cinaruco bed sediments. Second, there are many wind-blown sand deposits along the Río Cinaruco, so most of the bed sediments are well-rounded and fall in a narrow size range typical of wind-blown sands.

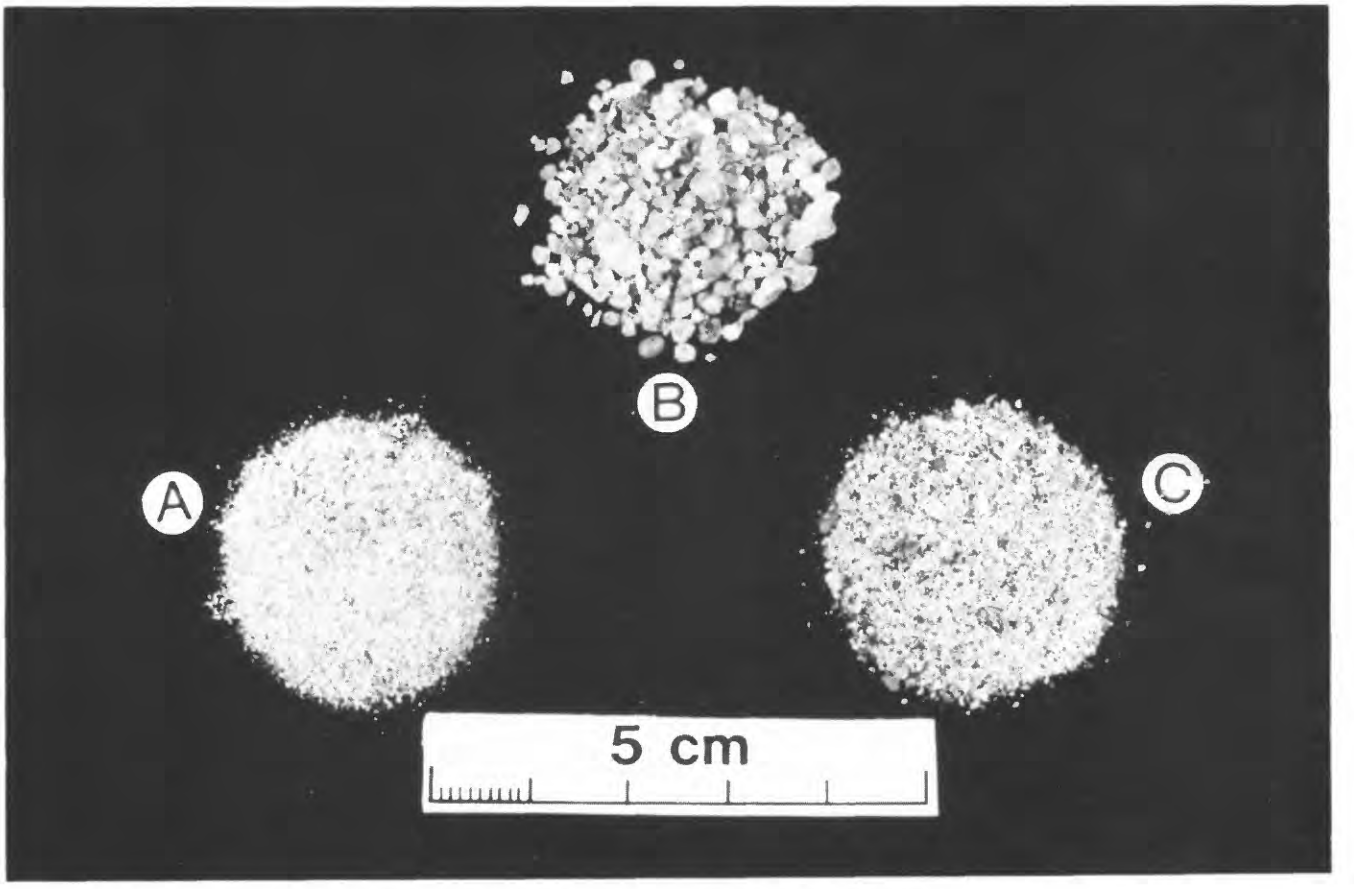

Figure 9. Bed sediments from (A) Río Cinaruco, (B) Río Parguaza, and (C) Río Meta.

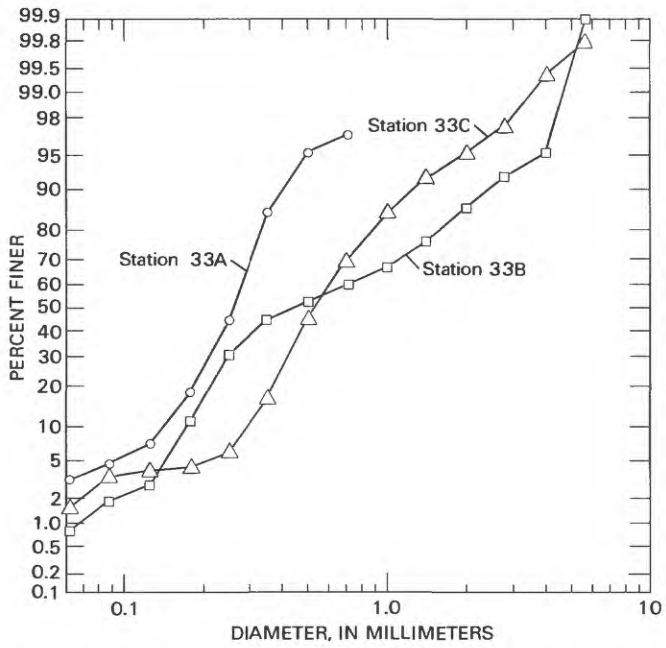

Figure 10. Size distributions of bed-material samples from station 33. (See table 4 for sample localities.)

Perhaps the most striking characteristic of the bed-material samples of the Río Orinoco mainstem was their great size variability, both across the channel at any given cross section and along the reach. The cross-channel variability shown in figure 10 for station 33 is typical. Median diameters for these samples were 0.26 mm at station 33A, 0.45 mm at station 33B, and 0.54 mm at station 33C. The sample at station 33A consisted mostly of fine to medium sand; 100 percent of the material is finer than 1.0 mm and about 3 percent of the sample consists of sizes finer than sand (<0.062 mm). Samples from stations 33B and 33C contain 33 and 16 percent, respectively, of sizes coarser than 1.0 mm and 5 and 14 percent gravel.

Three samples of bed material were collected at Musinacio near the cross section normally used by Ministerio del Ambiente y de los Recursos Naturales Revnovables hydrologists for water discharge measurements. This is a fairly wide section, about 2,700 m at bankfull stage. During low flows, a large bar (fig. 11) is exposed in the right half of the channel, and flow is confined to the left-hand channel, which is about 1,300 m wide. The size distribution of three samples collected approximately equally spaced across the section are plotted in figure 12. The sample collected at station 56C in 9-m depth along the right-hand side of the channel was mostly fine to medium sand and contained no gravel. Samples from stations 56B and 56C contained coarse sand and small percentages of gravel, but not the range of particle sizes found at stations 33, 70, and 72 (see table 5).

Median diameters, d_{50}, and sorting coefficients, σ, were computed for each sample and are listed in table 6. The sorting coefficient, σ, is defined by

$$\sigma = 1/2 \left(\frac{d_{84}}{d_{50}} + \frac{d_{50}}{d_{16}} \right), \quad (1)$$

where d_{16} is the size for which 16 percent by weight is finer, d_{84} is the size for which 84 percent by weight is finer, and d_{50} is the median diameter for which 50 percent by weight is finer. Variations of d_{50} and σ with distance upstream of the river mouth plotted on figure 13, show the large variabilities in the median diameters and sorting coefficients and indicate no tendency for reduction of particle size in the downstream direction, a peculiarity the Río Orinoco shares with the Río Amazonas (Nordin and others, 1980). Probably, the coarser sediments from the shield just offset the reduction in size along the river due to hydraulic sorting.

SUSPENDED SEDIMENT

Depth-integrated suspended-sediment samples were collected at eight localities along the Río Orinoco and on the Río Cinaruco and Río Meta. These samples were collected using a large-volume collapsible bag sampler and were partially processed aboard ship using procedures described by Nordin, Cranston, and Mejía (1983). Concentrations of these samples are given in table 7.

A few of the samples were sieved aboard ship so that concentrations could be determined separately for sand sizes and for the fine sediments containing silt and clay sizes. Except for the Río Meta, though, the concentrations of sands were so small that only traces were caught on the 0.063-mm sieve, so only total concentrations were determined for most samples.

The largest concentration observed was in the Río Meta: 106 mg/L (milligrams per liter), of which 42 mg/L was sand. The concentration of the Río Cinaruco, 15 mg/L, was the smallest concentration sampled.

Samples at stations 26 and 27 on Río Orinoco were composites of three depth-integrated samples collected at approximately equal centroids of flow. Surprisingly, the concentrations are almost the same for these two samples, even though station 26 was upstream and

Figure 11. Aerial photograph of the reach near Musinacio. Flow is from left to right.

station 27 was downstream of the Río Meta. Possibly, flows of the Río Meta were so small relative to flows of the Río Orinoco that the suspended-sediment contribution from Río Meta is diluted to negligible concentrations. This possibility is suggested by the fact that the concentration at station 36 on Río Orinoco, just upstream of Río Apure at river km 900, also is 23 mg/L, the same as the concentration at station 26. Other possibilities are (1) backwater from the Río Orinoco at the mouth of the Río Meta causes substantial deposition before the sediments reach the Río Orinoco, or (2) in taking samples at only three centroids, we simply missed the thread of higher concentrated flow from the Río Meta along the left bank. In any event, we were not able to detect the higher concentrations of the Río Meta at either station 27 or station 36.

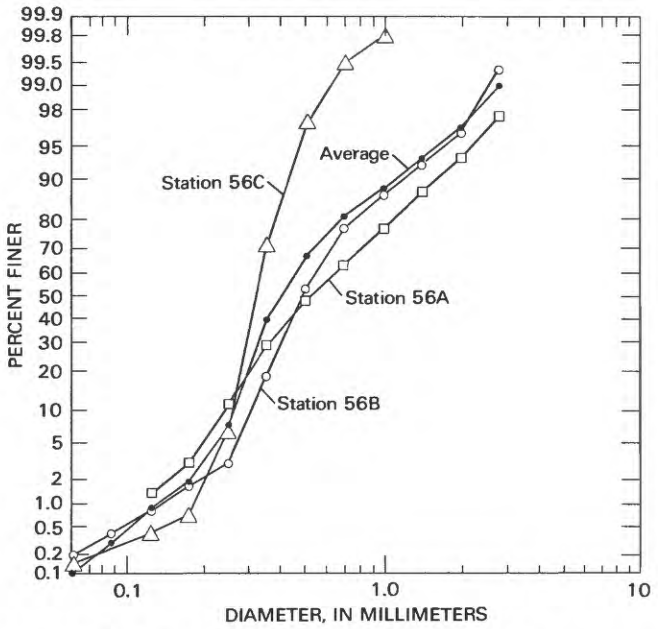

Figure 12. Size distributions of bed-material samples from station 56, Río Orinoco at Musinacio. (See table 4 for sample localities.)

The higher concentrations in flows from the Río Apure were easily detected. The average concentration on March 15, 1982, at station 36 above Río Apure (river km 900) was about 23 mg/L, the same as the upriver concentrations, but at station 37 downstream of the Río Apure (river km 867) the concentration was 78 mg/L, more than three times that above the confluence (table 7). The three depth-integrated samples at station 37 were composited, but it was evident when we sampled that there were higher concentrations along the left side of the channel due to sediments from the Río Apure. On March 17, another set of five samples was collected at Cabruta, station 38, about 20 km downstream of station 37. The sediment concentrations varied from 46 mg/L along the left bank to 19 mg/L along right bank, again reflecting Río Apure sediments in the flow. This cross-channel difference in concentration is even more striking when examined visually. Aerial photographs obtained April 4, 1982, of the reach near Cabruta (fig. 14) show clearly the interface between the higher concentrated Río Apure flows and the main channel flows. This abrupt interface is not detected in our samples, probably because the lighter main channel flows ride over the heavier mixture from the Río Apure, so the depth-integrated samples traverse through water from both rivers and show a fairly uniform cross-channel gradient of concentration even though the surface appearance might suggest an abrupt transition.

The samples at station 38 were collected at equal widths across the channel, but not at equal centroids of flow. Furthermore, the nozzle diameters of our sampler and the vertical transit rates were not constant from one vertical to the next, so the average concentration at this cross section is not the arithmetic average of the values in table 8; instead, it must be determined by weighting each concentration, C, the product of mean velocity, U, and depth, D, at that vertical. The mean concentration estimated by this weighting procedure was 35.

At cross sections downstream of Cabruta, the mean concentrations of suspended sediments were 38 mg/L at Las Bonitas (river km 782); 37 mg/L at Musinacio (river km 657); and 29 mg/L at El Almacén (river km 486).

The sample collected at station 56C for the Musinacio cross section shows a substantially lower concentration of suspended sediments than those at stations 56*A* and 56*B* (table 7). This difference can be attributed to clear water inflow upstream from the Río Caura, which dilutes the concentrations of the Río Orinoco. Complete vertical and cross-channel mixing of the Caura and Orinoco waters occurs many kilometers downstream of the Musinacio station.

We did not measure water discharge during these reconnaissance studies, so the only estimate of suspended-sediment discharge was for the rated gaging station at Musinacio. The flow at this station was 6,520 m^3/s, so the suspended-sediment discharge was 241 kg/s or 20,800 Mg/d.

SAND WAVES AND BARS

The most common bed configurations of the alluvial reaches of the Río Orinoco are large sand waves. The sand waves usually are long-crested, with wave lengths ranging from 70 to 100 m and wave heights ranging from 2 to 3 m. These features commonly are called dunes by hydraulic engineers and subaqueous dunes or megaripples by geologists, but here they will be called sand waves, reserving the term dunes for wind-blown sands.

During the dry season, numerous large bars such as those shown in figures 11 and 14 are exposed along the channel. These bars commonly extend across the channel a kilometer or more and along the channel for several kilometers. The surfaces of the bars are covered with sand waves, which migrate over the bars and deposit their bed load along a continuous slip face at the downstream ends of the bars. The slip faces commonly are 8–10 m long and several times as high as the sand waves that formed them. The bars usually grow in height in the

Table 6. Median diameters and sorting coefficients for the size distributions listed in table 5 [d_{50}, median diameter; σ, sorting coefficient; mm, millimeters]

Station No.	d_{50} (mm)	σ	Station No.	d_{50} (mm)	σ	Station No.	d_{50} (mm)	σ
1	0.43	1.47	28C	0.55	2.03	46C	0.26	1.35
2	.29	1.29	29A	.36	1.33	47	.27	1.40
4	.29	1.26	29B	.76	1.64	48	.30	1.51
5	.28	1.48	29C	.67	1.85	49	.43	1.30
6	.20	1.34	30	.51	1.38	50A	2.18	4.85
7	.35	1.63	31A	.45	1.78	50B	.52	1.48
8	.39	1.90	31B	.46	2.03	51	.24	1.97
9	.30	1.49	31C	.39	2.43	52	.54	1.56
10	.41	1.26	32	.27	1.46	53	.45	2.06
11	1.45	1.59	33A	.26	1.46	54	.32	1.62
12	.42	1.21	33B	.45	3.18	55	.06	1.83
13	.39	1.43	33C	.53	1.71	56A	.52	2.13
14	.09	1.85	34A	.29	2.85	56B	.48	1.63
15	.61	1.96	34B	.42	1.50	56C	.32	1.21
17	.74	2.33	34C	.35	1.53	57	.43	2.15
18	.26	1.52	35	.46	1.50	58	.45	1.55
19	.36	1.94	36A	.37	1.70	60	.40	1.40
20	.46	1.48	36B	.44	1.44	61	.57	1.75
21A	.24	1.85	36C	.42	1.53	62	.28	1.90
21B	.44	2.53	37A	.40	2.09	63	.33	1.42
21C	.41	1.78	37B	.62	4.20	64	.30	2.05
22	.46	1.66	39	.18	1.45	65	.31	1.28
23	.72	2.74	40A	.47	1.79	66	.26	1.52
24	.15	1.67	40B	.41	1.75	67	.11	1.33
25A	.50	2.32	40C	.30	1.25	68	.38	1.59
25B	.32	2.10	41A	.37	1.64	69A	.54	4.10
25C	.29	1.56	41B	.44	1.64	69B	.12	3.65
26A	.29	1.68	41C	.56	1.89	70A	.62	1.83
26B	1.07	2.08	42A	.57	2.39	70B	.43	2.84
26C	.50	1.55	42B	.40	1.49	70C	1.77	2.03
27A	.32	1.33	42C	.34	1.38	71	.59	2.05
27B	.35	1.38	43	.36	1.38	72A	.28	8.65
27C	.63	1.54	45	.42	1.41	72B	.55	2.05
28A	.48	2.13	46A	.29	1.20	72C	.37	1.84
28B	.38	1.60	46B	.45	1.88	73	.56	1.53
						74	.54	1.81
						75	5.85	1.50

downstream direction, and their highest points near their downstream faces generally stand no more than 2 m below the flood plain.

The exposed bars exhibit great variety of size, shape, and orientation, as shown in the index map of aerial photographs for the reach from Cabruta to Río Cuchivero (fig. 15). It is difficult to specify the factors that control a bar's location and formation. However, a few generalities can be drawn. The Río Orinoco has very little tendency to meander, probably because heavy sediment loads from tributaries draining the Andes push the river over against the Guayana Shield. As a consequence, point bars are not well developed, and certainly they are not prominent features as in most rivers. The one at Cabruta shown in figure 14 perhaps is typical. It is considerably smaller than the bar that extends along the outside of the bend across from Cabruta.

Center bars may form where the channel expands, such as the almost circular bar in the reach between

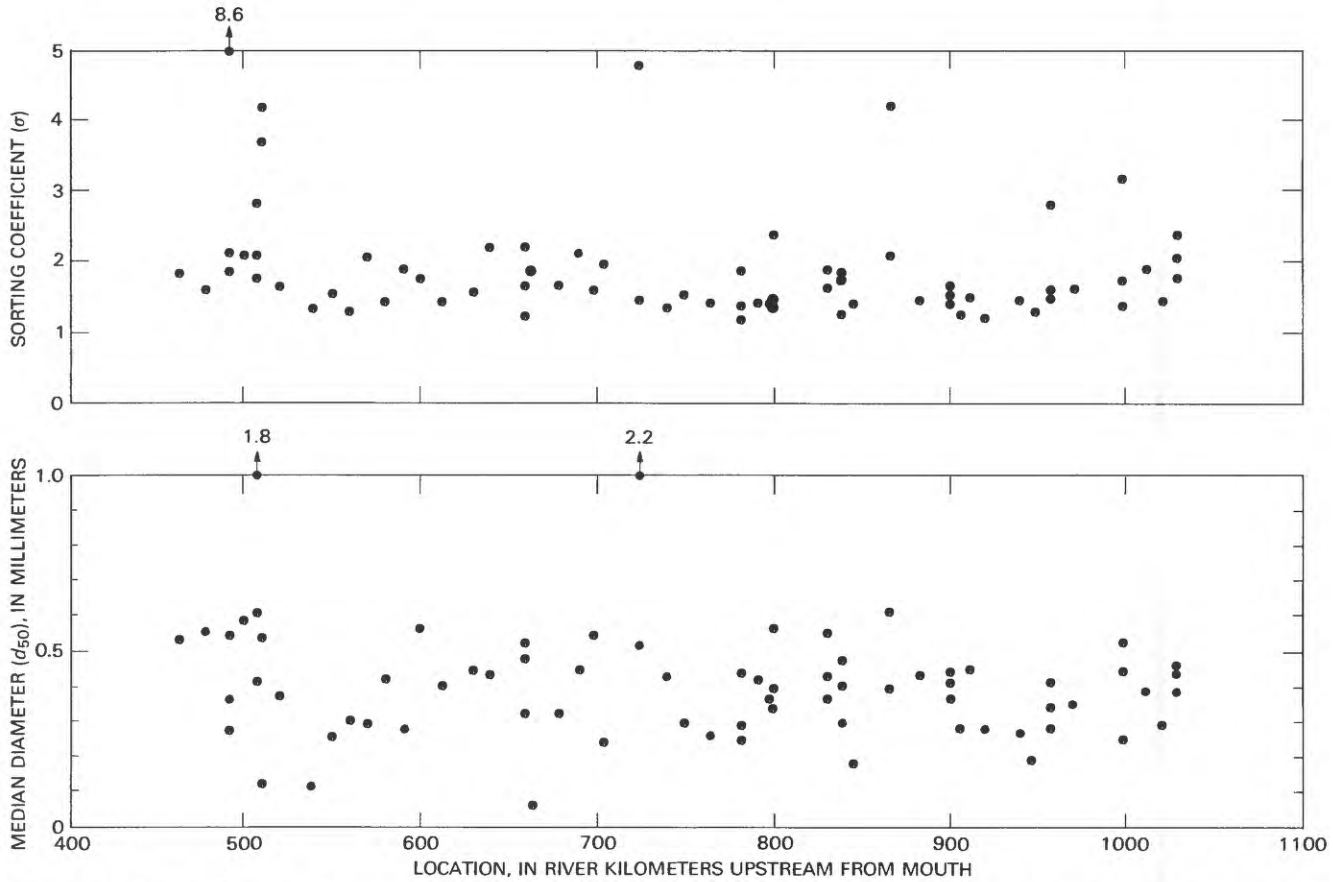

Figure 13. Values of median diameters and sorting coefficients plotted against location along river. (See figure 7 for river kilometer reference points.)

Cabruta and Caicara (fig. 15). However, center bars also form in straight reaches. The large bar shown in figure 16 formed in a fairly straight reach of the river. There are no peculiarities of channel alignment upstream that might lead one to predict the formation of a center bar at this location. Many of the bars along the sides of the channel form in zones of flow separation downstream of obstructions along the banks. The bar at Punta Brava, shown in figure 17, is typical. In the reach between Puerto Ayacucho and Cabruta, the river flows through several rapids, and large bars form just downstream of the rapids. An example of the bars downstream of the rapids "Raudal San Borja" is discussed in the next section. Finally, delta-like bars form at the mouths of some of the tributaries. The one at the mouth of the Río Meta during both March, 1982 and March 1983, was quite large, extending almost three-fourths of the way across the channel of the Río Meta and rising at least 2 m above the low-water surface.

It was not possible during the reconnaissance studies of 1982 to establish horizontal control and survey any of the bars in order to determine from year to year their rates of migration and changes in size and shape. It was possible to visit sites A, B, and D, (fig. 7) in both 1982 and 1983. Here we measured the lengths and heights of some of the sand waves composing the bars and observed some of the small-scale features formed by both water and wind. The observations at sites B and D are summarized in the next section. The observations at site A concerned mostly armoring by wind action along the downstream end of the bar; these observations are reported later in the section "Lag deposits and armoring."

Ground Observations of Sand Waves

The lengths and heights of sand waves on exposed bars at sites B and D (fig. 7) were measured during both 1982 and 1983. In addition, it was possible to obtain records with an echosounder near both sites during higher flows to compare with measurements made on the

Table 7. Concentrations of suspended sediment samples
[mm, millimeters; leaders (---) indicate values are not determined]

Date (March 1982)	Station No.	Location	Concentration (milligrams per liter)			Remarks
			Size less than 0.062 mm	Size greater than 0.062 mm	Total	
11	18	Río Meta, 3 kilometers above mouth.	64	42	106	Composite of two verticals.
13	26	Río Orinoco above Río Meta	23	0	23	Composite of three verticals.
13	27	Río Orinoco below Río Meta	21	1	22	Composite of three verticals.
14	32	Río Cinaruco, 4 kilometers above mouth.	---	---	15	One vertical.
15	36A	Río Orinoco above Río Apure	28			
	36B	------do------	21	1	23	
	36C	------do------	17			
15	37	Río Orinoco below Río Apure	76	1	78	Composite of three verticals.
17	38A	Río Orinoco at Cabruta			46	
	38B	------do------			34	
	38C	------do------			30	
	38D	------do------			26	
	38E	------do------			19	
17	46	Río Orinoco above Las Bonitas			38	Composite of three verticals.
18	56A	Río Orinoco at Musinacio			43	
	56B	------do------			41	Mean=37.
	56C	------do------			28	
20	72A	Río Orinoco at El Almacén			32	
	72B	------do------			28	Mean=29.
	72C	------do------			27	

ground. Data also were collected during 1983 at a number of locations in connection with sedimentological studies of the internal bedding structures and cross-stratifications of the bars and sand waves. Those data are reported in another paper of this series (McKee, 1989) and will not be repeated here.

Site B is located at approximately latitude 6°4′ N. and longitude 67°27′., just downstream of the rapids "Raudal San Borja" (fig. 18). Sand-wave measurements were made along the right bank downstream of a large rock that is across from the downstream tip of Isla Chimborazo. In 1982, a few observations were made just above Isla Pañuelo, and in 1983 some measurements were made in the right channel around Isla Chimborazo. Wave lengths, L, were measured with a tape, height, H, were measured with a hand level, and crest-line lengths transverse to the flow, B, were determined either by tape measurements or by pacing. Figure 19 is a sketch of the area surveyed in 1982; the same numbering system was used in 1983. The observations are summarized in table 9. The average values of wave length and height listed in table 9 exclude the first wave because its length is not representative.

This bar had some peculiarities not found on other bars. There was a large scour hole about 4 m deep just downstream of the rock shown in figure 20*A*. The face of the scour hole and the upstream end of the bar were composed mostly of coarse sand and fine gravel, evidently the result of hydraulic sorting during the flood season when water flows over the rock. The face contained small amounts of silt and clay that apparently seeped into the coarser bed material as the flows receded. These fine sediments were slightly cohesive and imparted a stability to the face of the scour hole that allowed it to stand at an angle of almost 45°, considerably greater than the angle of repose for the bed material. Downstream of the rock, the faces of the sand waves were eroded slightly by water waves from winds blowing upstream. In addition the faces had lenses of fine material impregnating their surfaces to a few centimeters depth, imparting some stability to the faces so that they stood at angles of about 35°. The angles of the underlying slip faces measured at a few locations (fig. 20*B*) were 27°–30°, about the repose angle of the sediments composing the sand waves.

Figure 14. Aerial photograph of the reach near Cabruta. Flow is from left to right. Point bar along left bank is site D.

At some locations, large scour holes had formed in the troughs of the sand waves and several of these contained stagnant water (fig. 20*C*). Apparently, the wash load carried by the river settles quickly in these still waters and forms an almost impermeable layer to prevent the water from seeping into the sand bed. Some of these fine sediments also settle in the intercrest areas; figure 20*D* shows the typical mud polygons formed when the material dries and cracks. The layers of fine sediments were about 8 mm thick downstream of the crest lines and thinned toward the next crest.

The crests of the sand waves generally extended from near the right bank down into the water, so the lengths of the crest lines probably were much greater than shown in table 9. Only three of the sand waves had discontinuous crests. The crest lines were straight to

Table 8. Data for samples at station 38

Sample	Depth, D (meters)	Velocity, V (meters per second)	Sample volume, v (liters)	Sample concentration, C (milligrams per liter)
A	13.7	1.06	4,500	46
B	6.4	1.10	1,350	34
C	7.0	1.27	3,350	30
D	7.6	0.96	1,330	26
E	4.6	0.76	1,400	19

Mean concentration, $\bar{C} = \frac{\Sigma Cv}{\Sigma v} = 34.6 = 35$,

or $\bar{C} = \frac{\Sigma CVD}{\Sigma VD} = 34.5 = 35$.

slightly sinuous and veered upstream near the right bank, probably because of lower flow velocities along the bank when they were formed. None of the crests continued all the way to the bank; the turbulence and vortex action of the flow due to bank roughness were sufficient to maintain a small channel along the bank which was devoid of any bed configurations.

It is interesting that scour holes form in connection with long-crested sand waves. Migrating scour holes produce trough cross-bedding with festoon pattern and this type of cross-bedding normally is associated with three-dimensional or short-crested subaqueous dunes (McKee, 1989). Apparently, this type of cross-bedding also occurs in connection with scour holes downstream of long-crested sand waves such as the one shown in figure 20*C*.

Sand waves also were exposed along the upstream end of Isla Pañuela (fig. 18); the waves averaged about 80 m long and 2 m high. The wave troughs appeared to have filled some, so the ripple index, L/H, of 40 probably is larger than the ripple index under water.

During March 1983, observations were made in the downstream end of the right channel around Isla Chimborazo. Results are shown schematically in figure 21. Only the downstream seven waves were measured; their average wavelength was 106 m and average height was 2.1 m, for a ripple index L/H of 50. The waves all were long-crested, but were broken up near the center of the channel by rock outcrops (fig. 21). Upstream of the rocks, most of the crests were continuous across the channel, which is about 800 m wide, but were somewhat sinuous. The crest of wave 7 was 1,050 m long.

A few sediment samples were collected at site B in 1982; the localities of samples B1 through B4 are shown in figure 19. Sample B1 was material armoring the back of the bar just downstream of the scour hole. Samples B2 and B4 were from trenches cut in the faces of the sand waves to expose the underlying cross-stratification, and B3 was a sample of the fine materials deposited in the intercrest areas, presumably representative of the river's wash load. Sample B5 was an assemblage of heavy minerals and fine to coarse sand at the water's edge along Isla Pañuela, accumulated by wave action. Sample B6 was from the underlying sediments composing the slip faces of the sand waves. Particle-size distributions of five of the samples are plotted in figure 22. The lag deposit armoring the upstream end of the bar, sample B1, was composed of very coarse sand and fine gravel, with a median diameter of 1.3 mm and a sorting coefficient, σ, of 1.35. The trench samples B2 and B4 were somewhat finer with median diameters of 1.02 and 0.96 mm, respectively. Across the river on Isla Pañuela (sample B6), sediments were finer, with a median diameter of 0.61 mm. The heavy minerals sample (B5) had a median diameter of 0.46 mm.

The fine material deposited in the intercrest areas contained 10 percent clay, 68 percent silt, and 22 percent sand, and had a median diameter of 0.022 mm. The sand-size material in this sample may have settled out of suspension, but more likely it represents part of the bed material on which the fine sediments settled that was trapped when the mud dried and cracked.

Site D was the point bar along the left bank downstream of Cabruta (fig. 14). The numbering of the sand waves (fig. 23) was the same both years. Wave heights were measured near the water surface because the crests toward the left bank had been drastically eroded by the wind. Even so, the wave heights observed probably have been modified by wind and water and are smaller than the wave heights under water. A summary of the measurements is given in table 10. Notice that average wave lengths were somewhat greater in 1983 than in 1982, but average heights are almost the same.

Wind erosion at site D was quite spectacular. The sand-wave crests were substantially modified except close to the water, where apparently there was sufficient moisture in the crests to prevent much wind erosion. Examples of the sculpturing by the wind are shown in figures 24*A* and 24*B*. The intercrest areas at most locations were almost filled with blown sand, (fig.24*C*). The backs of the blown sand sheets in the intercrest areas were covered with ripples about 7 cm long and 0.25 cm high in 1982, (fig. 24*D*), and 5 cm long and 0.2 cm high in 1983.

Figure 15. Aerial photograph mosaic of the reach from Cabruta to Río Cuchivero. Flow is from left to right.

Figure 16. Aerial photograph of exposed bar 20 km upstream of the mouth of Río Caura. Flow is from left to right.

The two lines faintly visible in figure 24*D* apparently are the result of vortices formed behind two small clumps of erosion-resistant silt protruding through the ripples in the intercrest area. The vortex trails were 110 cm apart and extended downwind almost 70 m.

Wind erosion and the upriver transport of wind-blown sands were evident at this site in both 1982 and 1983, but clearly the erosion of sand wave crests was greater in 1982. At other locations along the river during both years there seemed to be enough very coarse sand

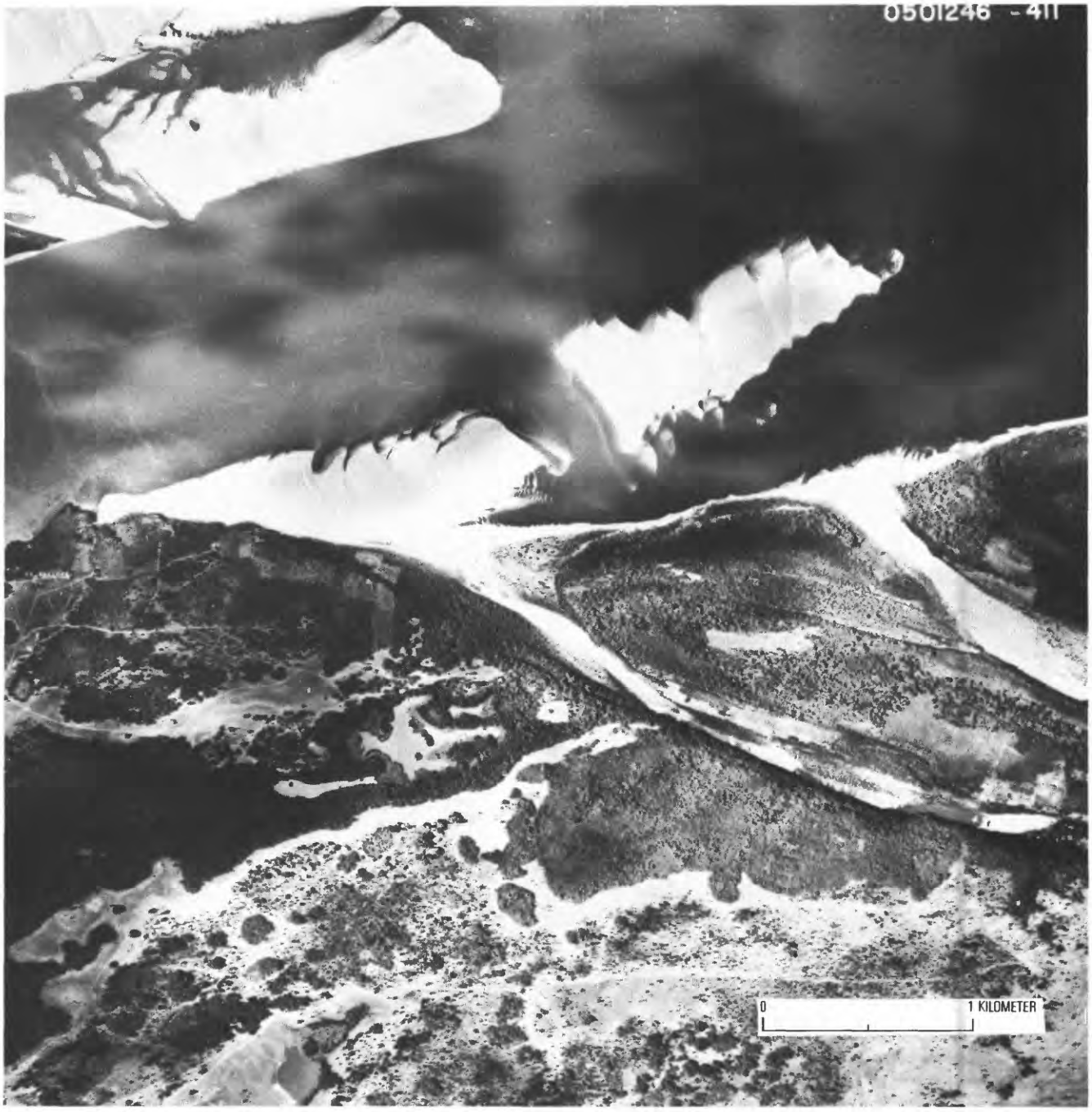

Figure 17. Aerial photograph of the bar at Punta Brava, April 4, 1982. Flow is from left to right.

and fine gravel to armor the bars and prevent further wind erosion, but at site D there was not. Perhaps the point bars are devoid of coarser sediments because hydraulic sorting tends to transport finer material toward the inside of the bend.

Lengths and Heights from Sounding Records

Echo soundings were obtained near site B in June and November 1982, and near site D in November 1982.

Table 9. Sand-wave measurements, in meters, at site B (fig. 19)
[Leaders (---) indicate values not determined]

Sand wave No.	1982 Wave length, *L*	1982 Wave height, *H*	1982 Crest length, *B*	1983 Wave length, *L*	1983 Wave height, *H*	1983 Crest length, *B*
1	250	1.0	42	260	1.1	98
2	52	1.0	84	95	1.3	80
3	72	1.4	160	38	2.0	120
4	59	1.7	110	73	1.4	70
5	74	1.2	58	90	1.7	120
6	77	2.1	[1]32	99	0.3	140
7	79	2.2	80	40	1.0	[1]70
8	---	---	---	31	.2	[1]40
9	---	---	---	30	1.7	140
10	---	---	---	101	.5	160
11	---	---	---	118	1.3	100
Average[2]	--- 69	1.6	---	72	1.1	---

[1]Crest lines are not continuous to the water.
[2]Excluding wave 1.

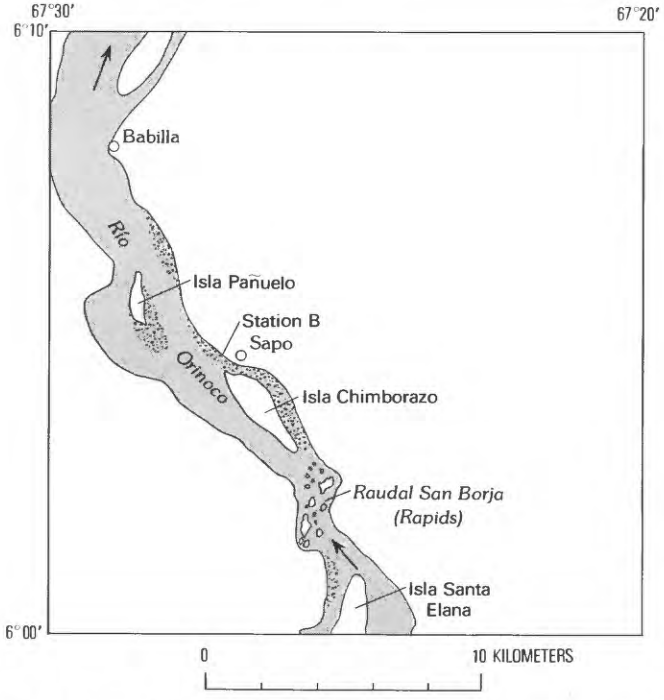

Figure 18. Sketch map of the Río Orinoco in the vicinity of site B (fig. 7).

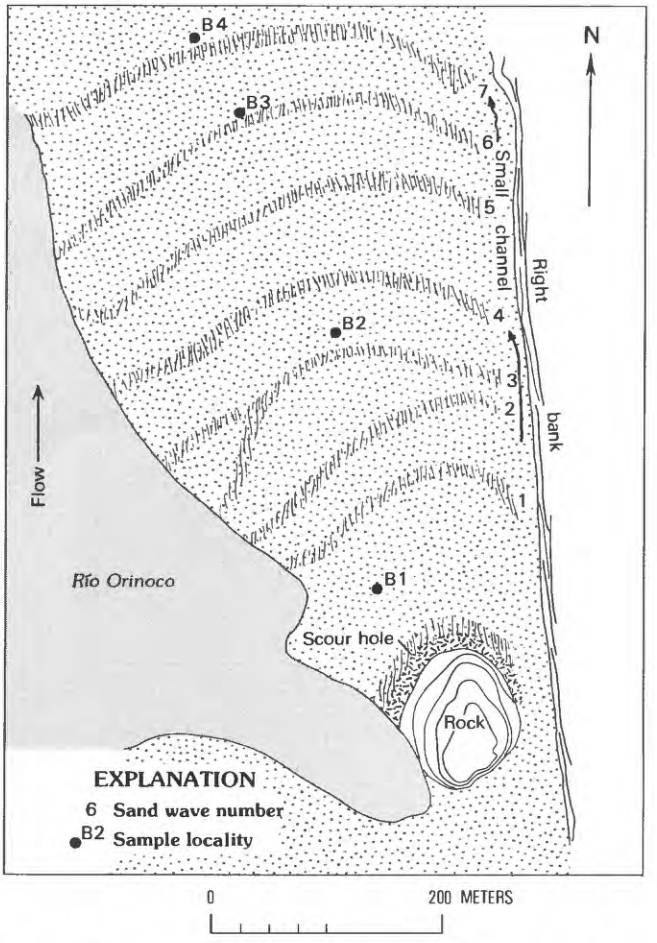

Figure 19. Sketch map of the bar at site B identifying dune crests and sample localities. Scale is approximate.

In June, the sounding line was close to the line measured on the ground in March. Horizontal distances along the sounding line were estimated from the average speed of the barge, 7 knots or about 220 m per minute, so these distances are not too accurate. In November, river stage was falling so the sounding line was slightly farther from the bank than in June. Distance along the sounding line in November was determined by electronic positioning equipment (Nordin, Cranston, and Mejía, 1983) and should be accurate to within a meter. The average flow depth along the sounding line was 7.6 m in June and 5 m in November.

The lengths and heights of sand waves and a few statistics are given in table 11. There are no significent differences in the observations for the two dates, but the average lengths under water were about 10 m less than those measured on the ground (table 10). However, the sounding lines were not identical and neither was in the exact location of the low-flow observations, so the differences between the data of table 10 and 11 probably are not significant.

Figure 20 (above and facing page). Features at site B, March 1982. *A*, Scour hole just downstream of a rock outcrop along the right bank. *B*, Cross-stratification in the slip face; sample B-2 was collected here. *C*, Scour hole downstream of the sand-wave crest. *D*, Mud cracks in the intercrest area.


C


D

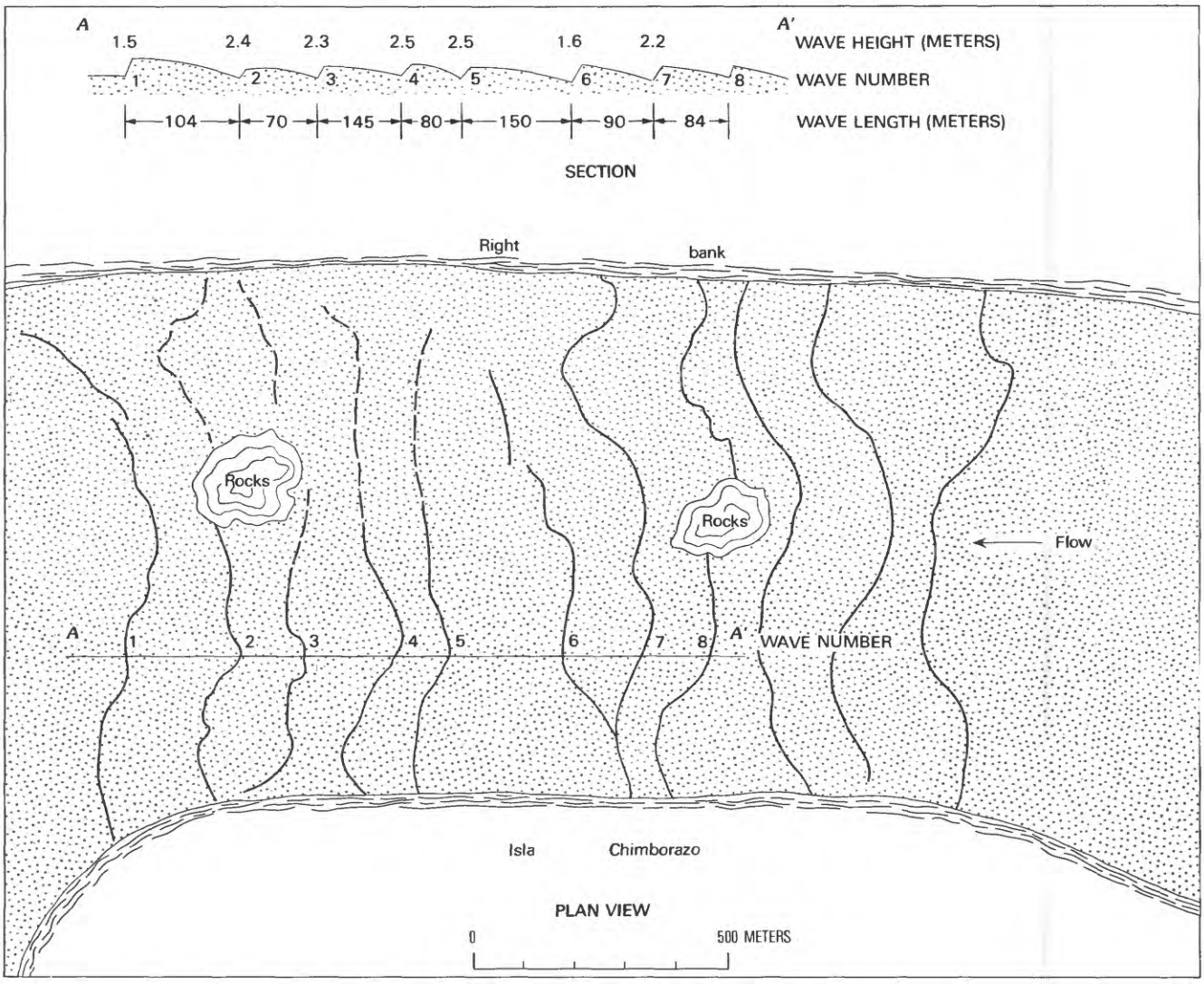

Figure 21. Sketch of sand waves along line *A–A'* observed March 1983, near Isla Chimborazo. Scale is approximate.

Changes in the sizes and shapes of sand waves composed of fine sand tend to lag changes in discharge (Lane and Eden, 1940), with larger sand waves occurring after the flood peaks, but from our data sand waves composed of medium to coarse sand and fine gravel appear to retain about the same shape through the entire hydrograph. The shape could easily be retained if the surfaces of the sand waves become armored with coarser sediments on the receding flows, and there is some evidence, presented later, that this happens.

In November 1982, one additional sounding was made commencing 100 m below the downstream tip of Isla Chimborazo and running 4 km downriver. Bed samples then were collected at each river kilometer along the sounding line. The properties of the sand waves along each kilometer are listed in table 12, and the size distributions of the bed samples are plotted in figure 25. With distance from the island the sediments become finer and the sand waves become higher relative to their length; that is, the ripple index L/H decreases with particle size, which accords with experimental findings (Simons and others, 1965).

Soundings over the point bar near Cabruta, site D (fig. 7), were made in November 1982 along three lines roughly parallel to the bank and about 100 m apart (fig. 26*A*). The first line was about 50 m from the bank. Samples of bed material were collected at three points along the center sounding line. The soundings are traced

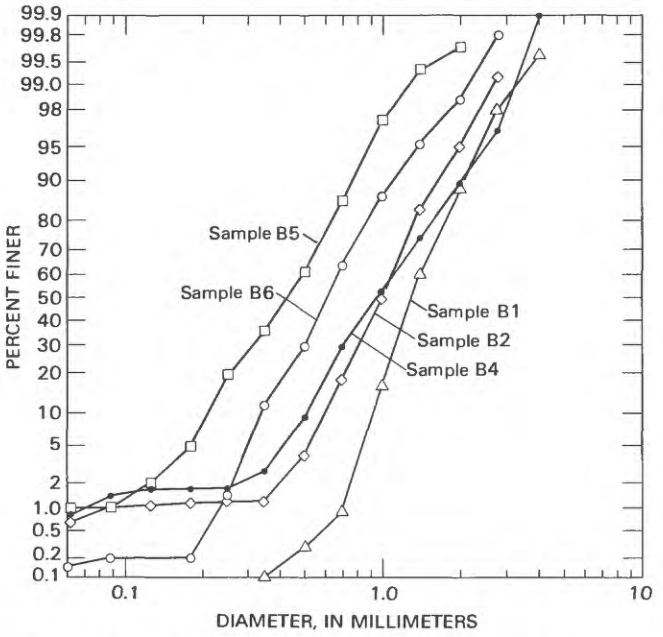

Figure 22. Size distribution of samples from site B.

to scale in figure 26*B*. Notice the vertical scale distortion. Several interesting features are evident from the records. First, the waves along lines 1 and 2 average 115 m long and 2 m high, about the same lengths as observed in March 1982 and 1983 (table 10); however, the November waves were about 0.4 m higher, supporting the earlier supposition that wave heights probably are reduced by wind and water action as the crests are exposed during falling river stages. Second, the wave crests are continuous across sounding lines 1 and 2, but seem to break up in the deeper flows along line 3. Third, the large sand waves near the bank have smaller waves superposed on them. These smaller waves form at about 1/3 L to 1/2 L downstream of the crest and grow in height and length toward the next crest where they attain heights of 30 or 40 cm and lengths of 10–20 m.

The median diameters and sorting coefficients of the bed samples are shown on figure 26*A*. Values of d_{50} varied from 0.37 to 0.55 mm and values of σ ranged from 1.35 to 2.13. The variability seems typical of the Río Orinoco bed sediments.

Three additional soundings were obtained during March 1982, to define lengths and heights of sand waves. Statistical summaries of these data are given in table 13. The soundings were along the thalweg. The average sand wave heights are from one-third to one-fifth of the flow depths. These ratios of average wave height to flow depth are greater than the ratios normally observed in large rivers, probably because the waves formed at higher flows and retained their shapes as the stage dropped.

Observation at Site C

Site C was along the right bank near river km 864, about 6 km upstream of Cabruta (fig. 7), at a place called Las Culatas. It is immediately downstream of the river gage at Capuchinos, which is located at km 865. At this location, rock outcrops protrude into the channel (fig. 27*A*). Downstream of the rocks, an accumulation of sediments extended about 100 to 200 m wide and 400 or 500 m downstream. The bar was not composed of sand waves as were other sites investigated; instead, it seemed to be a temporary depositional feature resulting from the accumulation of sediments during the 1981 flood season, and it showed a peculiar combination of features formed by water and wind.

The back of the bar was covered with wind ripples of various sizes. These ripples reflected both the strength of the wind and the sources of sediments available for transport. For example, figure 27*B* shows on the right a sheet of small wind ripples of fine sand overriding the older ridge-like features on the left, which are composed of coarser sediments and are much larger. At the upstream end of the bar, the blown sand had accumulated in a small dune about 2 m high (fig. 27*C*). Midway along the bar, the surface was covered with wind ripples of medium to very coarse sand from which protruded tubes of silt-size material (fig. 27*D*) 2–3 mm in diameter and as long as 15 to 20 cm. These perhaps were worm tubes or escape burrows of organisms buried by the incoming sediments during rising flows that later were exposed by wind erosion (see, for example, Reineck and Singh, 1975, p. 141–144).

Trenches were dug at two locations to expose the underlying sediments. In both trenches, the cross-stratification revealed slip faces oriented downstream with angles between 25° and 27°. These angles of repose suggest sediments were deposited by water, because eolian sands have steeper angles of repose (about 33°). The particle sizes of the underlying sediments apparently became finer with distance downstream from the rock outcrops (fig. 28), reflecting the hydraulic sorting downstream of the channel obstructions. Sediments from the upstream trench had a median diameter of 0.54 mm and contain 10 percent very coarse sand. Sediments from the downstream end of the bar had a median diameter of 0.30 mm and contain only 0.3 percent very coarse sand.

Wave No.	Wave length, *L* (meters)	Wave height, *H* (centimeters)	Length of crest line, *B* (meters)	
1	60	100	40	*B* not well defined; modified by wind
2	24	30	20	
3	30	70	20	
4	80	>100	50	
5	240	>200	100	
6	200	>200	~200	
7	30	<100	150	
8	70	>200	200	
9	224	>200	>300	
10	72	>200	~200	

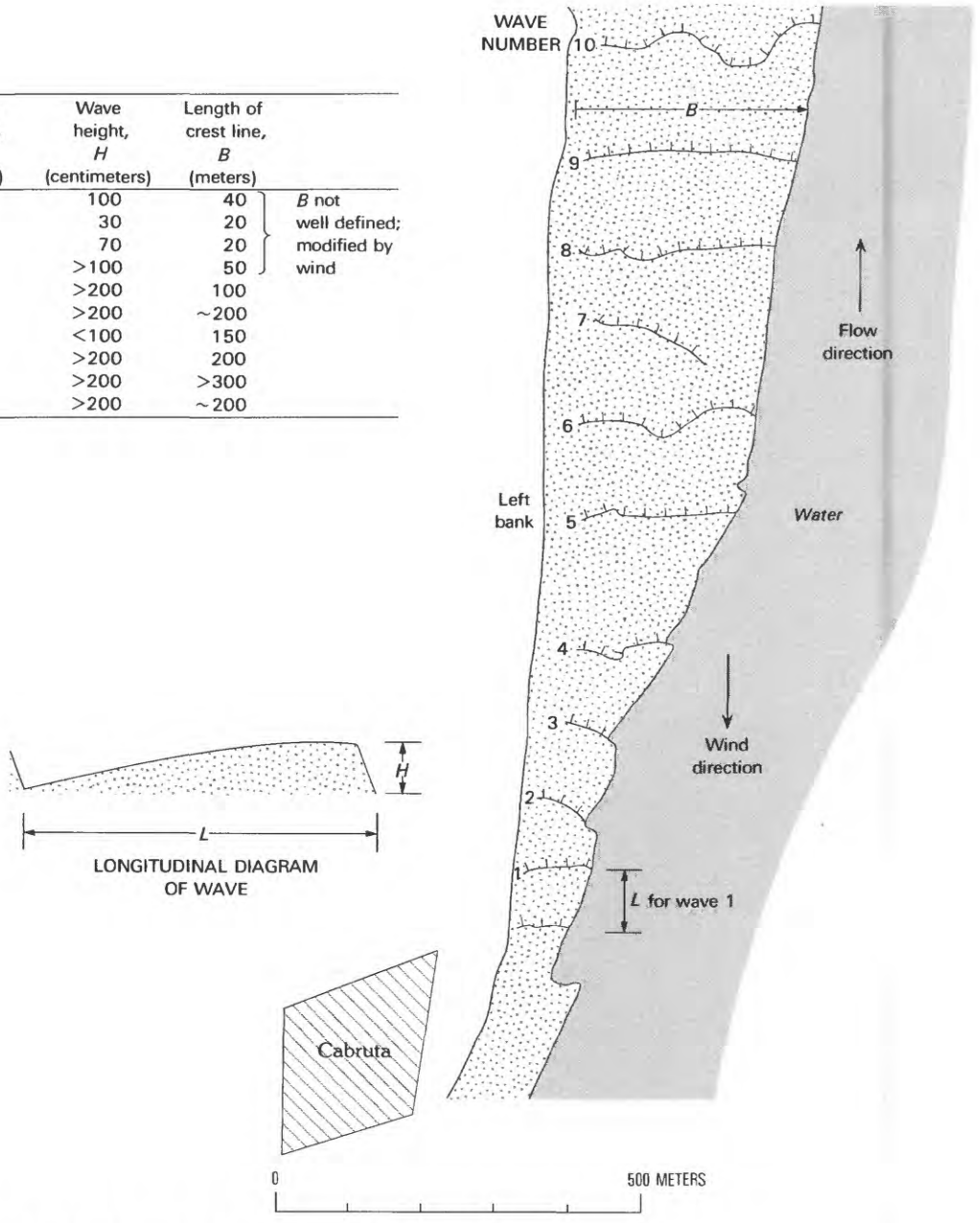

Figure 23. Map of the bar at site D, near Cabruta (fig. 7). Scale is approximate.

Samples also were collected of the material composing the small wind ripples and the larger features shown in figure 27*B* and of the wind ripples shown in figure 27*D*. Size distributions of these samples are plotted in figure 29. The sands of the small wind ripples (fig. 27*B*) have a median diameter of 0.32 mm and are almost the same size as the material collected from the trench at the downstream end of the bar. The larger features shown on the left in figure 27*B* are composed of material with a median diameter of 0.75 mm and containing 80 percent coarse and very coarse sand. The small ripples shown in figure 27*D* are composed of materials ranging from very fine to very coarse sand with a median diameter of 0.50 mm.

The larger features shown in figure 27*B* have their slip faces oriented upstream like the wind ripples, but they probably were formed by water, either the result of reverse flows from eddies that formed behind the rocks

Table 10. Sand-wave measurements, in meters, at site D (fig. 7)
[Leaders (---) indicate values not determined]

Sand wave No.	March 1982			March 1983		
	Wave length, *L*	Wave height, *H*	Crest length, *B*	Wave length, *L*	Wave height, *H*	Crest length, *B*
1	60	1.0	[1]40	90	2.0	116
2	34	0.3	[1]20	216	3.0	170
3	30	.7	[1]20	169	1.5	150
4	80	1.1	50	88	1.0	220
5	240	2.0	100	108	2.5	295
6	200	2.1	220	131	0.3	320
7	30	.9	150	100	1.5	[1]64
8	70	2.1	200	111	.5	---
9	224	2.6	320	109	2.0	500
10	72	2.4	270	---	---	---
Average	--- 104	1.5	---	125	1.6	---

[1]Crest lines are not continuous to the water.

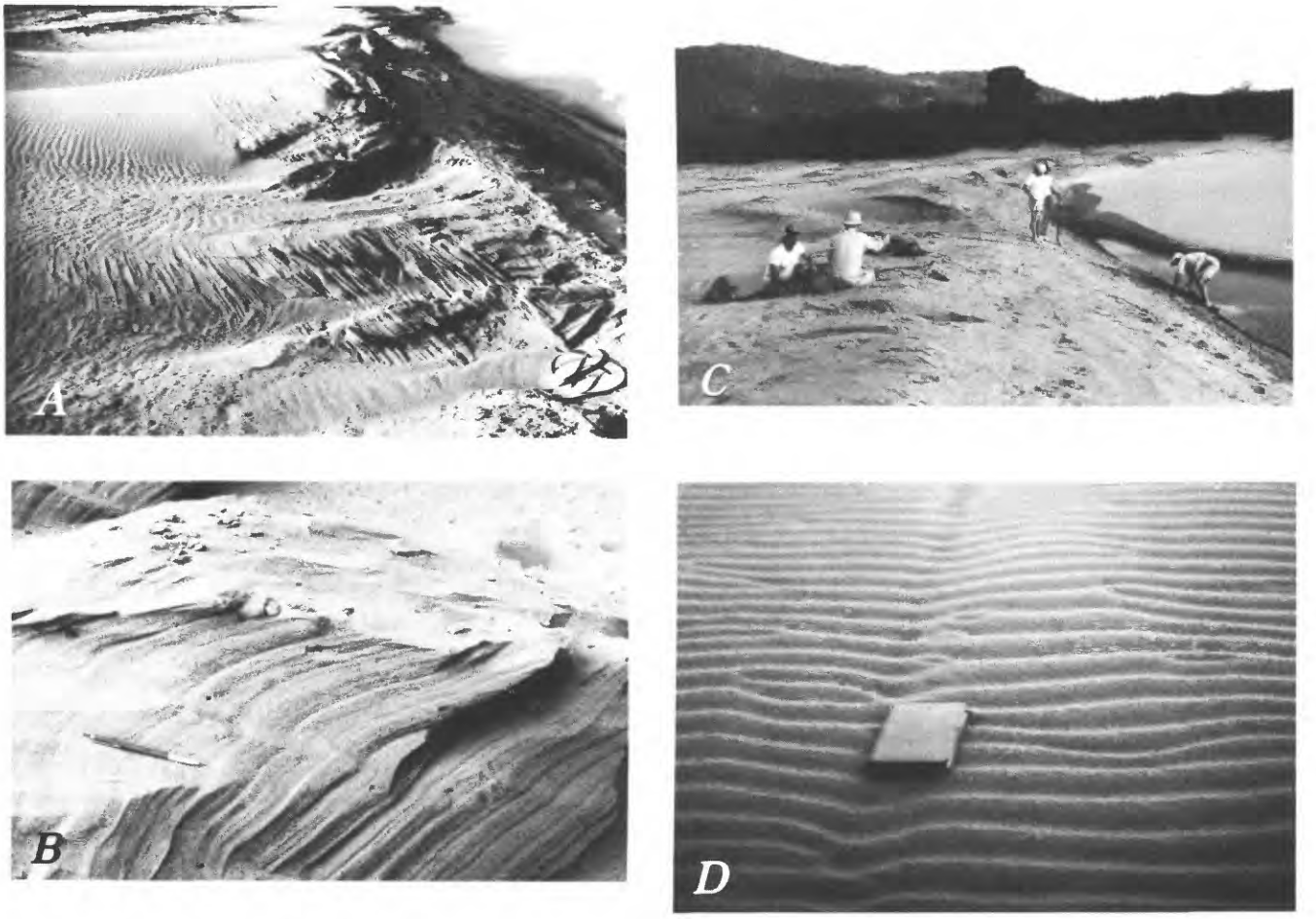

Figure 24. Wind erosion features at site D, near Cabruta (fig. 7). *A*, Wind erosion of sand wave crest; note beach shoes for scale. *B*, Close-up view of wind erosion; pencil is 15 cm long. *C*, View toward the left bank. *D*, Wind ripples and vortex trails; field notebook is 12 cm wide and 18 cm long.

Table 11. Sand-wave lengths and heights, in meters, at site B from sounding records
[Leaders (---) indicate values not determined]

Sand wave No.	June 12, 1982		November 19, 1982	
	Wave length, *L*	Wave height, *H*	Wave length, *L*	Wave height, *H*
1	66	1.2	52	1.2
2	40	0.9	38	2.6
3	31	1.2	114	1.5
4	66	1.5	60	0.9
5	62	2.4	60	2.4
6	73	1.1	62	1.5
7	26	0.8	32	0.9
8	48	1.8	58	2.4
9	57	2.1	70	2.0
10	48	1.8	48	1.4
11	42	1.5	21	0.8
12	136	1.2	35	2.4
13	44	1.4	96	1.0
14	55	2.0	54	2.0
15	44	1.2	138	3.2
16	49	1.9	30	1.4
17	40	1.8	62	2.4
18	158	1.8	114	2.3
19	55	2.0	66	2.2
20	48	1.3	67	1.3
21	44	2.3	93	2.3
22	132	2.0	49	1.3
23	---	---	45	1.9
24	---	---	39	0.9
25	---	---	41	2.6
26	---	---	82	1.9
27	---	---	48	1.3
28	---	---	74	2.1
29	---	---	41	1.0
30	---	---	31	2.0
Average	62	1.6	61	1 8
Standard deviation	35	0.5	28	0.6

on receding flows or from wind waves on the water surface. In either event, as these small sand waves are exposed and dried by the wind, some deflation occurs, leading to the relatively coarse size distribution shown in figure 29.

WIND-BLOWN SANDS

From our field observations, we estimated that as much as 30–40 percent of the bed in the alluvial reaches along the Río Orinoco might be exposed during the average low flows. This estimate was confirmed by inspection of 1:25,000-scale aerial photographs obtained April 3 and 4, 1982, of the reach between river km 860 near Cabruta to the rapids at El Infierno, river km 620. Typical large bars are shown in figures 11, 14, and 16. The aerial photography mosaic along the reach extending from 5 km upstream of Cabruta to 12 km downstream of the mouth of the Río Cuchivero, reproduced in figure 15, shows the extent of the exposed bars; by planimeter, the area of the channel is 180 km^2 and the bars occupy 62 km^2, or about 35 percent of the active channel, very close to our preliminary estimate. By April 4, however, the

Table 12. Properties of sand waves from soundings downstream of Isla Chimborazo, Nov. 19, 1982
[Measurements of wave height and length are in meters. d_{50}, median particle size in millimeters, mm]

Distance from Isla Chimborazo (meters)											
100–1,000			1,000–2,000			2,000–3,000			3,000–4,000		
Sand wave No.	Wave length, *L*	Wave height, *H*	Sand wave No.	Wave length, *L*	Wave height, *H*	Sand wave No.	Wave length, *L*	Wave height, *H*	Sand wave No.	Wave length, *L*	Wave height, *H*
1	56	1.0	13	80	1.5	30	25	1.0	52	72	2.4
2	114	1.9	14	125	3.0	31	30	1.0	53	51	1.4
3	50	0.6	15	74	2.2	32	39	0.8	54	24	1.1
4	47	0.8	16	65	2.0	33	40	0.8	55	50	2.1
5	49	1.1	17	88	1.8	34	30	1.1	56	59	1.8
6	160	1.8	18	58	1.1	35	32	1.4	57	82	1.7
7	58	1.3	19	43	1.8	36	39	1.4	58	30	1.0
8	33	2.4	20	42	1.2	37	36	1.0	59	48	1.5
9	108	1.2	21	45	2.2	38	25	0.9	60	46	1.4
10	54	1.6	22	92	1.7	39	37	1.0	61	50	1.4
11	102	2.5	23	45	1.0	40	34	1.7	62	70	1.0
12	31	2.4	24	40	0.7	41	60	1.4	63	54	1.9
			25	30	1.5	42	50	1.3	64	122	2.6
			26	75	1.4	43	44	1.7	65	91	2.2
			27	54	1.4	44	41	0.6	66	98	2.2
			28	66	1.1	45	66	2.2	67	50	2.1
			29	58	2.1	46	74	2.1			
						47	50	1.9			
						48	42	1.9			
						49	53	1.8			
						50	64	1.9			
						51	73	2.7			
Average ------	72	1.6		64	1.6		45	1.4		62	1.7
Standard deviation ---	40	0.7		24	0.6		15	0.5		26	0.5
L/H ---------	45.0			40.0			32.0			36.5	
d_{50} ----------	1.04			0.76			0.40			0.40	
Sorting coefficient --	1.49			1.46			1.35			1.35	
Mean -------- Depth (meters) ----	4.5			4.0			6.5			8.4	

river stage had risen to 50–60 cm above the early March stages. In addition, river stages during the low-flow season of 1982 were not especially low. The water discharge estimated for Musinacio on March 19, 1982, of 6,520 m^3/s is considerably greater than the average of the low flows (table 1), so our estimate of 40 percent exposed channel probably is a fair estimate for the average low flow. The average channel width is about 2.5 km, so for every kilometer of length along the reach, about 1 km^2 of the bed is exposed. Between Ciudad Guayana and Puerto Ayacucho, then, about 1,000 km^2 of bed is exposed at low flow. If we consider the channel below Ciudad Guayana and the delta, the area of the active channel exposed during low flows probably would be several thousand square kilometers.

During the dry season, trade winds from the Atlantic blow upriver. The winds are strong and persistent, blowing almost every day, but they are not continuous. On several occasions during the March 1982 investigations, data collection had to be postponed either

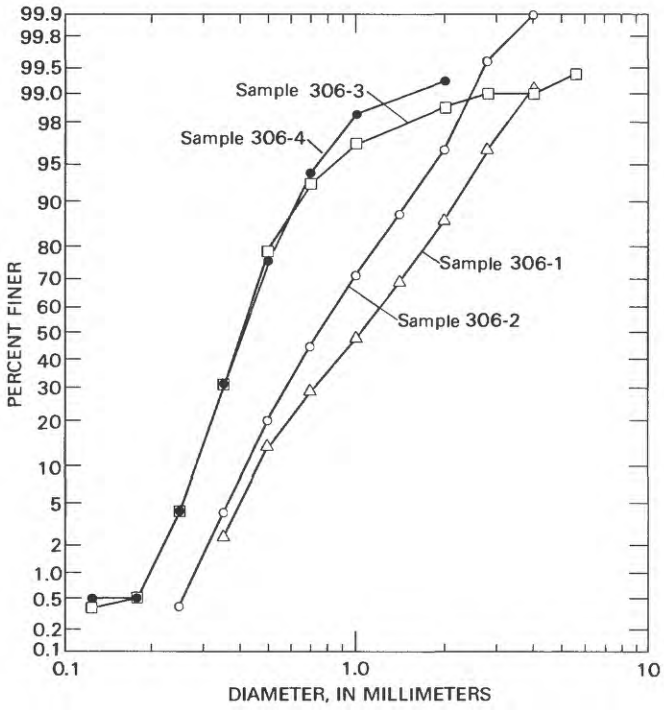

Figure 25. Size distribution of bed material along the sounding line downstream of Isla Chimborazo, Nov. 19, 1982.

because blowing sand obscured visibility or because the wind-generated water-surface waves were so violent that we could neither safely launch a small boat nor hold the barge in position long enough to collect velocity readings or suspended-sediment samples. The winds in 1983 were not so strong. We worked along the same reach from Puerto Ayacucho to Ciudad Guayana during March 9–21, 1983, and there were no occasions when strong winds prevented working. The diminished intensities of winds in 1983 also can be inferred by comparing the size distributions of armored layers along the downstream faces of the exposed bars. These data are presented in a later section of this report.

The action of the wind both modifies the surface expression of the exposed fluvial bed configurations and imposes on them a great variety of eolian features, as shown in figures 24 and 27. In addition, eolian transport along the river has several important implications. First, large quantities of exposed sediments from the stream bed are blown out of the channel and across the flood plain to form extensive dune fields and other wind-blown deposits. Second, large quantities of the sediments transported by the Río Orinoco at high flows are recycled sediments; that is, some of the material passing any cross section during floods and deposited in the channel downstream on falling stages is blown back upriver during the dry season. Some part of this material accumulates in the channel or on the flood plain where it remains until it is re-entrained on rising flows and transported once again downstream. The bed sediments of Río Cinaruco, for example, have the characteristic appearance of recycled wind-blown sands (fig. 9). Third, if enough coarse sand and gravel is present in the exposed bed, the surface will become armored with a lag deposit caused by deflation. The lag deposit protects the surface from further erosion by wind and also maintains the shape of the surface on rising flows until the flow strength is sufficient to move the particles composing the armor layer. Each of these implications is considered in the following sections.

Prominence and Distribution of Wind Deposits

Extensive deposits of wind-blown sands have accumulated west and southwest of the Río Orinoco. Some of these deposits are visible clearly on satellite imagery and on radar maps compiled in 1969 by Petroleras de Venezuela S.A. The approximate location and extent of these deposits are shown in figure 30. Tricart (1974) attributed these deposits to Wisconsin age, but Oswaldo de Sola (oral commun., 1982) believed that the age of these deposits are Pleistocene to Modern. Judging from the active erosion and sand transport observed along the river, substantial quantities of dust and fine sands likely are accumulating in these same areas today.

Local sand dunes occur on the flood plains adjacent to the river channel at many locations along the reach. Sand accumulates in fairly large dunes that extend in height many meters above the flood plain. With the large precipitation in the area and the ability of the sand to absorb and retain moisture, these accumulations are rapidly stabilized by vegetation. They are important centers for habitation, being well above the annual flood, and, once covered with vegetation, not subject to either excessive wind or water erosion. Many small communities, mostly along the left bank, are situtated above flood level on these sand accumulations. According to Roosevelt (1980, p. 166) these sand dune areas also are important out in the plains (llanos). In her study of archeological sites of the Parmana region, a 500-km^2 area of flood plain along the left bank about 50 km downstream of Cabruta, Roosevelt states: "Between the plateau and the highlands, the only land surfaces that regularly escape summer flooding are the elevated natural levees of the inner Orinoco flood plain and a few high places out in the plain. These areas are kept out of

Table 13. Summary of sand-wave statistics from soundings during March 1982

Sounding location	Numbers of waves observed	Length, *L* (meters)		Height, *H* (meters)		Average flow depth (meters)	Median diameter of bed material, (millimeters)
		Average	Standard deviation	Average	Standard deviation		
Downstream of Río Suapure, near station 28 -------	34	135	76	2.4	1.1	8.5	0.47
Near station 58 ----	16	56	29	2.0	0.5	6.2	0.45
Below station 74 -	35	154	96	3.8	2.5	20.7	0.54

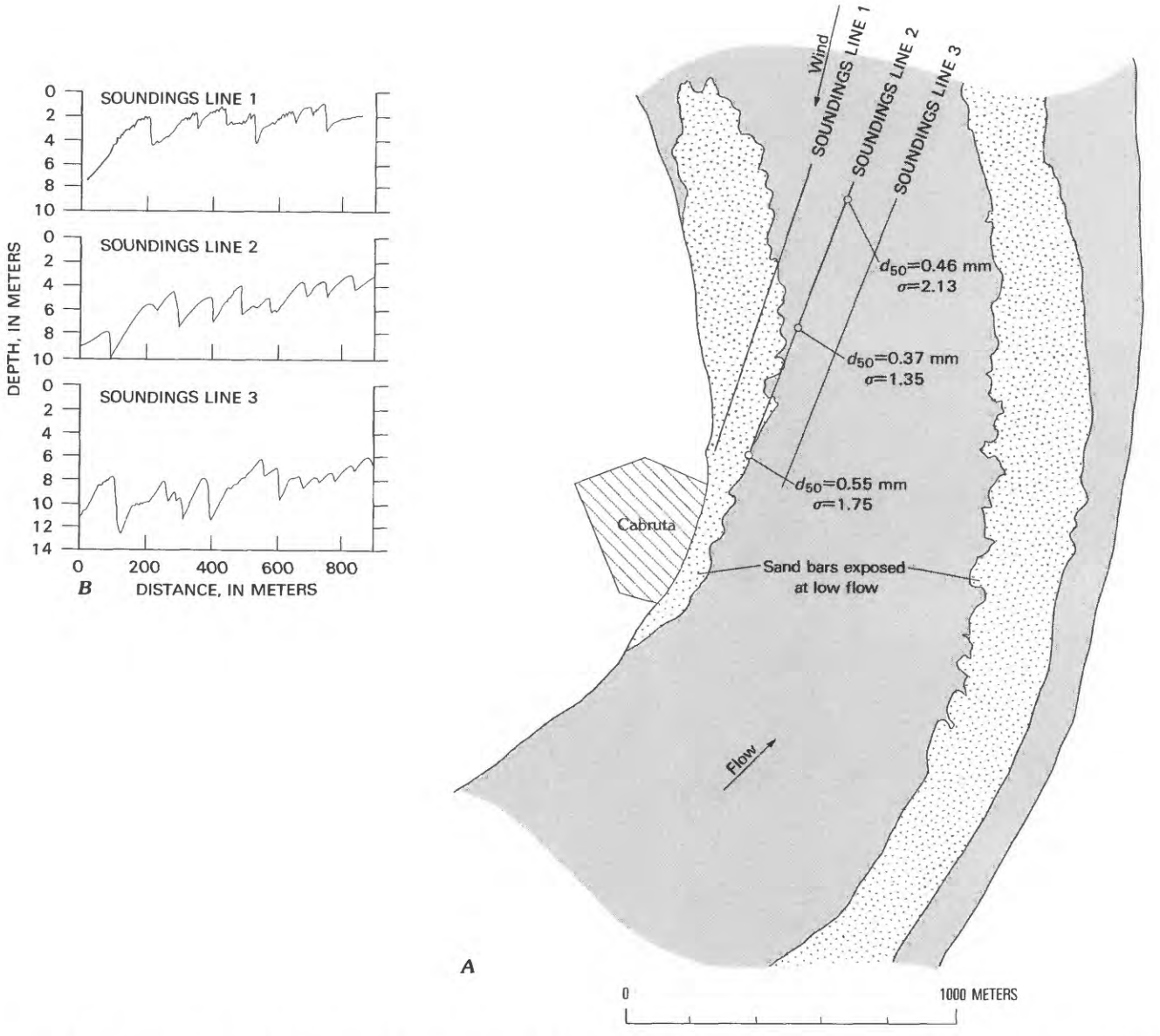

Figure 26. Soundings at site D (fig. 7), Nov. 30, 1982. *A*, Location of the sounding lines and bed sampling sites. Scale is approximate. *B*, Traces of the bed soundings.

Figure 27 (above and facing page). The bar at site C (fig. 7). *A*, View upstream to rock outcrops; *B*, wind ripples moving upstream (left, in photograph) over larger ridge-like features; *C*, dune at the downwind (upstream) end of the bar; *D*, coarse sand ripples and worm tubes (pencil is 15 cm long).


C


D

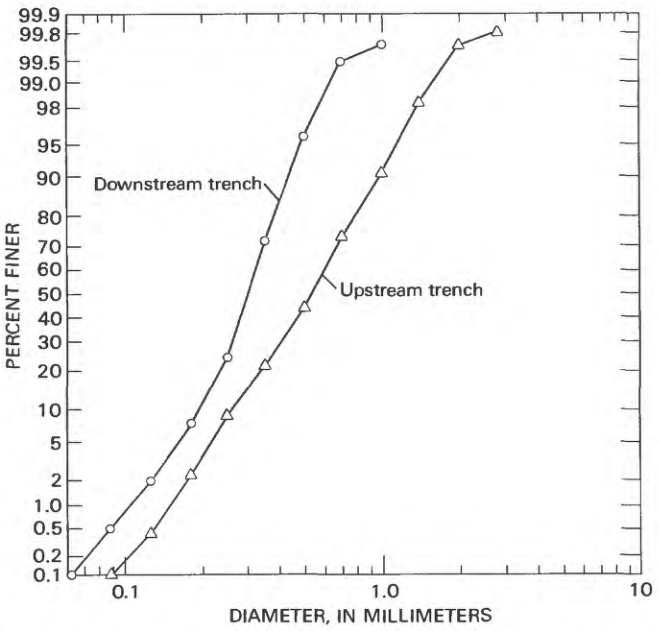

Figure 28. Size distributions of sediments in the bar at site C (fig. 7).

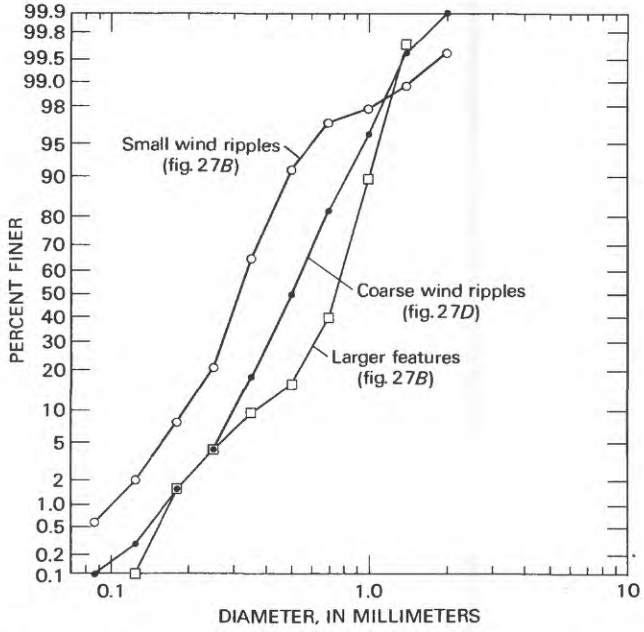

Figure 29. Size distributions of sediments forming the wind ripples shown in figures 27*B* and 27*D*.

the reach of the floodwater by the annual deposition of sand scoured by the wind from the riverbed during the dry season. All other land is subject to months of inundation during the rainy season * * * ."

When the wind rose along the Orinoco, usually by mid-morning, the surfaces of the bars would be obscured by dust and flying sand rising tens of meters above the surface. After an hour or so, some dust and finer sand moving in suspension would tend to thin out or disappear altogether, and the only visible transport over the bar would be the saltation within a meter or two of the bed.

Particles moving in saltation rarely attain heights greater than 2 m; most of the saltation transport occurs in a layer 10 or 20 cm above the bed. Thus, most of the saltating grains stay in the active channel, being deposited downwind along the bar or dropping into the water at the upstream (downwind) end of the bar. There are several conditions, though, when the coarser sands moving by saltation can migrate onto the flood plains. Many bars have tops less than 2 m from the flood-plain level, so in very strong winds the particles could move by saltation directly onto the flood plain. More commonly, blown sand migrates to the flood plain where large dunes build along the banks of the river and directly out onto the flood plain. One such migration investigated in 1983 was at Punta Brava (fig. 17). Punta Brava is a rock outcrop along the right bank. At high flow this outcrop creates flow separation and a large eddy of slow-moving water that allows the accumulation of sediment downstream. The deposited sediment forms a large bar about 4 km long and 800 m wide oriented with its long axis directly into the wind (fig. 17). During the dry season, the blowing sand accumulates in large dunes along the right bank just downstream of Punta Brava. In 1983 the downwind dune was 14 m high (fig. 31) and extended onto the flood plain. The size of the dunes at Punta Brava perhaps are exceptional, but at many locations along the channel, accumulations of blown sand grow to the height of the flood plain and move out across it. As mentioned earlier in this report, if these accumulations become stabilized with vegetation, they usually are inhabited, because they are well above the annual flood levels.

Quantity of Eolian Transport

The appearance of the blowing sand along the channel during high winds is spectacular. Clouds of dust and blowing sand extending upward 30–50 m at times envelop every exposed bar, and obscure completely the surfaces of the bars and the water surfaces upstream. It is readily apparent that large quantities of sediments are transported upriver by wind during the low-flow season. At present, no direct measurements exist to estimate these quantities, and during our reconnaissance of the reach we had neither the equipment to monitor wind

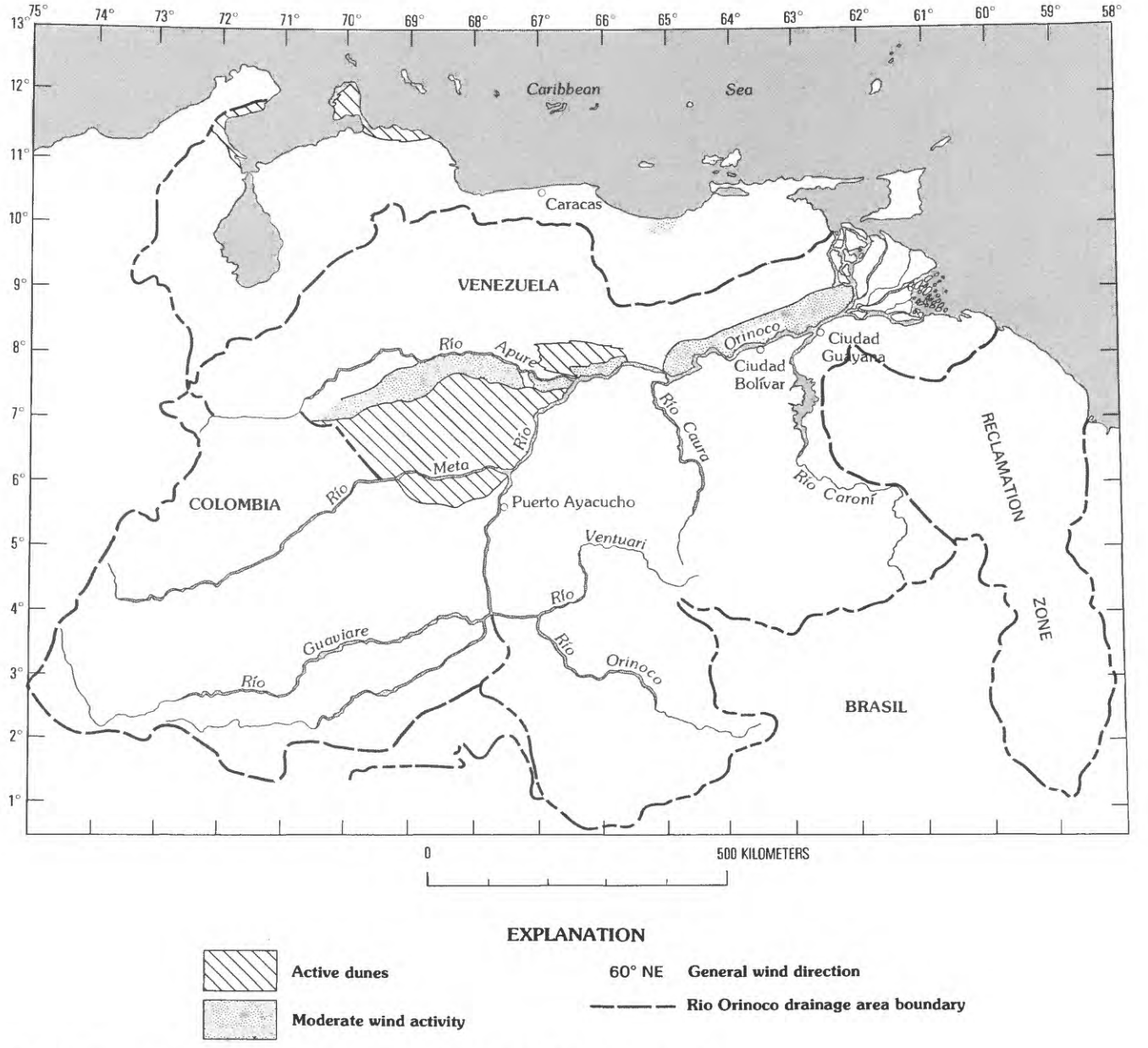

Figure 30. Location and extent of wind-blown deposits in Río Orinoco basin.

speeds and sand flux nor the time to undertake any quantitative measurements. Field studies of eolian processes are planned for 1985, but until these are completed, estimates of eolian transport have to be computed from wind speed and particle size.

It was estimated (de Sola, 1982a) that each year 60×10^6 m^3 of material are transported by wind to the dune fields of the Río Apure basin. This figure was speculative because no data were available to estimate either through computation or direct measurement the quantities of transport along the river. Nonetheless, de Sola's estimate was based on first-hand experience and knowledge about the area of concern; he had just completed a series of maps detailing the surficial geology of the flood plain between Cabruta and Ciudad Guayana (de Sola, 1982b). Assuming a sediment density of 2.65 Mg/m^3 and a volume concentration of 0.6, the volume of 60×10^6 m^3/y, is equivalent to 95×10^6 Mg.

Figure 31. The dune at Punta Brava. *A*, View from the river; *B*, view of the dune crest encroaching on the right-bank flood plain.

However, de Sola did not speculate on the sizes of wind-blown sediments or where the various sizes might be deposited. Presumably, coarse particles can move only by saltation, and they would remain in or near the channel. Finer sands could be transported in suspension and could form dune fields and other deposits away from the river. Dust could be deposited anywhere in the basin or could be carried entirely out of the basin. However, if the geomorphic processes in the basin are in equilibrium, the amount blown from the river channel each year must be resupplied to the river each year by erosion from the watershed, so large quantities of sediments transported by the river are recycled eolian sediment.

In a previous section, we showed that the annual suspended-sediment load at Musinacio was about 190×10^6 Mg/y. The total sediment transport, including the bed load, could be as large as 240×10^6 Mg/y (Meade and others, 1983). How much of this could be recycled sediment? Could it be as great as 40 percent, corresponding to de Sola's estimate? The questions obviously cannot be answered without some additional fairly detailed field studies, but we can at least determine some of the limiting factors that might control these quantities.

As a point of departure, we take de Sola's figure of 60×10^6 m^3 wind transport during the dry season and assume that half of this originates in the delta area and exposed channel downstream of Ciudad Guayana and the other half is derived from the reach between Ciudad Guayana and Puerto Ayacucho, a length of about 1,000 km. From the previous discussion, about 1,000 km^2 of the bed are exposed in this reach, so the erosion of 30×10^6 m^3 wind-blown sands would result in a uniform lowering of the exposed surface of about 3.0 cm.

Assuming the bed of the Orinoco everywhere to be composed of fairly uniform fine sand, the erosion of an average depth of 3 cm over the exposed bars is reasonable. Sand would begin to erode uniformly over the surface of an exposed bar wherever the wind was above the critical threshold to move the largest particles present in the bed. At the downstream (upwind) end of the bar, erosion would continue unchecked, there being no incoming supply of sand to replenish the material removed by the wind. Downwind, according to Bagnold (1941), the flow eventually should become saturated with particles at its capacity transport rate and the moving carpet of sand would protect the underlying bed from further erosion. Across the exposed surface, an equilibrium transport rate should exist that can be expressed in the general form

$$q_s = K(V - V_c)^3 , \qquad (2)$$

where q_s is the sand flux per unit width, V is the wind velocity, V_c is the critical or threshold velocity for the initiation of particle motion, and K is a coefficient that depends mostly on particle size and on the height at which the velocity is measured (Bagnold, 1941, p. 69). For naturally graded dune sand with a median particle diameter of 0.25 mm and wind velocities measured in meters per second at a level 1 meter above the surface, equation 2 becomes

$$q_s = 5.2 \times 10^{-4}(V - V_c)^3 , \qquad (3)$$

where q_s is in megagrams per hour per meter width. The critical velocity determined experimentally by Bagnold (1941) for natural dune sand is 4 m/s and for uniform particles of 0.25 mm diameter is 2.5 m/s. It is measured at the same height, 1 m, as the velocity, V.

Equation 3 with $V_c = 4$ m/s is plotted on figure 32. For wind speeds less than 6 m/s, the transport rate is small. However, the transport rate increases rapidly with wind velocity. An increase of wind velocity from 10 to 20 m/s results in a 20-fold increase in transport.

Consider now a typical exposed bar of the Río Orinoco, such as the one shown in figure 16, located about 20 km upstream of the mouth of the Río Caura. The bar is about 3 km long and 1 km wide. If it were lowered by deflation 3 cm uniformly over its surface and all the eroded materials were transported across the downwind end of the bar, the total sand transport would be 9×10^4 m^3. Assuming the sand in place has a volume concentration of 0.6 and a density of 2.65 Mg/m^3, this would amount to a sand flux of 14.3×10^4 Mg or 143 Mg per meter of width. From figure 32, we can estimate that this amount of transport could occur if winds persisted for 6.5 days with velocities of 16 m/s or for 48 days with velocities of 10 m/s. These velocities and durations are well within the range of conditions observed during March 1982, so the intensity and duration of wind would seem not to be a limiting factor in the transport of as much as 60×10^6 m^3/y from all the exposed bars between Puerto Ayacucho and the river's mouth, assuming the bed were of uniform fine sand.

Eolian Armoring

The situation described in the proceeding section, though, is not so simple. The great range of sizes of material composing the bed and the extreme variability both along the reach and across the channel at any cross

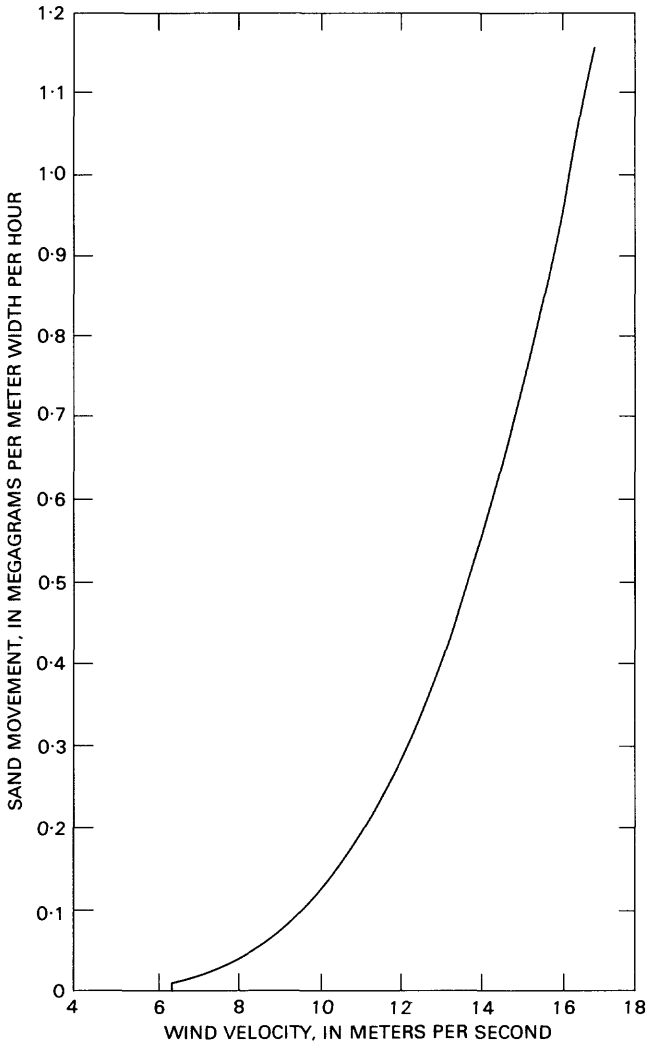

Figure 32. Relation between sand transport and wind velocity measured at 1 meter above the surface (modified from Bagnold, 1941, fig. 22).

section were discussed in a previous section. The size distributions in table 5 indicate that about 80 percent of the samples contain some gravel (particle size >2 mm). Thus, armoring of the bed seems to be a limiting factor on the availability of sand for transport. The finer particles are carried away by the wind, and eventually the coarser particles left behind form a protective layer that prevents further erosion.

On the average, the bed material of the Río Orinoco (table 5) contains about 2 percent gravel. Assuming again a density of 2.650 g/cm^3, a volume concentration of 0.6, and a critical wind velocity such that nothing coarser than sand is moved, the erosion of 3.0 cm from the exposed bed would leave about 0.095 g of gravel-size material on each square centimeter of the bed. A 2-mm quartz pebble weighs about 0.01 g, so the erosion could leave 9 particles covering a surface area of about 0.28 cm^2. Twenty-five particles with parallel center packing on a flat surface is probably the maximum number that could be placed on 1 cm^2; these would cover about three-fourths of the surface area and would require about 9 cm of deflation to be segregated out. Probably not this much degradation would occur, because the bed surface does not need to be completely covered with immobile particles for effective armoring to take place. The percentage of the bed area that must be covered with nonmoving particles to effectively armor a wind-blown surface has not been determined, but probably it is about the same as for armoring of a stream bed by flowing water. Harrison (1950) observed that sediment transport by water became negligible when 50 percent of the bed was protected. If this figure is adopted as an approximation, degradation of about 6 cm of the bed surface containing 2 percent gravel would effectively armor the bed and prevent further erosion. Over 1,000 km^2, the area of exposed bed between Puerto Ayacucho and Ciudad Guayana, this 6 cm of erosion would allow movement of 60×10^6 m^3 of the finer sand, so armoring should not be a limiting factor if the entire area were subject to uniform deflation.

Of course, the natural conditions along the river are much more complicated. Bars are rarely deflated uniformly because they are composed of large sand waves formed by the flowing water (fig. 16), so there is considerable relief across the surfaces of the bars. This relief tends to shelter large areas from the full force of the wind and provides locations at which blown sand can accumulate. On the other hand, some of the bars, especially the point bars on the insides of bends, are largely devoid of gravel. Here armoring does not occur at all. The only limitations to the rate of deflation of the bars are the speed and duration of the wind and perhaps the bar moisture content, which is influenced by the frequent local showers even in the dry season. Overall, these complications may balance out, so the preceding assumptions may be fairly reasonable. Some of these complicating factors will be considered in more detail in the next section.

We consider next the relation between wind speed and armoring. According to Bagnold (1941), there is a "fluid threshold" corresponding to the wind velocity at which particles just begin to move and an "impact threshold" required to maintain saltation. The impact threshold is about 80 percent of the fluid threshold. Thus, once general motion by saltation begins, the velocity required to maintain this motion is less than the velocity required to initiate it. A similar relation has been found

Table 14. Summary of wind records, Río Orinoco at Musinacio, 1970
[Measurements were at 10 meters above the surface; N, north; E, east; S, south]

	Jan.	Feb.	Mar.	Apr.	May	June	July	Aug.	Sep.	Oct.	Nov.	Dec.
Maximum velocity												
(meters per second)	13.6	17.2	16.4	19.4	15.6	21.1	18.3	21.9	20.0	13.1	16.9	16.4
Direction	ENE	ESE	ENE	ESE	SE	E	ENE	S	SSE	ENE	NE	ENE
Mean velocity												
(meters per second)	3.7	4.0	4.3	4.0	2.6	2.5	2.2	2.0	2.5	2.5	2.7	3.4
Direction	ENE	ENE	ENE	ENE	E	ENE	NE	ENE	ENE	ENE	ENE	ENE

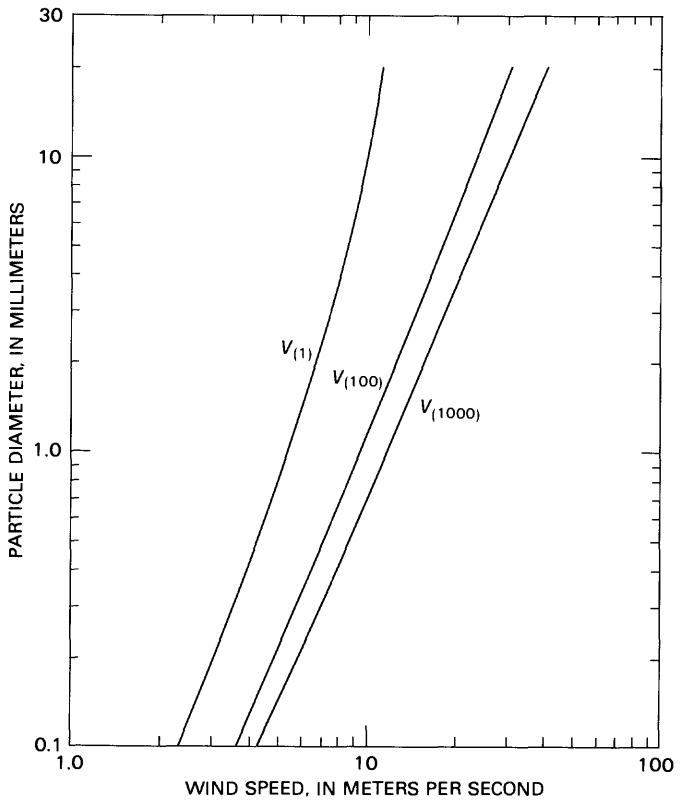

Figure 33. Relation of particle size to impact threshold wind speed, V_z, where z is measured in centimeters above the surface.

for water transport (Rathbun and Guy, 1967). For purposes here, we consider the impact threshold as the critical threshold for armoring.

Critical fluid and threshold velocities can be computed from the relations given by Bagnold (1941, p. 104–105). These can be written as

$$V_c = 5.75\,A\,(\frac{\rho_s-\rho_a}{\rho_a}gd)^{1/2}\log\frac{30z}{d}, \qquad (4)$$

in which A is an empirical coefficient, ρ_s is the density of the sand, ρ_a is the density of air, g is the acceleration due to gravity, d is particle diameter, and z is the distance above the bed at which the velocity is measured. At 25°C, ρ_a air density is about 1.185×10^{-3} g/cm^3, and for natural dune sands, $\rho_s = 2.65$ g/cm^3. The coefficient A is 0.1 for the fluid threshold and 0.08 for the impact threshold. The impact threshold velocities at $z = 0.01$, 1, and 10 m are plotted against particle sizes in figure 33. The velocity for 10 m is shown because this is the recommended height (according to World Meteorological Organization standards) for anemometers at weather stations.

In the preceding discussion, we showed that 3 cm deflation could occur, according to the relations of figure 32, if winds persisted for 6.5 days with velocities of 16 m/s or for 48 days with velocities of 10 m/s. According to figure 33, winds of these intensities would armor the bed with particles when $d > 4$ mm in the first case and $d > 1.2$ mm in the second. These are approximately the conditions found at site A, (fig. 7), the details of which are given in a later section.

Wind velocities of 15 m/s were measured in the channel along the left bank at Cabruta, using a portable digital anemometer, but no systematic records have been obtained. However, there is a weather station near the runway at Musinacio (see fig. 11) for which wind records are available. Data are summarized in table 14 and plotted in figure 34. These summaries indicate that maximum wind speeds and durations for this station are well above the 10 m/s minimum established using figure 32 for erosion along a 1,000-km reach of 30×10^6 m^3. The armoring of the bed and sheltering due to local topography over the bars, then, are more likely to limit the availability of material for sand transport than any other factors.

TRANSPORT BY WIND AND WATER—SOME APPROXIMATIONS

Thus far, we have considered only wind-blown sands that move by saltation or surface creep. For the most part, these consist of particles larger than about

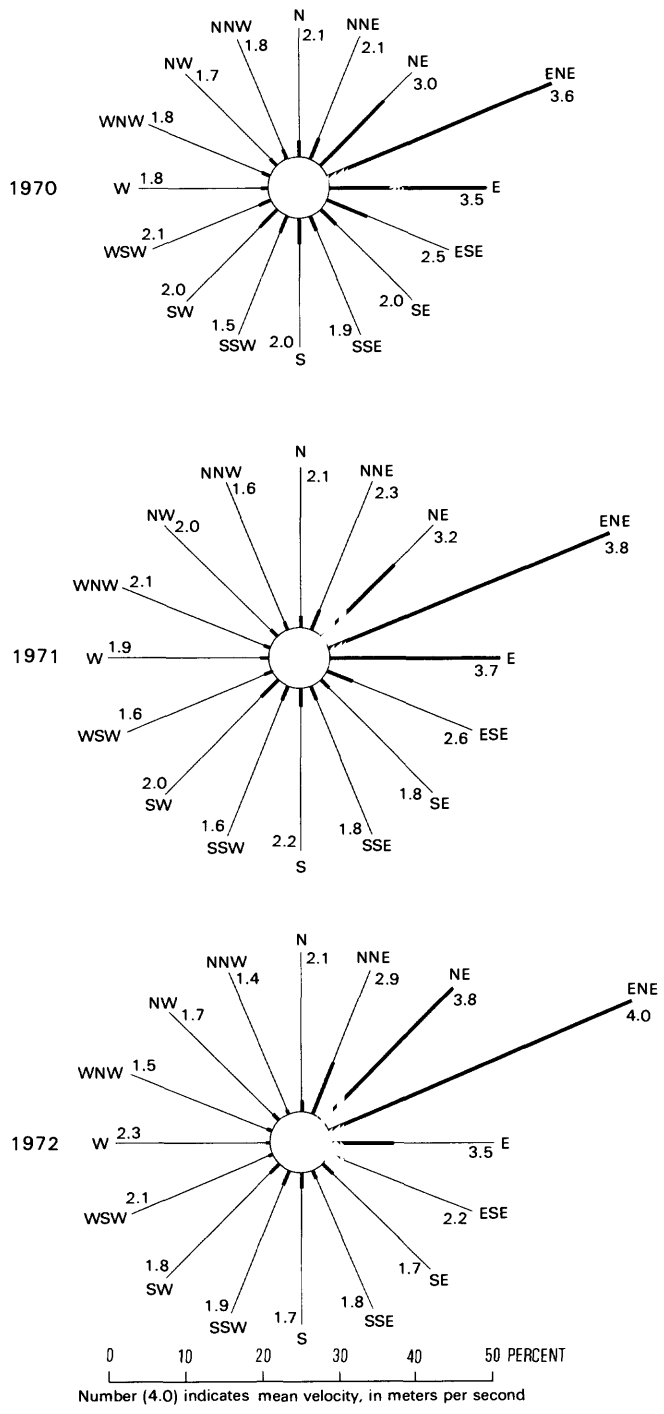

Figure 34. Summary of wind speeds and directions, Río Orinoco at Musinacio.

0.125 mm in diameter. Neither the stream bed nor the wind-blown deposits contain appreciable quantities of material finer than this size. On the other hand, the bulk of the sediments transported by the river are finer than 0.125 mm. The March 15, 1982, suspended sediment sample at station 37 (river km 867) just below the Río Apure contained only 2 percent sand; 98 percent of the material was finer than 0.062 mm. During the flood season, a sample collected at river km 857 contained 68 percent material finer than 0.062 mm and 80 percent finer than 0.125 mm (Nordin and others, 1983). Meade and others (1983) estimated that 84 percent of the total sediment load passing Musinacio is finer than 0.062 mm. Most of the sediment transported by the river is wash load, which by definition is the material finer than any sizes found in appreciable quantities in the bed (Einstein and others, 1940). It is interesting that the sizes of materials composing the wash load of the river are the same sizes most likely to be carried in suspension by the wind.

Wash Load and Dust

The finer sediments transported by winds are called dust. Dust carried by winds and the wash loads carried by rivers have many common characteristics. Both are composed mostly of fine sediments that move in suspension at about the same velocity as the flow and both are likely to be transported long distances. The most important similarities, though, are (1) the transport rates of dust and wash load depend on the rates at which these materials are made available to the flows and not on the capacities of the flows to transport them; that is, the flow is rarely saturated with these size particles because the energy required for their transport is very small; and (2) these sizes of sediments are not found in appreciable quantities in the beds of rivers or in wind-blown deposits that accumulate by saltation and surface creep.

The mechanisms whereby particles become suspended either by wind or water are not well understood, but it is generally agreed that a particle is likely to be suspended if the upward components of velocity exceed the particle's fall velocity, ω (Bagnold, 1941; Lane and Kalinske, 1939). Because turbulent-velocity fluctuations to a first approximation follow a normal probability distribution with zero mean, a measure of the intensity of the turbulence is given by the standard deviation of the velocity fluctuations, σ_v. The assumption then is made that a particle will be suspended if $\omega < K\sigma_v$ where K is a coefficient that has to be determined experimentally.

Turbulent-velocity fluctuations are not measured routinely, so it is useful to relate σ_v to some variable that can be measured or that can be computed from quantities that are easily measured. To this end, we can take advantage of the fact that in two-dimensional turbulent shear flow, the shearing stress, τ, is related to the density of the fluid, ρ, and the average correlation between the horizontal and vertical velocity fluctuations, u and v, according to the relation

$$\tau = \rho \overline{u\,v} \ . \tag{5}$$

Because u and v are correlated and u is generally proportional to v (Lane and Kalinske, 1939), equation 5 can be expressed

$$\tau/\rho = \sigma_v{}^2/B^2 \ , \tag{6}$$

$$\sigma_v = B\,U_* \ , \tag{7}$$

where B is a coefficient that varies from about 0.7 to 1.33 and averages about 1.0 (Lumley and Panofsky, 1964, p. 134–136), and U_*, the shear velocity, is $(\tau/\rho)^{1/2}$.

Sagan and Bagnold (1975) assume that particles are suspended when $\omega = U_*$, and similar relations have been proposed for suspension in water (Middleton, 1976). This assumption apparently was first proposed by Lane and Kalinske (1939). Engelund and Fredsφe (1976) suggested the criterion for suspension

$$\omega < 0.8\ U_* \ , \tag{8}$$

and this criterion will be adopted herein. Equation 8 seems to be well-supported by empirical evidence.

For uniform flow of water τ and U_* are easily computed from

$$\tau = \rho g D S = \rho\, U_*{}^2 \ , \tag{9}$$

where D is the flow depth and S is the water surface slope. For wind, the value of U_* is determined from the velocity gradient according to the logarithmic velocity relation (Bagnold, 1941)

$$\frac{U_z}{U_*} = \frac{1}{\kappa} \ln \frac{z}{K_s} \ , \tag{10}$$

where U_z is the velocity at height z from the bed, κ is von Karman's constant, equal to 0.4, and K_s is the length of a representative roughness element. If velocities U_1 and U_2 are measured at the levels z_1 and z_2 above the bed, the shear velocity is

$$U_* = \frac{(U_2 - U_1)}{\ln (z_2/z_1)} \ . \tag{11}$$

At times it is convenient to work directly with mean velocity rather than shear velocity, and some approximate relations can be derived for rivers from field data. For the flow of water over a flat sand bed, the relation between mean velocity, U, and shear velocity, U_*, is determined mostly by particle diameter (Dawdy, 1961, fig. 11) and can be expressed

$$\frac{U}{U_*} = 8.1\, d^{-0.62} \ , \tag{12}$$

where d is the median grain size in millimeters. For particles with 0.25 mm diameter, $U/U_* = 19.1$, or U_* is about 5 percent of U. For wind, mean velocity is not defined, but the ratio of shear velocity to the velocity measured at 1 or 2 meters above the surface turns out to be about the same, $U_* \cong 0.05\ U_z$ (see for example Bagnold, 1941, fig. 15, and Hsu, 1973, fig. 2). Applying this approximation to equation 8, particles will be suspended when

$$\omega < 0.04\ U \ , \tag{13}$$

where U is taken as the mean velocity in water and, for wind, is measured at 1 m above the surface.

The fall velocities in air of natural sand grains with a shape factor of 0.7 can be computed from the coefficient of drag and Reynolds number relations given in Federal Inter-Agency Sedimentation Project (1957) and fall velocities in water can be taken directly from the figures or tables of the same report. Those relations for air and water at a temperature of 25 °C (degrees Celsius) are shown in figure 35. From figure 35 and equation 13, it is easy to estimate approximately the velocity to suspend a given size particle. For example, particles of 0.1 mm diameter or less could be suspended in air when the velocity at 1 m is greater than 12 m/s and in water when the mean velocity is greater than 0.2 m/s.

Sagan and Bagnold (1975) proposed a quantitative definition of dust; it is material that can be suspended as soon as the critical tractive force at the bed is sufficiently great to initiate motion. This can be

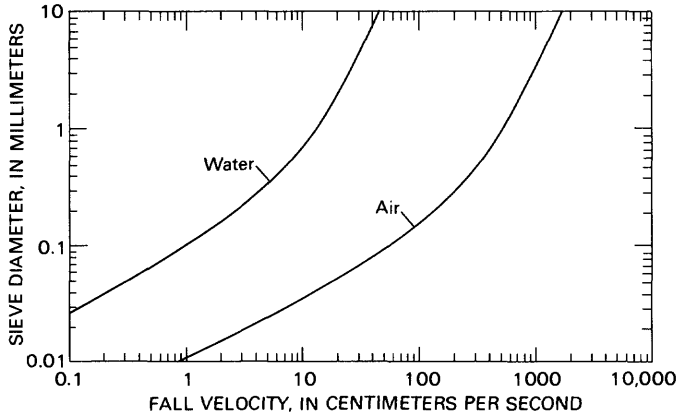

Figure 35. Fall velocity of natural sands in air and water at 25° Celsius.

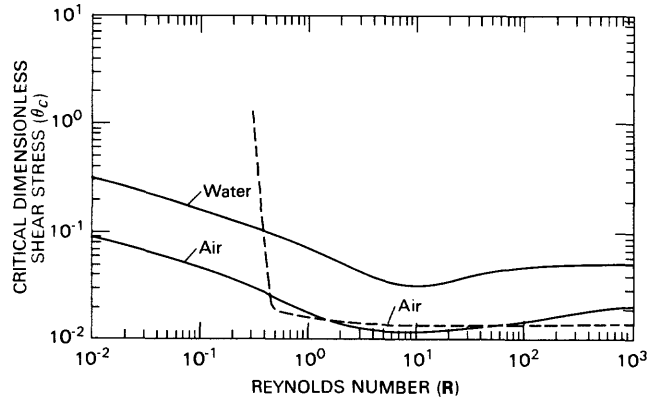

Figure 36. Shields diagrams for air and water, modified from Miller and Komar (1977) and Yalin and Karahan (1979). Dashed curve is from White (1979).

expressd in a form similar to equation 8,

$$\omega < 0.8\, U_{*c} \quad , \qquad (14)$$

where U_{*c} is $(\tau_c/\rho)^{1/2}$ and τ_c is the critical tractive force or shear stress at the bed required to initiate motion of a particle with diameter d and fall velocity ω. Apparently, no one has tried to define wash load quantitatively, but there is no reason why the same criterion, equation 14, should not apply, and we propose that this be adopted as a definition of dust in the atmosphere and wash load in rivers.

The critical tractive force usually is determined from Shields diagram in which the critical dimensionless

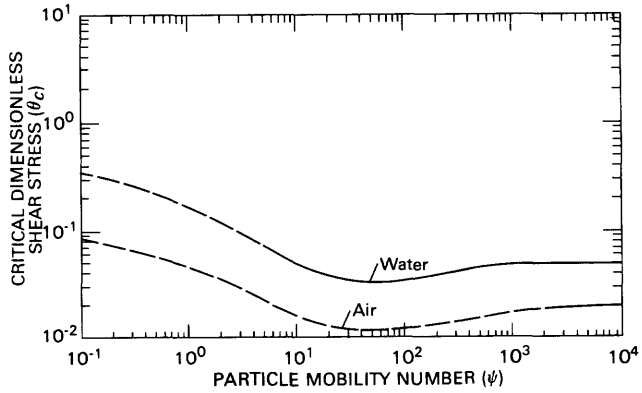

Figure 37. Relation between θ_c and Ψ.

shear stress, θ_c, is plotted against Reynolds number, **R**, where

$$\theta_c = \frac{\tau c}{(\rho_s - \rho) g\, d} \quad , \quad \mathbf{R} = \frac{U_* d}{\nu} \quad , \quad \theta_c = f\,(\mathbf{R}) \quad , \qquad (15)$$

where ν is kinemetic viscosity of the fluid. The relation of equation 15 first was defined empirically by Shields (1936); it since has been verified experimentally many times for water, and modified only slightly. There is a great deal of scatter in the experimental data. The average relation shown in figure 36 will be used here; it is similar to the ones proposed by Miller and Komar (1977) and Yalin and Karahan (1979). Notice that at high Reynolds numbers, θ_c assumes the constant value of 0.05 in water.

For some reason, Shields diagram as defined for water does not apply to the initiation of the motion of sand by air. For air flow, empirical evidence shows θ_c to be about one-third of the value for water and at low Reynolds numbers, the relation of increasing θ_c with reducing **R** rises much more sharply for air than for water (White, 1979, fig. 1; Maegley, 1976, fig. 2). The general shape of the empirical relation from White (1979) is sketched in figure 36.

The abrupt rise in θ_c with decreasing **R** (fig. 36) shown by the empirical data has been attributed to moisture developing cohesion between particles. At intermediate Reynolds numbers, values of θ_c must be obtained by trial because U_* appears in both the ordinate and abscissa. To avoid this θ_c can be plotted as a function of a particle mobility number Ψ (Yalin, 1977), where

$$\Psi = \left[\frac{(\rho_s - \rho)\, g\, d^3}{\rho\, \nu}\right]^{1/2} . \qquad (16)$$

The curves for these relations are shown in figure 37.

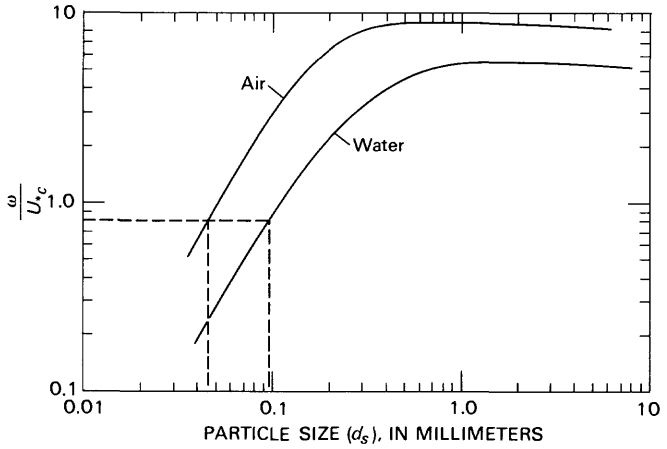

Figure 38. Relation between ω/U_{*c} and particle size.

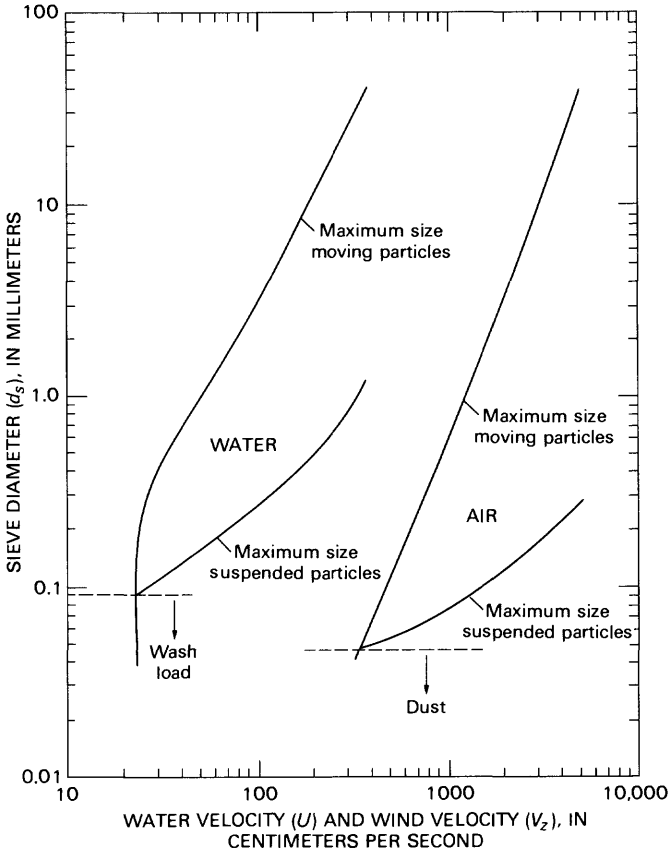

Figure 39. Largest particle suspended and largest particle moving at the bed as functions of flow velocity. Wind velocity is measured at $z=1$ meter.

Figures 35 and 37 provide the basis for quantitative definitions of dust and wash load. Values of ω/U_{*c} are plotted against particle sieve diameter, d_s in figure 38, with the values $\omega/U_{*c} = 0.8$ indicated. For air, the critical size is 0.045 mm and for water it is 0.095 mm. Figure 38 was prepared for air and water temperatures at 25 °C, which is a fair value for average temperatures along the Río Orinoco during the dry season. However, the relations in figure 38 are temperature-dependent and need to be defined for the range of temperatures encountered if they are to be applied to areas where air and water temperatures vary appreciably.

Largest Particle Suspended and Moving at the Bed

From the relations just given, we can now estimate for either wind or water the largest particle that can be suspended and the largest particle that will just begin to move as functions of the flow velocity (fig. 39). Relations for wind follow directly from equations 4 (V_c) and 13 (ω). The curves for water were developed first by obtaining U_{*c} from figure 37 and then using equation 13 and the assumption that $U=20U_{*c}$. The velocity for wind is for initiation of motion, not the impact threshold, so values in figure 39 are 25 percent greater than values from the curve of figure 33.

Both curves for initiation of motion are likely to be somewhat imprecise. For air, equation 4 applies only down to grain diameters of about 0.2 mm (Bagnold, 1941); grains smaller than 0.2 mm are partially imbedded in a viscous sublayer and the velocities required to initiate their motion are greater than predicted from equation 4. The curve for initiation of motion by water is based on the even more restrictive assumptions of flow over a flat bed with grain roughness only and a constant ratio between the shear velocity and mean flow velocity. These conditions are not likely to apply in the Río Orinoco except perhaps along the flat backs of sand waves and bars. Nonetheless, the curve agrees well with values computed under somewhat different assumptions by Sundborg (1956, fig. 13), and we will use it here as a first approximation with the reservation that it probably can be refined as better information on velocity distribution becomes available.

A few generalities can be drawn from the curves of figure 39. In the river, the wash load consists of particles finer than about 0.1 mm. These will be deposited in areas where flow velocities drop below 0.2 m/s. At velocities of 0.25 m/s, particles as large as 0.3 mm can move as bed load and particles as large as 0.1 mm diameter can be suspended. At intermediate flows with velocities of 1 m/s, particles as large as 3 mm will move at the bed and fine sand almost as large as 0.3 mm size can be suspended. At bankfull stage, where velocities can approach from 2.5 to 3 m/s in narrow sections of the river, the flows can move particles as large as 16 mm in diameter, the largest sizes found in the bed (table 5), and can suspend particles as

large as 0.7 mm diameter, which also are the largest sizes thus far found in suspension (Nordin and others, 1983).

For wind transport, material finer than 0.05 mm constitutes dust; it can be suspended as soon as its motion is initiated at wind speeds of about 3.2 m/s. At moderate wind speeds, say 10 m/s, particles as large as 0.6 mm can be moved, and sand as fine as 0.08 mm diameter can be suspended. At extreme wind speeds of 40 m/s, particles as large as 20 mm diameter, the largest sizes likely to be found on the exposed bars, can just be moved, but these winds could only suspend fine sands with diameters smaller than 0.23 mm. The large differences in sizes that can be suspended in air and water are accounted for by the much greater fall velocities of particles in air than in water.

Predictions of initiation of motion and particle suspension are likely to be more precise if they are based on shear velocities rather than flow velocities. These relations derived from figure 37 are shown in figure 40. Viscous effects are accounted for in these curves, so the curves have somewhat different shapes than those of figure 39. For convenience, an approximate velocity scale is included on the figure; it is based on the assumption that $U = 20\ U_*$. If shear velocities can be estimated from direct measures of the turbulent-velocity correlations, equation 5, for example, or even from velocity gradients, equation 10, the curves of figure 40 should give better predictions than those of figure 39.

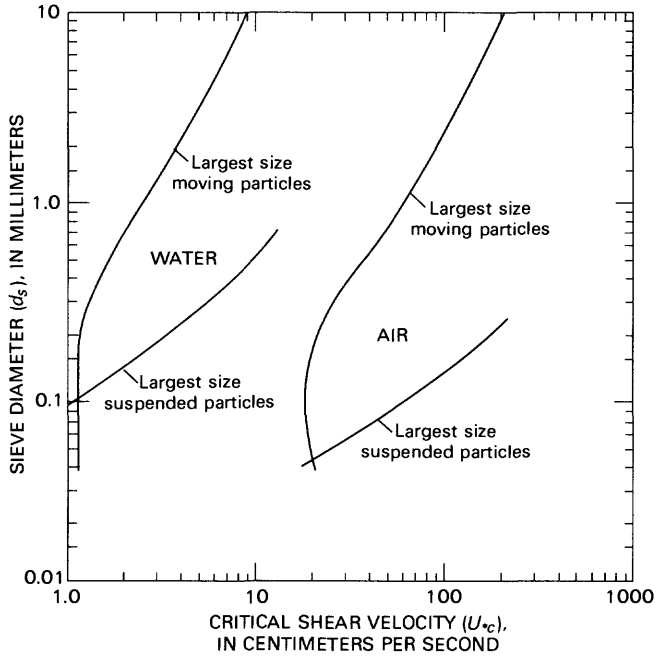

Figure 40. Largest particle suspended and largest particle moving at the bed as functions of critical shear velocity.

Because natural river channels do not have uniform cross sections, the velocities and shearing stresses vary from place to place across a section and along the channel, even under steady-flow conditions. Ideally, to predict local scour and fill and the bed-sediment transport, one needs the magnitude and direction of the velocity and shearing stress at every location. To a reasonable approximation, these values can be estimated along a short reach (Chiu and Hsiung, 1981; Chiu and Lin, 1983; Chiu and others, 1983). These computational techniques require the velocity isovels at the upstream section of the reach and details of the channel geometry and water-surface elevations along the reach. Usually, the detailed field data required to implement Chiu's model are not available, and one is reduced to working with average values at a cross section. But even relations based on average values can be useful if it is recognized that across any section in the stream there will be a distribution of values about the mean. In the following, we develop such approximate average-value functions for typical wide and narrow sections of the river, and we demonstrate the approximate range of variability that might be expected during high flows.

The relations to be developed provide means of estimating as a function of discharge the size of the largest particle that can just be moved at the bed and of the largest particle that can be suspended. These sizes can be taken directly from figure 40 if the relations between water discharge and the mean shearing stress of the cross section are known.

Pérez-Godoy (1984) has compiled a summary of discharge measurements made during 1969 through 1976 for the gaging station at Musinacio, as well as values of local and average water-surface slopes. Slopes were estimated by several methods. The average slope was determined from stage readings along the river between Puerto Ayacucho and Ciudad Bolívar. It is almost constant, equal to the topographic slope of 4.6 cm/km, or 0.000046. Local slopes were measured between the gage at Musinacio and the gage at El Piñal, 7 km upstream. The relation between local water-surface slope, S, and discharge, Q, will be used here; it is plotted in figure 41. The curve is a power function fitted by the method of least squares

$$S = (2.25 \times 10^{-6})\, Q^{0.30} \qquad (17)$$

Observed values vary by a factor of 4 from 0.00002 to 0.00008. At the mean daily discharge of about 30,000 m^3/s, the local slope is almost equal to the average topographic slope.

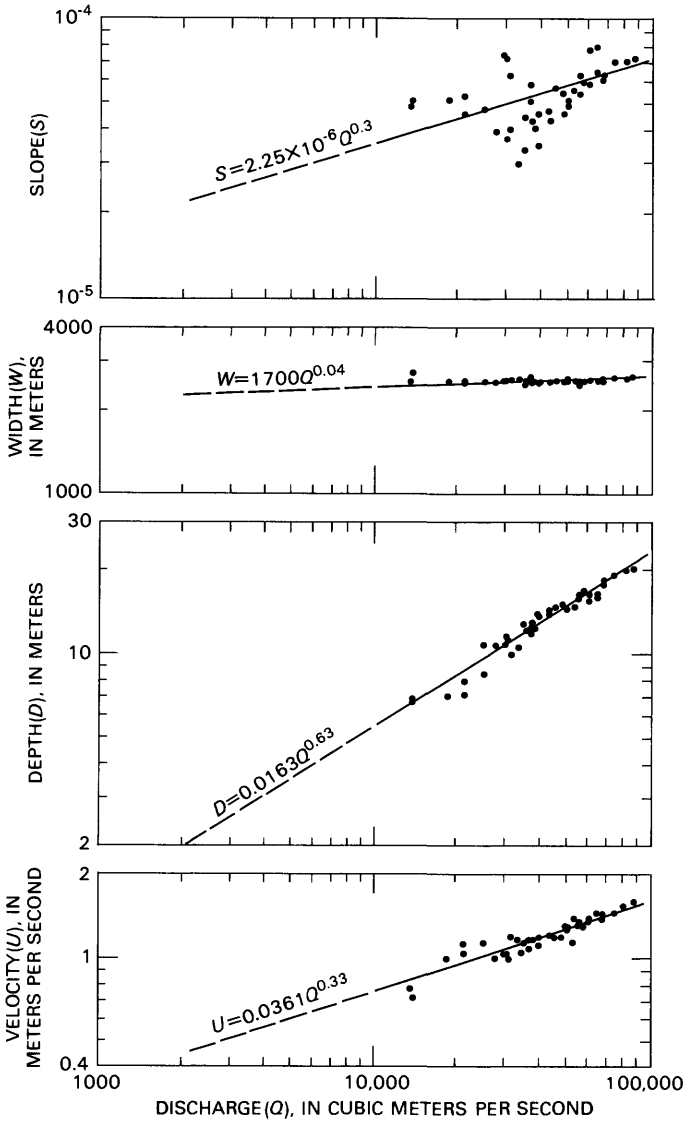

Figure 41. Hydraulic geometry for the Río Orinoco at Musinacio, measuring section of the Ministerio del Ambiente y de los Recursos Naturales Renovables.

The hydraulic geometry relations for the measurements used here also are plotted in figure 41. The mean relations fitted by eye are

$$W = 1700\,Q^{0.04} \quad ,$$

$$D = 0.0163\,Q^{0.63} \quad , \text{ and} \qquad (18)$$

$$U = 0.0361\,Q^{0.33} \, ,$$

where W is the channel width, D is the mean depth, and U is the mean velocity.

The gaging section at Musinacio is across from the landing strip, figure 13, at about river km 655. At discharges greater than 20,000 m³/s, the flows occupy almost the entire channel from bank to bank, a width varying from 2,500 to 2,700 m. The values of average shearing stress computed from the average depth and local slope are plotted against discharge in figure 42. The equation for the line fitted by the method of least squares is

$$\tau = (1.66\times10^{-3})\,Q^{-0.12} \quad \text{g/cm/s}^2 \quad . \qquad (19)$$

We assume the equation applies to "typical" wide sections and can be extrapolated to low flows because, although the river at Musinacio tends to channelize along the left bank with a width between 900 and 1200 m during flows less than 10,000 m³/s, many of the wide sections maintain almost their full widths at low flows and become very shallow. On several occasions we ran aground in the wider sections, even though the vessel draws only 1 m. We believe the extrapolated curve of figure 42 should represent fairly well the average shear stress in these kinds of sections.

To estimate the shearing stress at a "typical" narrow section of the river, we plotted the hydraulic geometry for four discharge measurements made during 1982 and 1983 in a narrow reach of the river at river km 652 just downstream of Musinacio (fig. 43). For discharges between 7,000 and 72,000 m³/s, width varied

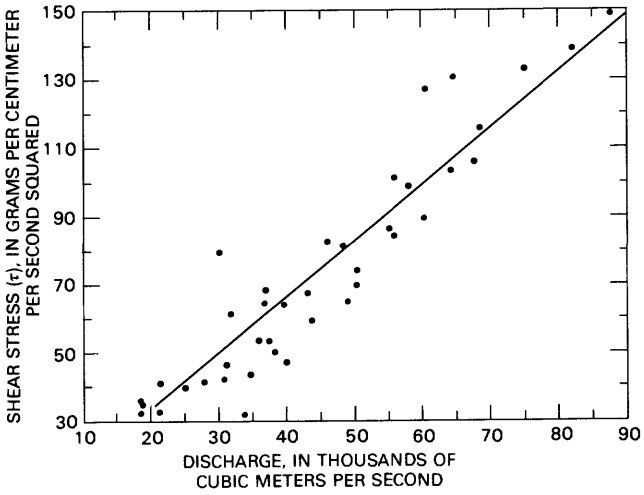

Figure 42. Relation between shearing stress and water discharge, measuring section of the Ministerio del Ambiente y de los Recursos Naturales Renovables.

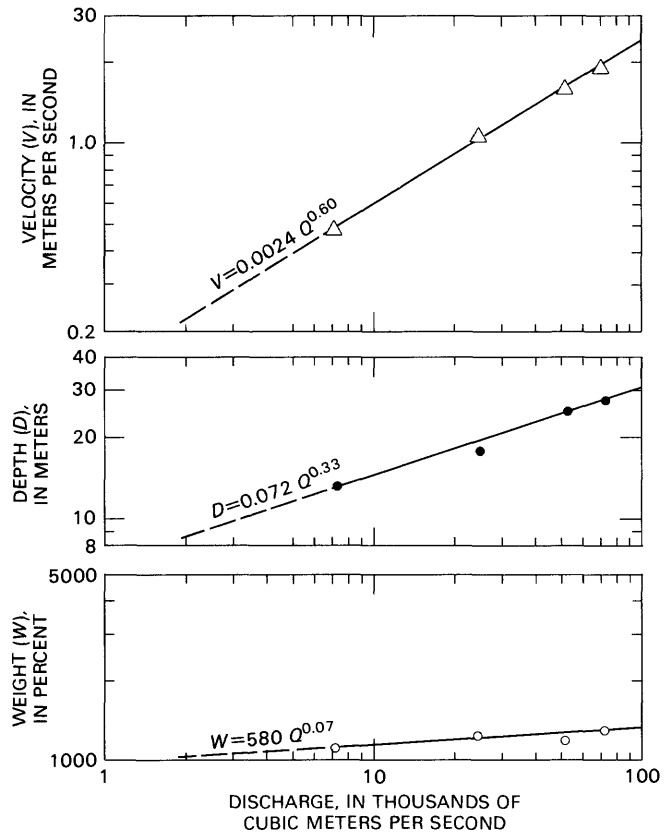

Figure 43. Hydraulic geometry for the Río Orinoco at Musinacio, measuring section of the U.S. Geological Survey.

between 1,100 and 1,300 m. These data are summarized in table 15. The hydraulic geometry relations for this section are fitted by eye,

$$W = 580\,Q^{0.07} \quad ,$$

$$D = 0.72\,Q^{0.33} \quad , \text{ and} \qquad (20)$$

$$U = 0.0024\,Q^{0.60} .$$

The cross section is very near the Musinacio gage, which is along the right bank about 2 km below the downstream end of the bar shown in figure 11, so the local slope should be fairly close to the energy slope for this cross section. To estimate the shearing stress for the section, we selected depths from figure 43 and slopes from figure 41 for a range of discharges. A direct correlation between discharge and shearing stress as in figure 42 would be preferable (Williams, 1983), but the slope data were not available for that approach.

Final results of the calculations are sketched in figure 44. Notice that the curves for initiation of motion and for suspension do not intersect, even at the lowest observed flows (table 1) of 1,050 m³/s. At the lowest flows, the wash load of the river on average can be transported through both wide and narrow sections. Material finer than 0.1 mm will be deposited on the bed only in areas of slack water along the banks and behind obstructions where the local shear stress falls below the average. In the wider sections, the bed load will be very small; nothing larger than 0.35 mm can be moved by the flow and the suspended load should contain almost no sand, the largest size in suspension being 0.1 mm. In the narrower sections, bed load as large a 1.7 mm can be moved by these flows, and sands as large as 0.2 mm can be suspended. Again, in either section the highest flows are capable of moving gravel sizes larger than any found in our bed samples.

Interpretation and application of the curves in figure 44 require information about the bed material and suspended-sediment size distributions for the station at Musinacio. Size distributions from five sets of bed samples and two width-depth integrated suspended samples are listed in table 16. The suspended-sediment size distributions, the mean size distribution of bed material, and the two curves for June and December 1982 are plotted on figure 45. The median diameter of bed material from the mean curve is 0.42 mm and the sorting coefficient from equation 1 is 1.90. The distribution is skewed toward the coarser sizes, with 5 percent of the material finer than 0.2 mm and coarser than 2.0 mm. Notice that between June and December, the bed material coarsens considerably. During this same period, the bed filled about 2 m (table 15).

In June, the suspended-sediment discharge for a flow of 51,850 m³/s was 10,300 kg/s or 892,000 Mg/d, of which 20 percent or 178,000 Mg/d was bed material. During the peak flows of August, at a discharge of 70,700 m³/s, the suspended-sediment load was 7,000 kg/s or 605,000 Mg/d, with 24 percent or 145,000 Mg/d bed material discharge. The size distributions of suspended sediments on the 2 days are similar, but the sizes of the bed material are appreciably different. The larger sediment loads on rising stage in June are associated with finer bed material, $d_{50} = 0.31$ mm, and a lower mean bed elevation than the flood flows in August or the falling stage in December, when the bed has coarsened to $d_{50} = 0.50$ mm. It can be inferred from figure 44 that during low flows, some of the finer sediments accumulate on the bed in the wider sections of the river because they cannot be suspended; during the rising stages these sediments move into and through the narrow sections. A

Table 15. Summary of discharge measurments, Río Orinoco at Musinacio, U.S. Geological Survey section
[°C, degrees Celsius]

Date	Stage (meters)	Discharge (cubic meters per second)	Width (meters)	Depth (meters)	Velocity (meters per second)	Water temperature (°C)	Local slope (from fig. 43)
June 22, 1982	23.93	51,900	1,208	26.2	1.64	27.0	0.0000584
Aug. 20, 1982	26.77	72,000	1,290	28.7	1.25	29.6	0.000645
Dec. 3, 1982	17.93	24,750	1,275	18.2	1.07	28.4	0.0000468
Mar. 19, 1983	11.97	7,240	1,120	13.4	0.48	30.2	0.0000326

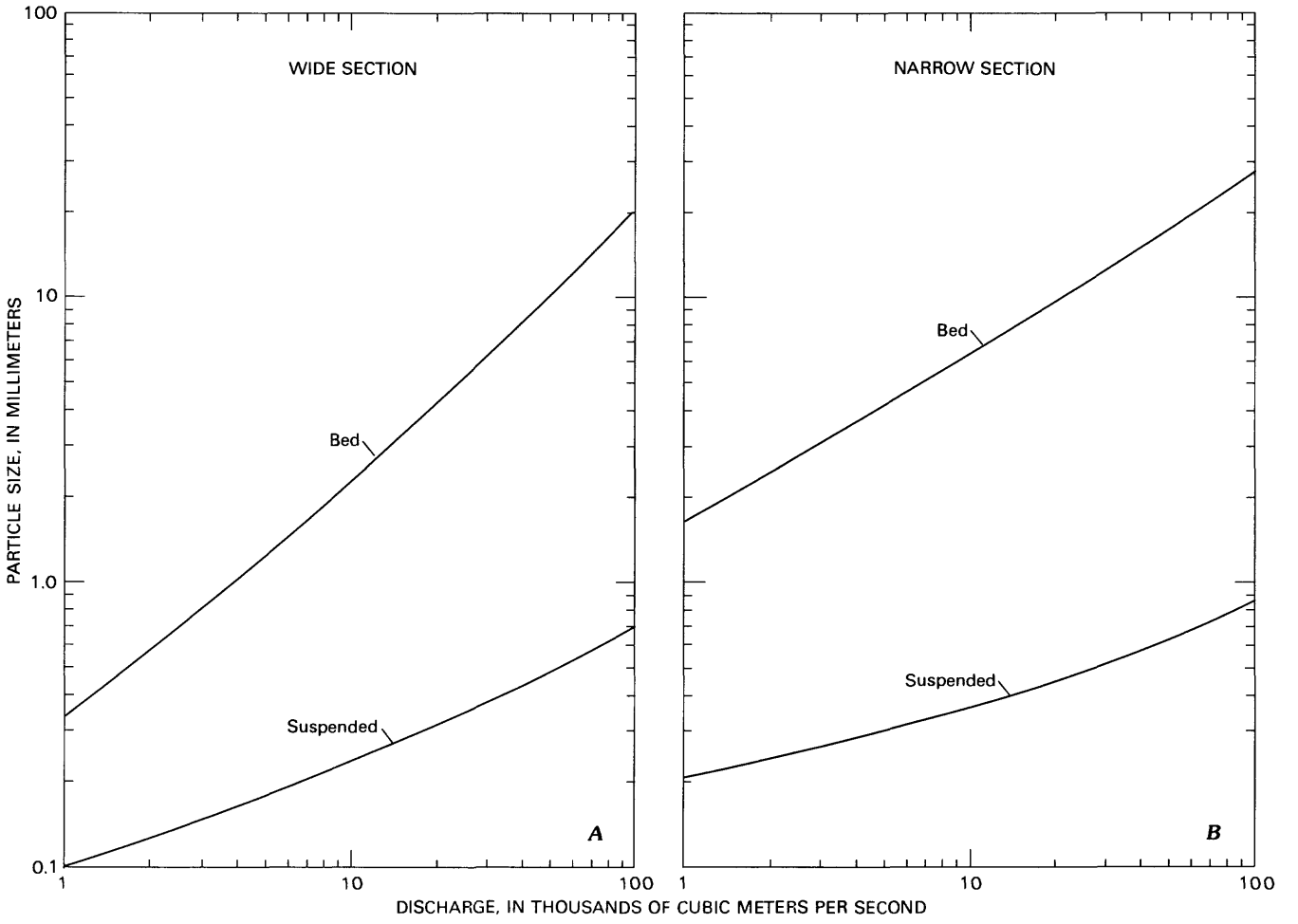

Figure 44. The largest particle that can just be moved at the bed and the largest particle that can be suspended for the indicated water discharge for *A*, a typical wide section, and *B*, a typical narrow section.

complex pattern of seasonal storage and re-entrainment of sediments along the Río Orinoco is reported by Meade and others (1983), and the seasonal difference in transport capacity between wide and narrow sections along the river is one of several factors contributing to this pattern.

The curves in figure 44 are based on shearing stresses and shear velocities computed from mean depths of the cross sections, as if the flows were one-dimensional. Usually, though, there are considerable differences in depth and velocity, and thus in the local shear velocity and shearing stress, across a normal river

Table 16. Average size distributions of bed material and suspended-sediment samples, Río Orinoco at Musinacio

Bed Material

Date	No. of samples	Percent finer than indicated size in millimeters															
		0.062	0.088	0.125	0.177	0.250	0.350	0.50	0.707	1.00	1.414	2.00	2.83	4.00	5.66	8.00	11.3
March 18, 1982	3	0.1	0.3	0.9	1.9	7.2	39.7	66.7	80.5	88.0	93.3	96.6	99.0	100			
June 22, 1982	7	0.	.3	1.9	10.1	26.1	62.8	79.5	88.3	93.4	95.8	96.8	97.0	97.3	97.4	97.5	100
August 20, 1982	5	0.	0.	0.	.4	4.1	20.8	50.3	68.4	83.1	91.4	96.2	98.2	98.9	99.5	100	
December 3, 1982	4	0.	.1	.8	2.4	9.8	31.4	51.8	64.5	75.6	84.9	92.4	97.1	98.8	99.4	99.8	100
March 19, 1983	6	1.1	1.4	2.7	3.2	8.5	30.2	61.2	75.4	83.3	88.8	93.2	96.3	98.1	99.3	100	
Average		.2	.4	1.3	3.6	11.1	37.0	61.9	75.4	84.7	90.8	95.6	97.2	98.6	99.1	99.5	100

Suspended Sediment

Date (1982)	Discharge (cubic meters per second)	Concentration (milligrams per liter)	Number of verticals	Percent finer than indicated size in millimeters												
				0.002	0.004	0.008	0.016	0.031	0.062	0.088	0.125	0.177	0.250	0.350	0.50	0.707
June 22	51,850	197	11	20.8	25.2	32.4	43.9	53.4	71.1	77.2	84.0	89.5	95.0	98.2	99.2	100
August 20	70,700	99	8	18.4	23.7	32.8	39.7	49.6	65.7	74.0	80.1	87.4	91.7	97.5	99.5	100

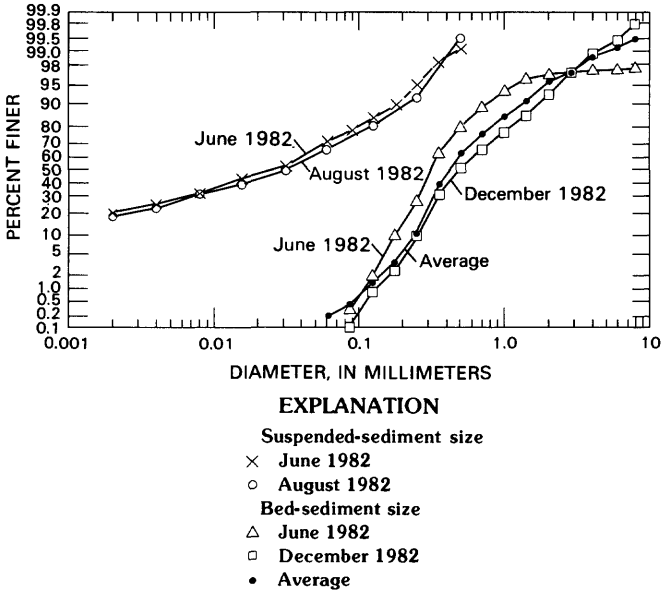

Figure 45. Size distribution of bed and suspended sediments, Río Orinoco at Musinacio.

section. To demonstrate the range of variability that might be expected, data from a discharge measurement on August 21, 1982, are compiled in table 17. For each of 22 verticals, U_* was computed from equation 11 and τ from equation 9. The data from vertical 1,270 could not be used. There are rock outcrops along the right bank, and perhaps these obstructions account for the peculiar velocity distributions observed near the bank.

The cross section is plotted in figure 46*A*, and the average shearing stress and individual values of the shearing stress at each vertical are shown in figure 46*B*. The individual values range from 2 to 1,000 g/cm/s^2 (equivalent to dynes per square cm), but the average of all values, 184, is close to the value computed from mean depth and local slope from figure 43, 180 g/cm/s^2. The average of individual values of U_*/U is 0.0671; the average for the cross section based on mean velocity of 1.94 m/s, is 0.0691. The predicted value based only on mean grain size from Dawdy's empirical relation, equation 12, is 0.0721. The agreement between the three values is quite remarkable but may be fortuitous. The relatively low value of U/U_*, 13.9, suggests that most of the roughness in this section at high flow is grain roughness.

The concentrations of suspended sands for depth-integrated samples collected at six verticals are plotted on figure 46*C*. The lower concentrations along the right half of the channel correspond roughly to the part of the channel with lower shearing stresses, but there is no definite correlation. A comparison of local shearing stress with size of bed material (Nordin, Meade, and others, 1983, table 14) shows no tendency for larger bed sizes to be associated with larger local shearing stresses. This is not surprising; the bed size is likely to reflect the long-term average shearing stress, because the changes in the bed sediments probably will lag changes in the bed stress. The heavier particles because of their inertia cannot react instantaneously to changes in the forces acting on them. The suspended sediments should respond fairly quickly to changes in the shearing stress and in the ratio U/U_*, but because the particles are being convected along at approximately the mean stream velocity, the concentration and size of suspended particles at any vertical will reflect upstream conditions rather than the instantaneous local shearing stress.

In previous discussion, it was assumed that $U=20\ U_*$ based on a particle size of 0.25 mm. The larger particle size at Musinacio of 0.42 mm results in the lower value of $U=13.9\ U_*$. If this ratio is known for any section of the river, the velocity scale on figure 40 can be shifted accordingly.

Relations between Sediment Discharge and Flow

As a final consideration of sediment transport by the river, it is useful to develop some approximate relations between water discharge and sediment discharge for the two idealized sections characterized by equations 18 and 20. Because of the sparse hydraulic data and uncertainties about water surface slopes for the narrow reaches of the river, extensive computations are not justified. Instead, the simple relation proposed by Engelund and Hansen (1967) will be used. Their transport equation is

$$f\phi = 0.1\,\theta^{2.5} \quad , \tag{21}$$

where f is a friction factor,

$$f = \frac{2gDS}{U^2} \quad , \tag{22}$$

ϕ is dimensionless transport function,

$$\phi = \frac{q_T}{\left[\left(\frac{\rho_s-\rho}{\rho}\right)g\,d^3\right]^{1/2}} \quad , \tag{23}$$

Table 17. Summary of data from discharge measurement, August 21, 1982, and computation of U_* shear velocity
[Leaders (---) indicate values not determined]

Cross-channel station (meters)	Depth, D (meters)	Mean Velocity U (centimeters per second)	Velocity, (centimeters per second) U_2	U_1	Distance from bed (meters) z_2	z_1	Shear velocity U_* (in centimeters per second)	$\frac{U_*}{U}$	τ (grams per centimeter per second squared)	Concentration of particles >0.062 millimeters (milligrams per liter)
158	14.6	58	78	38	11.68	2.92	11.5	0.199	133	57
272	22.5	173	190	156	18.00	4.50	9.8	.0567	96	---
316	22.5	174	208	140	18.00	4.50	19.6	.112	372	57
345	24.0	178	205	150	19.20	4.80	15.9	.0892	251	---
422	25.0	210	230	189	20.00	5.00	11.8	.0563	139	---
455	30.0	220	235	205	24.00	6.00	8.7	.0394	75	61
497	27.0	196	215	176	21.60	5.40	11.2	.0574	126	---
561	31.0	202	232	171	24.80	6.20	17.6	.0871	308	---
584	32.0	170	195	146	25.60	6.40	14.1	.0832	199	---
654	33.6	218	273	163	26.88	6.72	31.7	.146	1000	---
694	35.0	213	241	185	28.00	7.00	16.2	.0759	260	---
742	36.6	213	223	203	29.28	7.32	5.8	.0271	33	21
798	36.5	233	242	224	29.20	7.30	5.2	.0223	27	---
839	37.5	212	242	182	30.00	7.50	17.3	.0817	298	---
893	36.5	230	249	211	29.20	7.30	11.0	.0477	120	---
935	35.8	202	215	189	28.64	7.16	7.5	.0371	56	---
1,008	33.5	225	272	222	26.80	6.70	1.4	.0064	2	17
1,032	35.5	214	231	198	28.40	7.10	9.5	.0445	90	---
1,098	31.8	190	200	180	25.44	6.36	5.8	.0304	33	---
1,143	33.5	177	199	155	26.80	6.70	12.7	.0718	161	---
1,212	40.4	168	197	140	32.32	8.08	16.4	.0979	269	---
1,235	24.0	182	184	179	19.20	4.80	14.4	.0079	2	2
1,270	20.5	148	100	201	16.40	8.20	---	---	---	---
							Average of 22 values --------	.0671	184	

Θ is the dimensionless shearing stress at the bed,

$$\Theta = \frac{\tau}{(\rho_s - \rho)\, g\, d} \quad , \qquad (24)$$

q_T is the volume flux of sediment particles per unit width of channel, and d is the median diameter of the bed sediment. Engelund and Hansen used median fall diameter instead of sieve diameter for d in both equations 23 and 24. For naturally worn fine to medium sands, the differences are not very great (Federal Inter-Agency Sedimentation Project, 1957, fig. 7), but for coarse sands and fine gravels, the fall diameters are considerably less than the sieve diameters, depending mostly on particle shapes. By inspection of equation 21, it can be seen that for any given flow conditions, $q_T \sim 1/d$, and it is our experience that if the bed sediment is coarser than about 0.7 mm, equation 21 overestimates the sediment discharge if the smaller fall diameters are used instead of sieve diameters. Therefore, in the following computations, sieve diameters will be used.

Predictions using equation 21 agree very well with observed sediment discharges for both laboratory and field data so long as the range of grain sizes in the bed sediments is small enough for the mixtures to be characterized by their median diameter, d_{50} (Yang and Stall, 1976; Brownlie, 1981). However, if σ is much greater than 1.5 for log-normal distributions or if the distributions are skewed toward coarser sizes, which they usually are for river bed sediments, the mixtures should be characterized by some kind of "effective" diameter, d_m. This was first proposed by Meyer-Peter and Muller

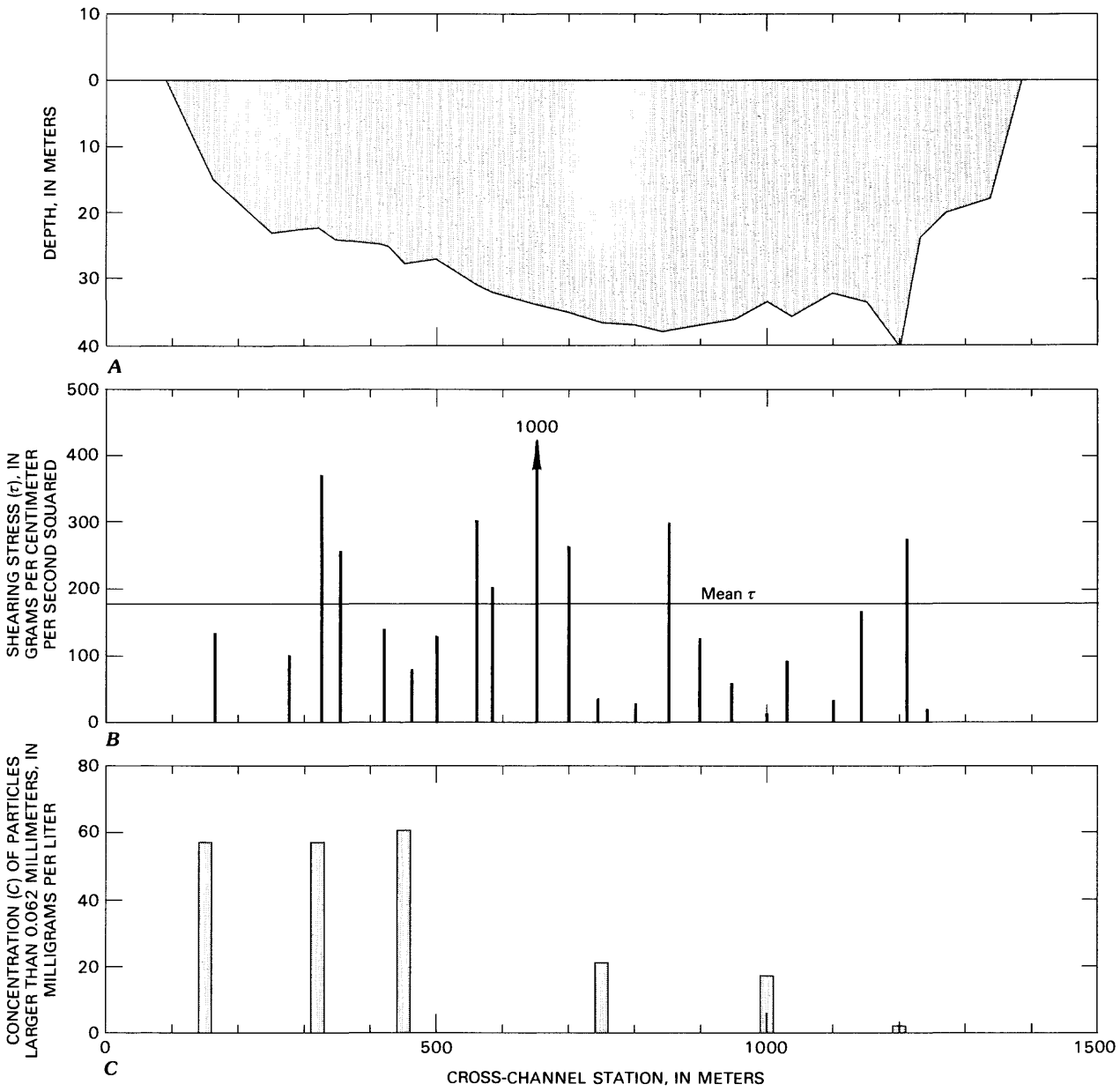

Figure 46. The U.S. Geological Survey measuring section at Musinacio. *A*, The cross section; *B*, the local shearing stress estimated from equation 11; and *C*, concentrations of suspended sands.

(1948), who defined an effective diameter as

$$d_m = \sum f_i \, d_i \quad , \tag{25}$$

where f_i is the fraction by weight of particles with mean diameter d_i. However, equation 25 doesn't seem to work very well—the effective diameter is too small. For applying the Engelund-Hansen equation to mixtures, we propose that the effective diameter should be computed from

$$d_m = \left(\sum f_i \, d_i^{\,3/2} \right)^{2/3} \quad . \tag{26}$$

The diameter from equation 26 is used in both Θ and ϕ. For the average size distribution curve of figure 45, the effective diameter is 0.91 mm.

Table 18. Data used to compute sediment discharge for a typical wide section

Water discharge (cubic meters per second)	Width (meters)	Velocity (meters per second)	Depth (meters)	Slope
7,000	2,420	0.67	4.31	0.0000320
15,000	2,500	0.86	6.97	0.0000403
25,000	2,550	1.02	9.61	0.0000469
50,000	2,620	1.28	14.9	0.0000578
70,000	2,660	1.43	18.4	0.0000639

Computations of sediment discharge were made for a narrow section at river km 652 using the observed data in table 15. For the wider section, river km 655, the values of width, depth, velocity and slope in table 18 were selected from the hydraulic geometry plots of figure 43. At both sections, the average local slopes are from equation 17.

Results of the calculations are plotted on figure 47. The curves intersect somewhere below 4,000 m^3/s, so the calculations predict that the sediment discharge at river km 652 will be greater than the sediment discharge at river km 655 about 95 percent of the time. Applying the flow frequencies of table 3 to the curves, the estimated annual sediment loads are approximately 34×10^6 Mg/y at the wide section and 54×10^6 Mg/y at the narrow section.

On the average, there should be continuity of sediment discharge along a river. The problem with the curves in figure 47 arises from using the same values of local slope along both reaches. If the average topographic slope is 5 cm/km, the extreme low or high values of local slope of 2 cm and 8 cm/km cannot persist over very long reaches. There must be local slope reversals along the river, somewhat as sketched in figure 48*A*. These kinds of slope reversals with changing stage seem to be common to all rivers (Seddon, 1900). The slope reverses between pools and riffles on gravel-bed streams, between bends and crossings on meandering streams, and between wide and narrow sections of relatively straight rivers like Río Orinoco. According to Seddon (1900), a riffle or crossing in a river acts as a weir, but a section like El Infierno, which is narrow and deep because of bed rock, acts as an orifice. The very narrow, deep reaches of the Río Orinoco such as El Infierno, Punta Angostura near Ciudad Bolívar, and Punta Cuchillo near Ciudad Guayana are presumed to be flowing through old channels cut in the bed rock during times of lower sea level.

It is fairly easy to show that slope reverses in reaches of the river upstream of Cabruta, where the gages are spaced uniformly along the stream. For

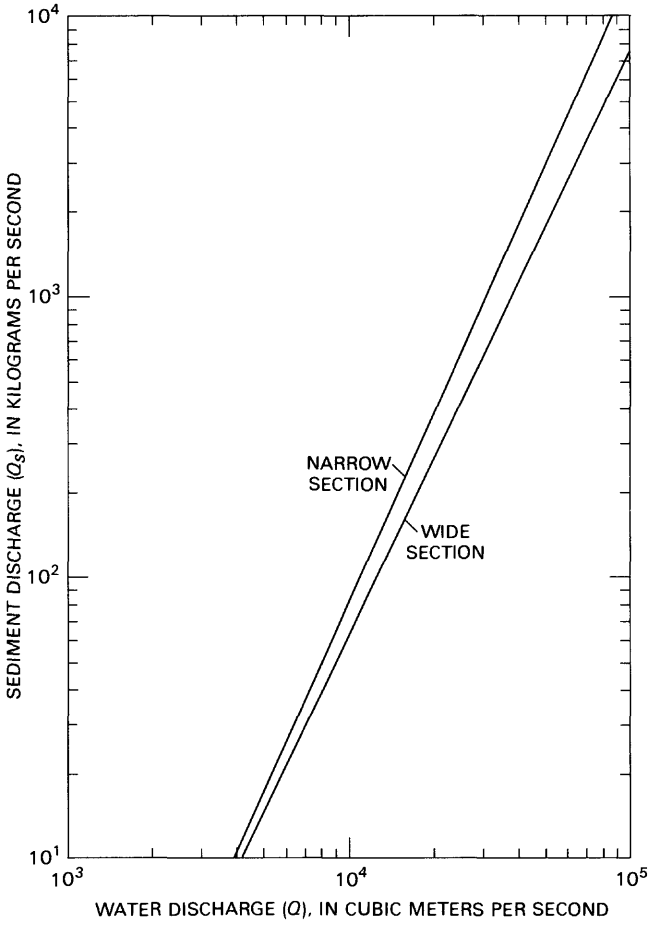

Figure 47. Relations between sediment discharge and water discharge for a wide and narrow section computed using local water-surface slope.

example, figure 49*A* shows the stage hydrographs for several years for the gages at El Burro (river km 930), Parguaza (river km 908), and Las Ventanas (river km 887). The slopes at highest and lowest stages for 1972 and 1973 are plotted in figure 49*B*. The slope reversals are clear. Downstream of Cabruta, the gages seem not to be spaced uniformly enough to detect this same kind of reversal. For example, the reach from Musinacio to El Infierno is 5 times as long as the reach from El Pinal to Musinacio that was used to determine local slope for the preceding computations. When stages are plotted for these three stations, there is no evidence of slope reversal in the lower reach, probably because the reach is too long to detect the local water-surface changes. If the gages were more closely spaced below Musinacio, we believe the local slopes would behave about the same as those shown in figure 49*B*.

The local slope plotted in figure 41 should apply to the wide section at river km 655, as it is within the

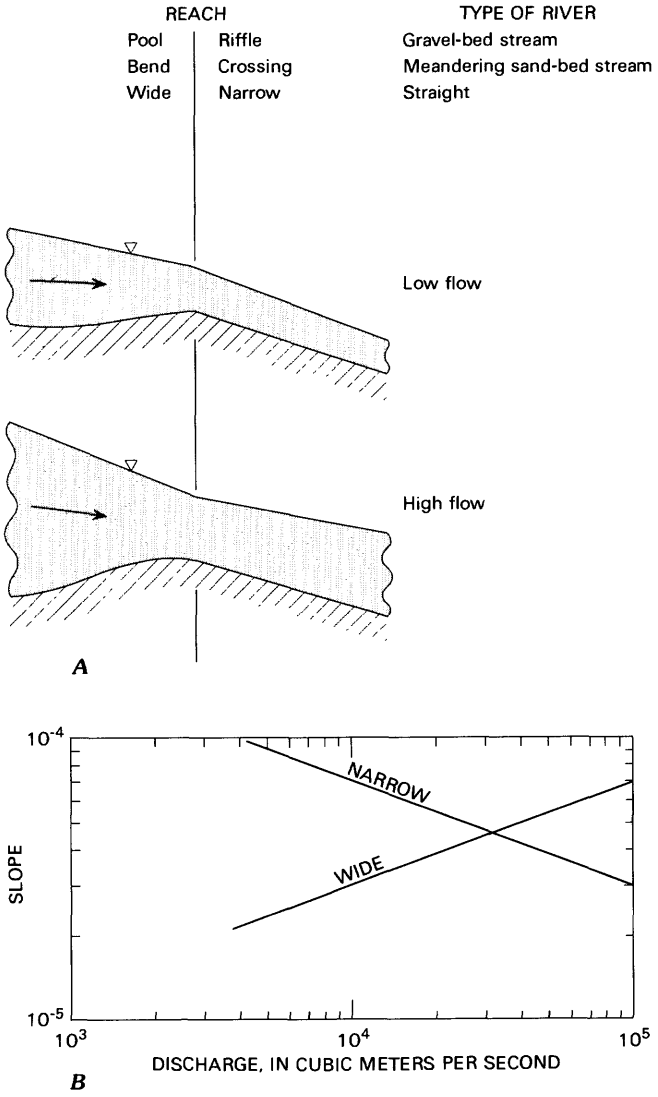

Figure 48. Water surface-slope reversals along a river. *A*, According to Seddon (1900); *B*, postulated for the reach near Musinacio.

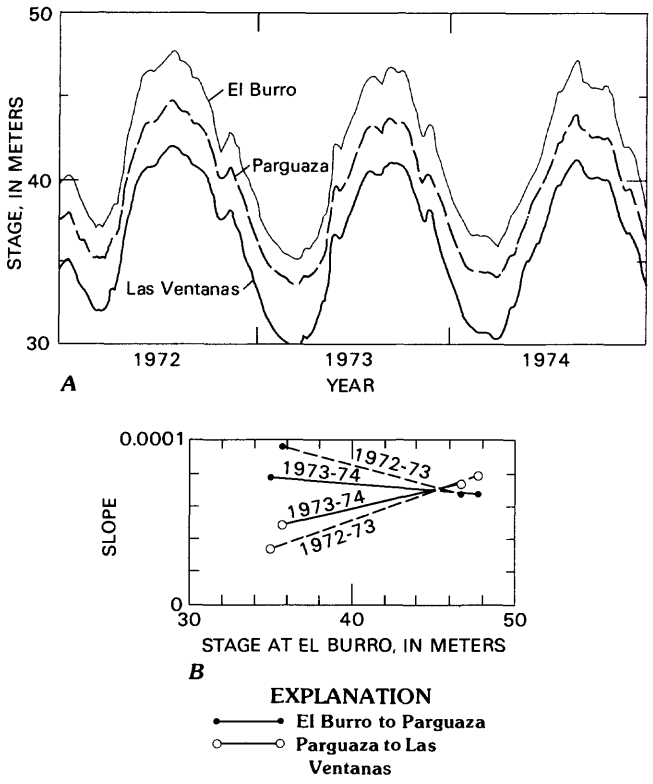

Figure 49. *A*, Stage hydrographs for three stations. *B*, Water-surface slopes at lowest and highest stages.

reach where slope was measured. The narrow section at river km 652, though, is probably in a reach where slope trends are the reverse of those along the wider reach. The relation postulated for this narrower reach is shown in figure 48*B*, as is the mean curve of local water-surface slope from figure 41.

Using these slopes in the calculations, the transport relations shown in figure 50 are estimated. The mean annual sediment loads for the sections are now computed at 34×10^6 Mg/y for river km 655 and 31×10^6 Mg/y for river km 652, a fair agreement. The average of the two curves shown by the dashed line should represent the mean condition if one were to apply average hydraulic conditions over a long reach that included representative cross sections from both wide and narrow parts of the river.

According to the relations of figure 50, the wider sections of the river will fill relative to the narrow sections during periods when flows are less than 40,000 m^3/s, and they will scour relative to the narrow sections for flows greater than 40,000 m^3/s. This would account for the observations that bed sediments in June at river km 652 were finer than later in the year.

The curves of figure 50 of course are only approximations. The observations of Pérez-Godoy (1982) and Meade and others (1983) show that the sediment rating curves for Río Orinoco are looped, with larger sediment discharges on rising then falling stages. This looped sediment-rating curve reflects mostly the storage and re-entrainment of wash load and finer bed sediments, and the calculations using average hydraulic relations cannot reflect these complications. Pérez-Godoy (1982), using the modified Einstein method, estimated the bed load plus suspended-sand discharge of the river at Musinacio to be 35×10^6 Mg/y. The

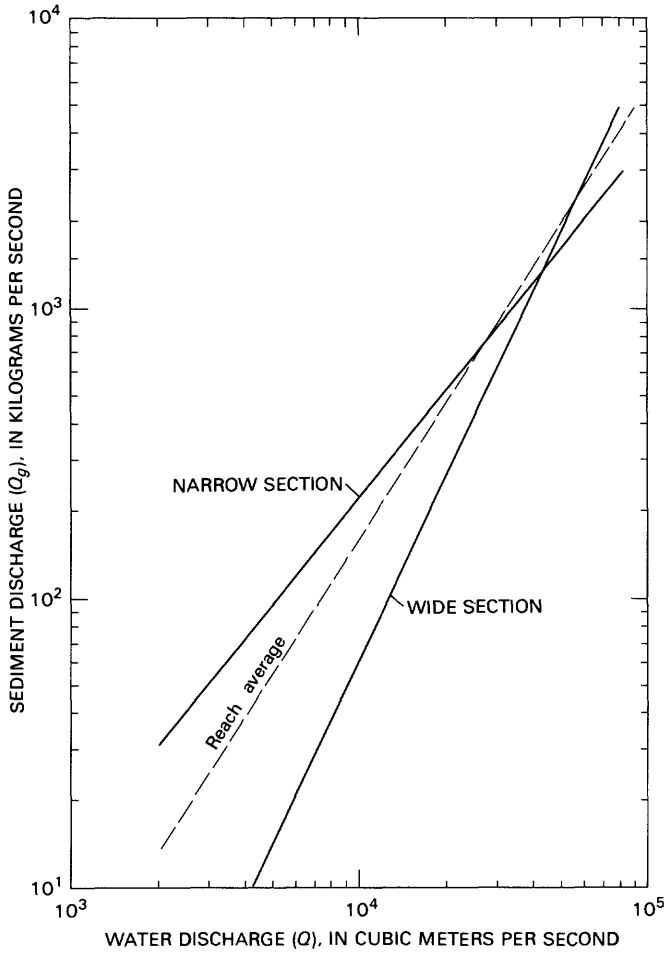

Figure 50. Relation between sediment discharge and water discharge computed using slopes of figure 48.

computations with the Engelund and Hansen (1967) equation are in good agreement with his estimate.

LAG DEPOSITS AND ARMORING

The surfaces of most of the bars contained lag deposits and were armored. This condition clearly resulted from deflation by wind action on some bars, but appeared to result from hydraulic action during the high flows on a few bars.

Armoring by Wind

The most striking example of wind armoring was at site A (fig. 7), where a few observations were made during both 1982 and 1983. Observations were confined to the downstream end of a large bar that occupied approximately the right one-half of the active channel. Plan and profile views of the downstream part of the bar as it appeared in 1982 are sketched in figure 51. The face of the bar and the crests of the sand waves forming it generally were perpendicular to the downstream direction (fig. 51*A*), suggesting that the flows over the bar mostly were parallel to the banks. The face and the back of the bar across the several downstream sand waves were armored by wind action.

The height of the bar from water surface to crest was 4.3 m (fig. 51*B*), and the heights of the sand waves varied from 0.8 to 1.5 m. Shallow trenches were dug at the crest and toe of the bar to reveal the underlying cross-stratification, and the angles of the slip faces measured with a Brunton compass were 28.5° at the crest and 27° at the toe. The strata appeared to be continuous along the 9-m length of the face, although we did not trench along the entire face to confirm this. However, later detailed examinations by McKee (1989) showed that the strata of the downstream faces of similar bars generally were continuous.

Near the toe of the bar beneath the water surface, small ripples oriented upstream had been formed by wind-generated water waves; these features were 20–30 cm in wavelength and about 1 cm high. On the back of the bar in the intercrest areas downwind of the bar face, accumulations of coarser sands and fine gravel were formed into long-crested, ripple-like features that were called pebble ridges by Bagnold (1941) and granule ripples by Sharp (1963). These pebble ridges were 50–70 cm from crest to crest and 2 or 3 cm high. The crests were parallel to the crests of the larger sand waves; that is, perpendicular to the channel, indicating that the winds that formed them blew generally upriver.

The plan form of the bar and the orientation of the crest lines over it in 1983 (fig. 52) suggest that the flow patterns over the bar during 1983 were much more complicated than during 1982. Apparently some fairly strong cross-channel flow patterns developed during the 1983 flood season.

The armor layer in 1982 contained substantial amounts of gravel with particles as much as 16mm in diameter, as shown in figure 53*A*. In 1983, the sizes of materials armoring the bar were smaller, and a large pebble ridge had formed right at the crest of the bar (fig. 53*B*). Smaller pebble ridges almost at right angles to the crest line had formed down the face of the bar (fig. 53*C*) and in the intercrest areas over the back of the bar, indicating that strong winds in 1983 had blown cross-channel from right to left bank. The downstream face of the bar in 1983 showed several bands of fine light sand (fig. 53*D*) where wave action from upstream winds had modified the appearance and slope at the toe of the bar.

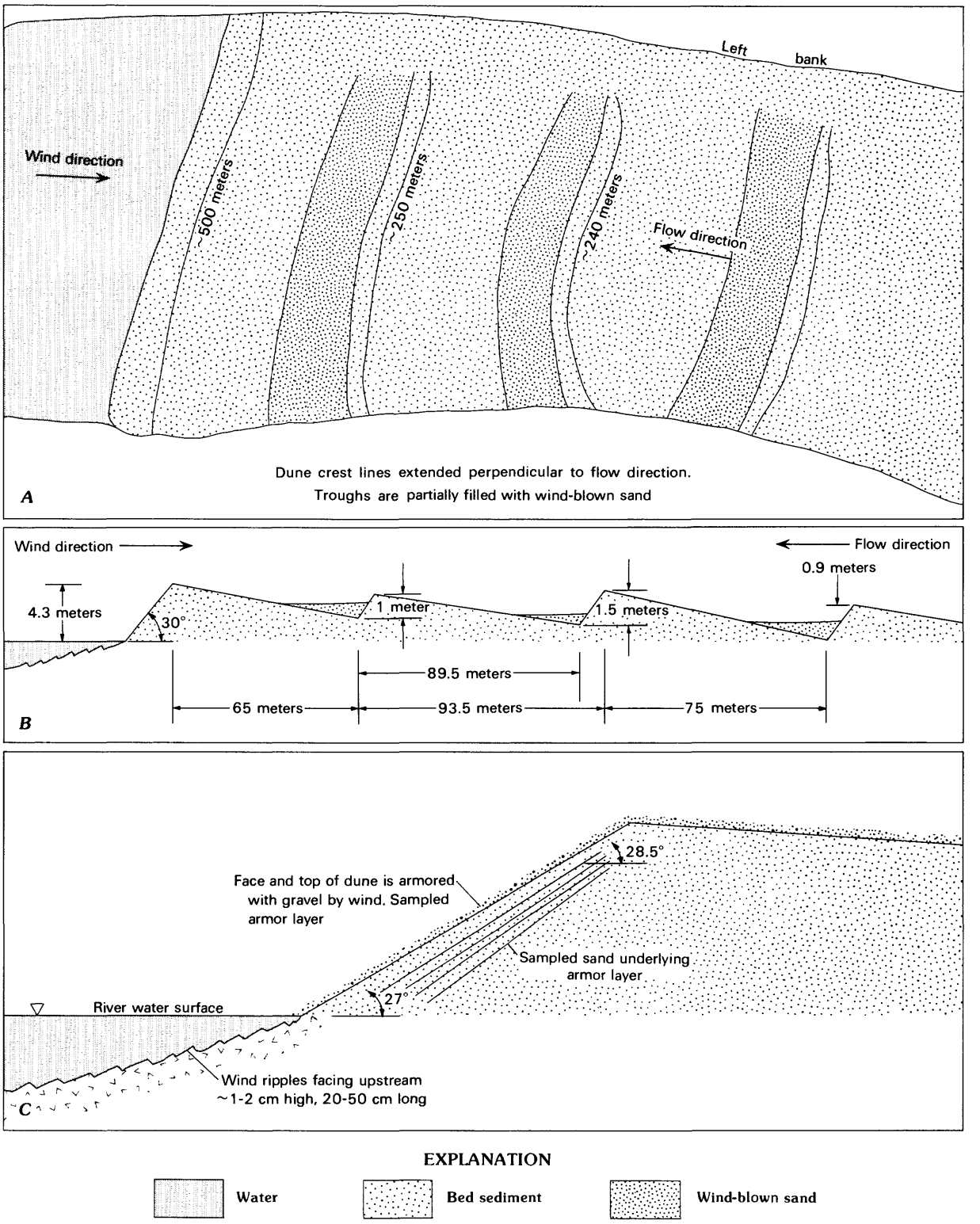

Figure 51. Sketch of the bar at site A, 1982. *A*, Plan; *B*, profile; *C*, profile, downstream slip face.

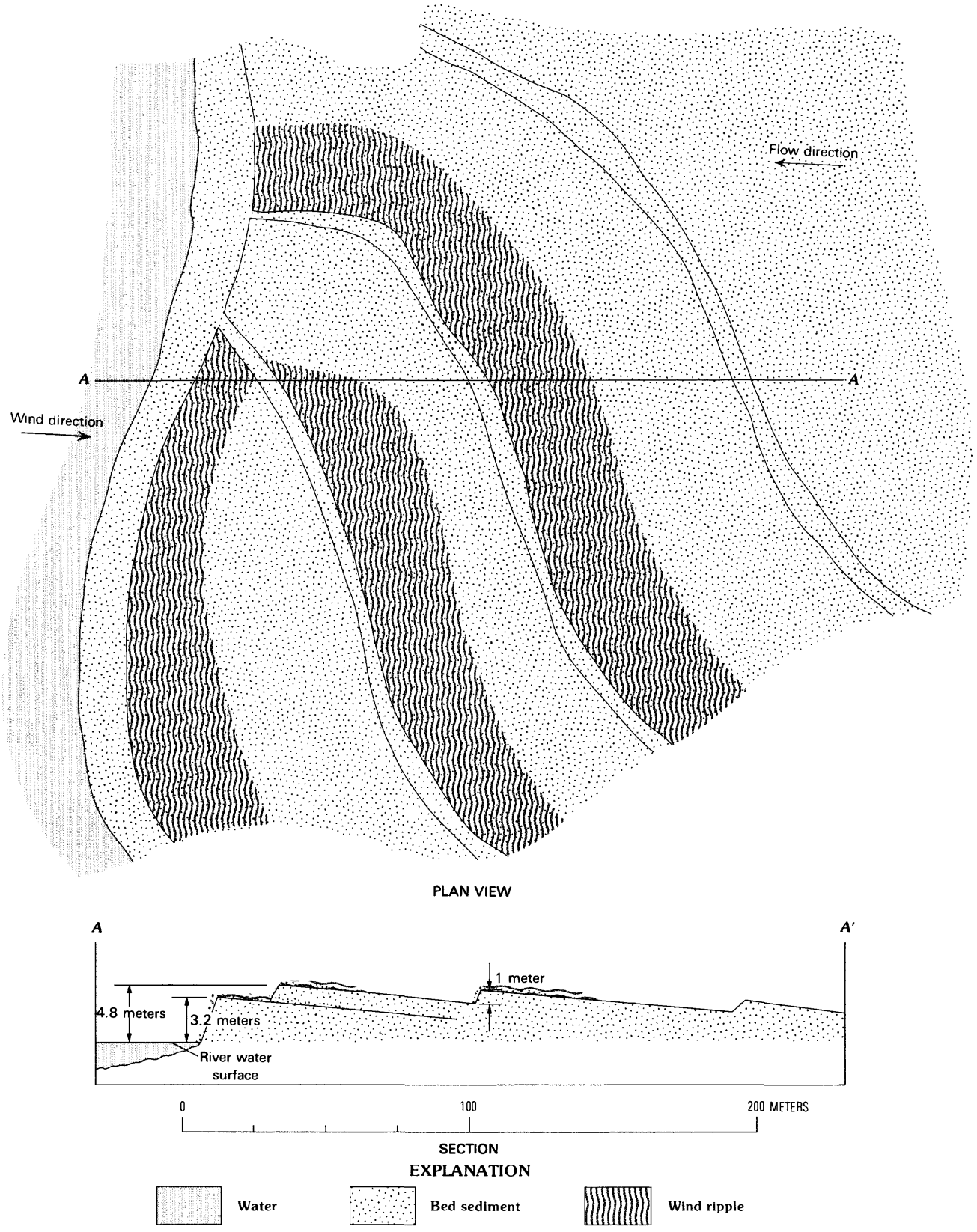

Figure 52. Sketch of the bar at site A, 1983.

The face of the bar above the bands of sand shown in figure 53*D* was armored by wind action, whereas the lower part of the bar was not, suggesting strong winds early in the flow recession but not later as the water dropped, uncovering the toe of the bar.

The particle-size distribution for the armored layer shown in figure 53*A* is plotted in figure 54, as well as size-distribution curves for the underlying material and for the bed-material sample collected at station 8, a few kilometers downstream of site A. The channel bed material and the material underlying the armor layer contain only small quantities of gravel (less than 4 percent), whereas the armor layer contains 52 percent gravel. Most of the material between 0.5 and 2.0 mm presumably was removed from the suface by the wind.

The size distribution of the armoring in 1983 at this site is shown in figure 55. Fifty percent of the material is coarser than 1 mm, but only 3 percent is gravel. At the pebble-ridge crest, 83 percent of the material is between 1 and 2 mm.

The cumulative distributions of figures 54 and 55 are replotted as relative frequency bar graphs in figure 56. The difference in the size distributions of the armored layers for the 2 years is striking. In 1982, the median size of the armor was between 4 and 8 mm, whereas in 1983 it was between 0.7 and 2.0 mm.

The strengths of the winds that formed the pebble ridges are fairly easy to determine. According to Bagnold (1941, p. 156), for pebble ridges to persist, the wind must never reach the threshold strength at which it can begin to dislodge the crest grains. The geometric-mean size of the crest grains is about 1.4 mm, so from figure 33, we infer that wind speeds at 1 meter above the surface did not exceed 11 m/s.

The coarse sand and fine gravel forming the pebble ridges do not move by saltation; rather, these particles move by surface creep imparted by the impact of finer grains moving in saltation. The momentum of a particle impacting from saltation is great enough to impart movement to particles whose diameters are equal to 6 times that of the saltating particle (Bagnold, 1941). Thus, a pebble surface can be formed by the momentum of saltating grains composed of medium sand.

The size distribution of the armor layer of March, 1982 (fig. 56*A*) is a bit more difficult to interpret, but surely the winds that formed it were much stronger than the winds of 1983. The geometric-mean size of the armor layer is close to 8 mm, and from figure 33, these size particles should armor the bed with wind speeds of about 20 m/s.

In a previous section, we assumed that 50 percent of an erosion surface should be covered with nonmoving particles in order to effectively protect the surface from further erosion. This value was based on empirical observations that seem to apply for the armoring of a streambed by flowing water (Harrison, 1950). However, the appearance of the armor layer in 1982 (fig. 53) suggests that the value of 50 percent is too large for a flat erosion surface. Even where the surface is not flat, but rather is covered with granule ripples, the value of 50 percent probably is too large. Sharp (1963, p. 634–635) observed that "a concentration of larger grains giving a surface coverage of at least 50 percent in the crestal area seems required before granule ripples become well developed" and "Large grains compose no more than 10–20 percent of the surface material in the troughs of the granule ripples, the rest being average dune sand." Our observations of grain-size distributions from the ripple crest and the armor layer (fig. 55), which would correspond roughly to the surface material in the troughs, agree exactly with Sharp's observations. More than 50 percent of the ripple crest is composed of material coarser than 1.4 mm, whereas only about 24 percent of the armor layer is coarser than 1.4 mm.

The kind of armor layer that will form under conditions of strong wind transport seems very difficult to predict analytically because, ultimately, it involves the random placement of a random number of particles over the erosion surface. The sizes of the material composing the armor layer can be specified, though; they must be larger than the threshold size that can be moved by the strongest winds that blow during the dry season.

For a highly idealized case, the fraction of the bed that can be sheltered by a given size particle can be estimated. The most efficient armoring occurs when there is no overlapping; that is, no two particles shelter the same area, so the fraction of the bed sheltered by a single particle should give an approximate lower limit for the fraction of the bed that needs to be covered with nonmoving particles in order to check further erosions.

Bagnold's (1941) qualitative observations on particle saltation and surface creep contain all the essential information needed to make the computations. Bagnold observed that saltating particles of size d_s could impact the bed with sufficient force to impart movement by surface creep to particles of size $d_a = 6\ d_s$. Not all saltating particles can do this; only the particles whose trajectories carry them high into the flow will attain sufficient momentum. They will strike the bed at the

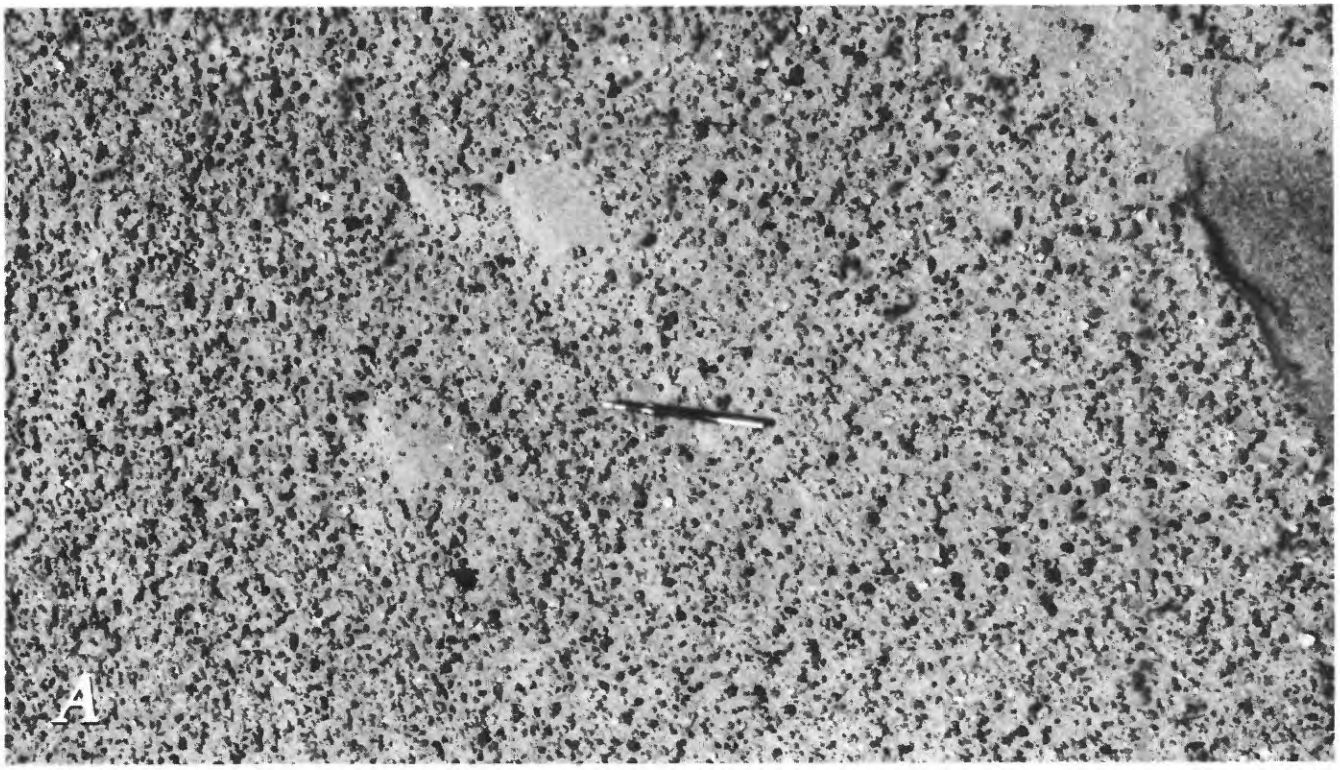

angle α to the horizontal, and if they have spent sufficient time in the flow, their downward velocity will be their terminal fall velocity and their horizontal velocity will be approximately equal to the mean wind speed through the upper part of their trajectory.

For purposes of computation, we consider the sheltering effect of a particle of size d_a with a threshold impact velocity V_c measured 100 cm above the bed. V_c is from figure 33. The saltating particles have a diameter of $d_s = d_a/6$, and they strike the bed at the angle α, where

$$\tan \alpha = \frac{\omega}{V_c} \quad . \tag{27}$$

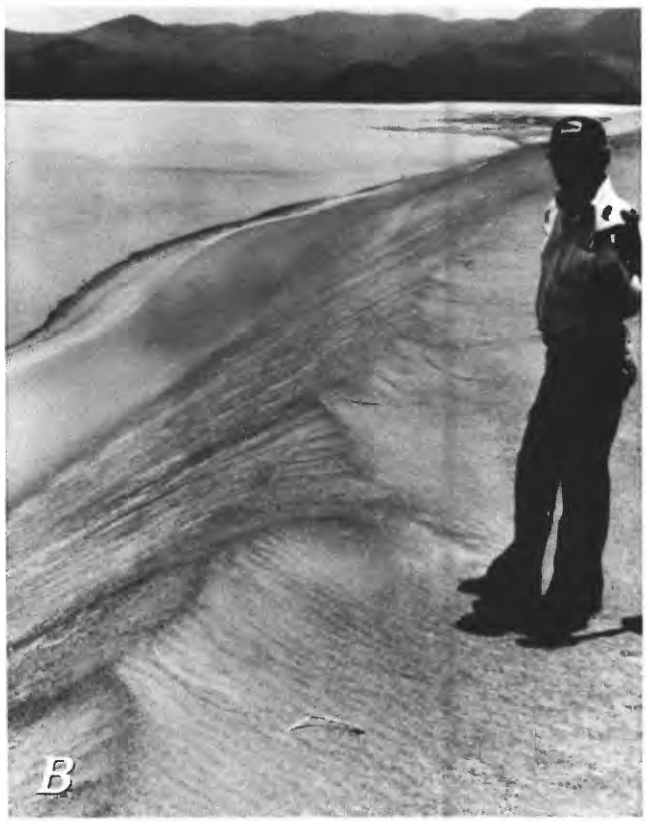

Figure 53 (above and facing page). Photographs of the bar at site A. *A*, Wind armor in 1982 (pen is about 15 cm long); *B*, large pebble ridges along the face of the bar in 1983; *C*, small pebble ridges along the downstream face of the bar; *D*, wave action has modified the appearance and slope of the bar face. Note the turtle nest and tracks in center of photograph.


C


D

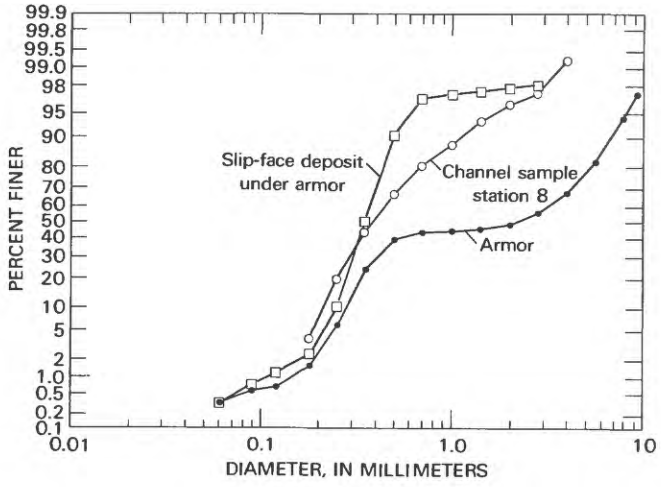

Figure 54. Particle-size distribution of the armor layer, the underlying sediments, and the channel samples at station 8, 1982.

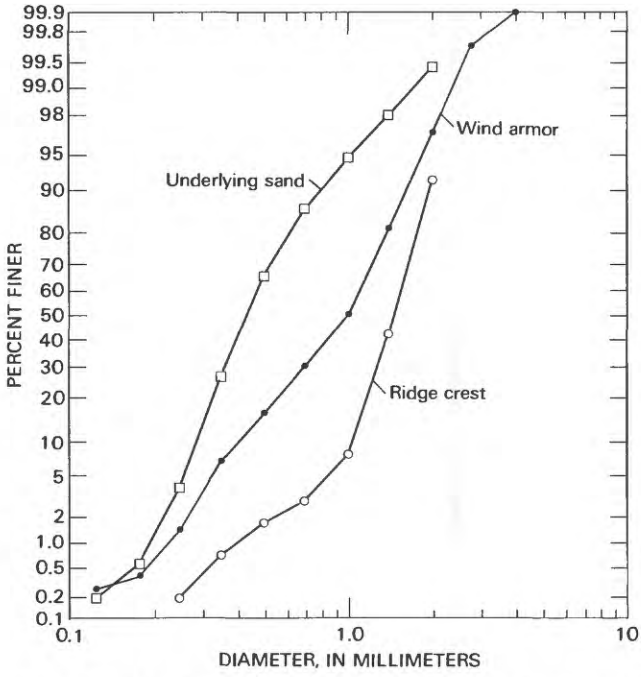

Figure 55. Particle-size distributions of the wind armor and pebble-ridge crest, 1983.

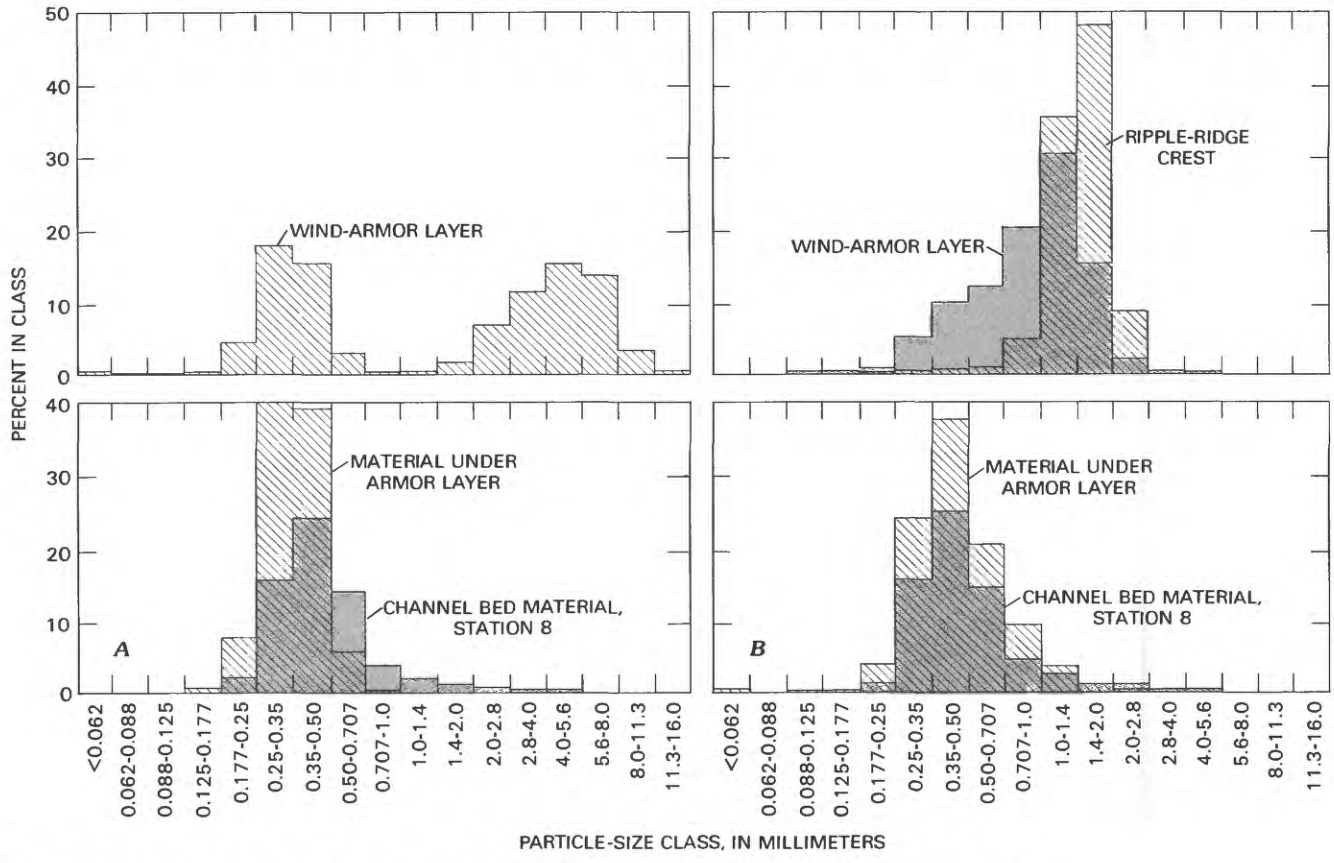

Figure 56. Relative-frequency histograms of the data in figures 54 and 55. *A*, 1982; *B*, 1983.

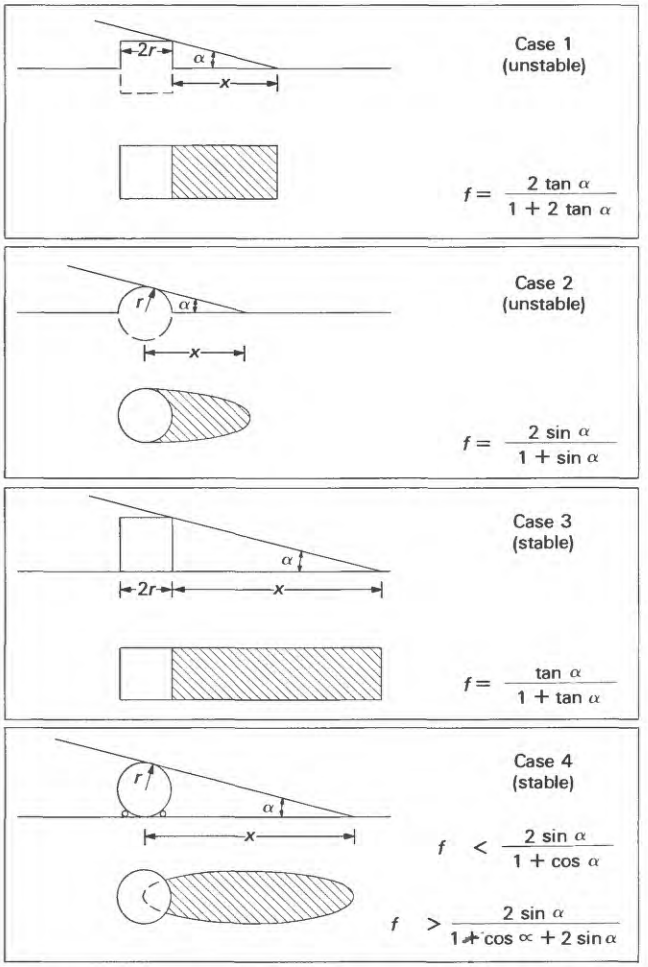

Figure 57. Ideal cases for the fraction of the bed, *f*, that needs to be covered with nonmoving particles in order to protect the surface from further erosion.

The fall velocity, ω, is taken for d_s from figure 35. The fraction, f, of the bed that needs to be covered by particles of size, d_a, in order to protect the surface from further erosion is the ratio of the projected area of the particle, A_p, to the total area of the bed, A_s, that is sheltered from the saltating particles,

$$f = \frac{A_p}{A_s} \quad . \tag{28}$$

Only two particle shapes are considered, a sphere and a cube, assuming naturally worn particles fall somewhere between these extremes.

It turns out for these ideal conditions that f depends on d_a, on particle shape, and on the degree of particle exposure; that is, on whether or not the armoring particle is partially buried in the bed.

The four ideal cases for which computations were made are sketched in figure 57. The computations are summarized in table 19. The values of f shown for each case depend only on the angle, α. The first two cases are considered unstable because if the winds persist long enough, saltating particles striking upwind of the armoring particle will continue to erode the bed until case 3 or case 4 obtains. These cases are considered stable in the sense that additional erosion of the bed only will occur if the wind velocity increases sufficiently to move the armoring particles. Case 4, of course, would not be stable on a perfectly flat surface, but on any erosion surface there always will be a few small particles around the lower part of the sphere to prevent it from rolling easily.

Values of f for the first three cases are exact; they follow from simple geometry. Case 4 is not so simple, because it will depend to some extent on the placement of smaller particles around the sphere that keep it from rolling, and this cannot be specified. However, it is fairly easy to specify upper and lower limits for f. The sheltered region is an ellipse with area $A_e = \pi r x / 2$, so

$$\frac{A_p}{A_p + A_e} < f < \frac{A_p}{A_e} \quad . \tag{29}$$

where r is $d_a/2$ and x is the major axis of the ellipse shown in figure 57.

Values of d_a and f are plotted against wind speed in figure 58. The curves have similar shapes for all cases, their positions along the ordinate depending on particle shape and degree of particle exposure. At high wind speed, the curves approach asymptotically their upper limiting values. Case 3 and the lower boundary of case 4 are of most interest; they represent the ideal lower limit for the fraction of the bed to be covered by nonmoving particles to check further erosion. The two curves are almost identical; they show that at great wind speeds the bed can be completely protected with less than 25 percent of its area covered with nonmoving particles. The highest limit, case 2, requires a fraction of about 45 percent, but as suggested, this case is unstable; if the winds persist and there is an adequate supply of saltating particles, the curve would shift toward case 4 as more and more small particles are eroded upwind of the nonmoving armor particle.

The shapes of the curves are a bit surprising in that a much smaller fraction of the bed needs to be covered with nonmoving particles to armor its surface for low

Table 19. Values used to compute the curves of figure 58

Size of armor particle d_a (centimeters)	Critical wind speed, V_c (centimeters per second)	Largest saltating particle, $d_a/6$ (centimeters)	Fall velocity, ω (centimeters per second)	Impact angle α (degrees)	Tan α
0.1	950	0.0167	95	5.71	0.100
0.2	1,250	.0333	210	9.54	.168
0.3	1,480	.0500	305	11.64	.206
0.4	1,650	.0667	385	13.13	.233
0.6	1,920	.100	510	14.88	.266
0.8	2,140	.133	600	15.66	.280
1.0	2,320	.167	670	16.11	.289
1.2	2,500	.200	740	16.49	.296
1.4	2,650	.233	800	16.80	.302
1.6	2,780	.267	855	17.10	.308

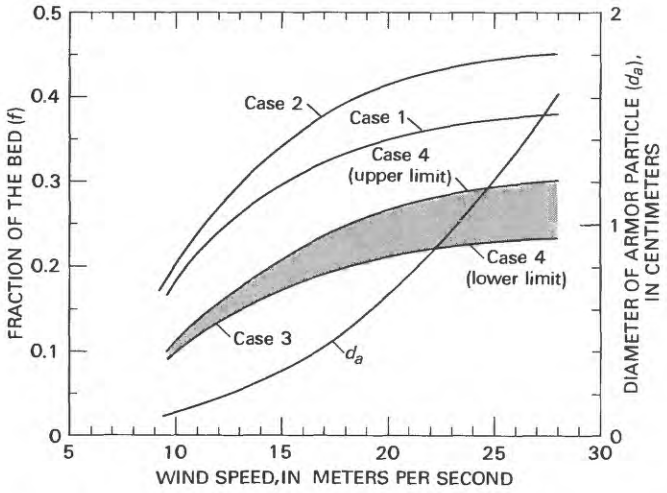

Figure 58. Fraction of the bed, f, covered by nonmoving particles of size d_a as a function of wind speed for the cases shown in figure 57.

wind speeds than is required for high winds. For example, at winds of 10 m/s, the bed can be armored with 10 percent of it surface covered with 1-mm-diameter particles, whereas at 25 m/s, the bed will armor with 23 percent of its surface covered with particles of 12 mm diameter.

The reason for this peculiarity is in the angle, α, which increases systematically with wind speed, as shown in figure 59. The range of computed values, from 6° to 17°, agrees fairly well with the range of observed values, from 10° to 16°, reported by Bagnold (1941, p. 16).

The smaller impact angle in the case of low wind speeds and finer saltating particles is explained easily by considering particle-fall velocities (fig. 35). For a given grain shape, the terminal fall velocity of small particles ($d < 0.1$ mm) varies as their diameter, whereas the terminal fall velocity of larger particles ($d > 0.3$ mm) varies as the square of their diameter; however, the impact threshold velocity shown in figure 33 bears almost a linear relation with diameter. Therefore, with increasing wind speeds, tan α increases and approaches a constant limiting value of about 0.32, close to the maximum value observed by Bagnold (1941).

The agreement between the predictions of figures 58 and 59 and the empirical observations of Bagnold (1941) and Sharp (1963) is encouraging. In addition, the general appearance of the erosion surface shown in figure 53*A* lends at least qualitative support; the fraction of the surface covered with armoring particles is not very large, probably not more than 20 or 30 percent.

The curves in figure 58 now can be used to estimate approximately the amount of degradation required for armoring. Consider for example a unit volume of the bed with a particle volume concentration of 0.6 and with the coarsest 5 percent by weight of the material consisting of particles of diameter $d_a = 4$ mm. The critical wind speed from figure 58 is 16.5 m/s, on average there will be almost one particle of size d_a per cubic centimeter of the bed, and when exposed by 1 cm of erosion, the particle will protect an area of the bed equal to A_p/f, where f from figure 58 is about 0.2. Thus, a particle of size $d_a = 4$ mm will protect 0.625 cm², so complete armoring should occur with less than 2 cm of erosion. If d_a is 2 mm, however, there would be 7 particles per cubic centimeter of the bed, the critical wind velocity is 12.5 m/s, and each exposed particle will shelter an area A_p/f, where f is about 0.15. Thus, 7 mm of erosion would expose enough particles to armor the surface.

The processes involved in armoring an erosion surface by wind are so complicated that one should not expect much correspondence between observations and

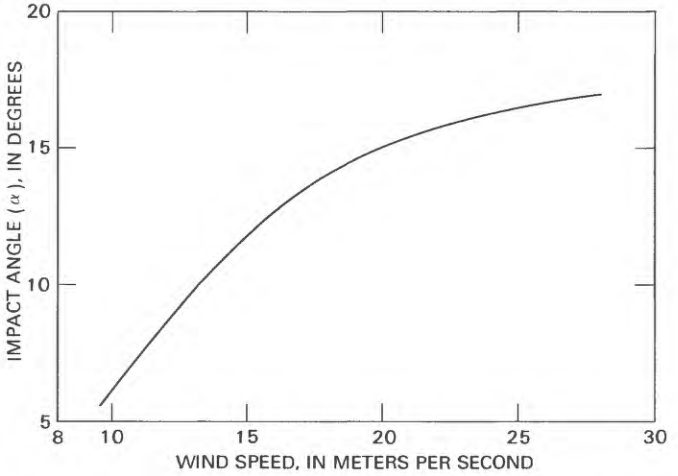

Figure 59. Relation between impact angle of saltating grains and the wind speed measured 100 centimeters above the surface.

the simple theories outlined here. In fact, it will be very difficult to extend either the collection of field data or the theory to accommodate some of these complications. For example, it is not clear how to sample the armor surface to obtain a meaningful particle-size distribution. Probably, an areal concentration determined by photographic techniques would be best. The bulk samples of figure 56 were simply scraped from the surface and contain both the armoring particles and the underlying matrix.

A second complication arises from the fact that the armor layer forms with time. If the initial surface is mostly fine sand, only a few of the particles will gain sufficient height in their saltation trajectories to attain horizontal velocities equal to the wind velocity and downward velocities equal to their terminal-fall velocities (Bagnold, 1941). These few particles are the only ones capable by virtue of their high momentum of initiating surface creep of the coarser particles in the bed, so initially the armoring process will proceed slowly. The percentage of particles moving in saltation above a given level increases with wind speed and depends strongly on particle shape (Williams, 1964); spherical particles on the average saltate higher than angular particles. Thus, the time progression of armoring must depend on both particle shape and wind speed.

As erosion progresses with time, more and more pebbles are exposed on the surface. The saltation process now is drastically modified, and a larger percentage of the saltating particles attain high trajectories (Bagnold, 1941, fig. 10). The impacting particles then will maintain a substantial surface creep of the coarser sediments, and the armoring should proceed rapidly until either the bed surface becomes protected or the supply of saltating particles is depleted. Thus, the length of time required to form the armoring depends not only on wind speeds and particle shapes but also on the initial size distribution of the deposit and on the supply of particles for saltation. For the exposed bars along the Río Orinoco, the supply of saltating particles depends on river stage. As the water surface drops, larger and larger areas of the bars are exposed to the wind, providing a continuous supply of sands for transport. At the downstream (upwind) end of a bar where a single continuous slip face exists, such as the one shown in figure 53, the situation is simple; there is no additional supply of sand beyond that of the face and the initial erosion surface. Downwind on the bar surface, though, the integrated effects of wind and water levels may be extremely complex.

Another major complication arises from the fact that the armor layer will consist of a range of particle sizes from d_a, the diameter corresponding to the maximum wind speed, to d_m, the maximum size in the bed-sediment mixture, and this range could easily extend over an order of magnitude or more. The final composition of the armor layer depends on the relative proportions of particles of size d_a and larger, assuming the wind persists long enough for a complete armor to form. The calculations for the curves in figure 58 assume that the armoring is due to a single particle of size d_a. In reality, there always will be a range of particle sizes, various degrees of overlapping of the areas sheltered from saltation, and various degrees of armor-particle exposure, ranging from partial burial to complete exposure.

Finally, the river environment is much more complicated than the desert environments where wind processes normally are studied. The effects of channel alignment, vegetation, river stage, and hydraulic sorting that lead to wide variations in particle sizes from place to place along the channel all must have substantial influences on wind transport and armoring. Large quantities of sands and finer sediments are blown from the exposed channel of Río Orinoco during the dry season, and deflation and armoring must control the amount of material eroded from many of the bars. However, quantities of wind-transported material cannot be estimated without additional information on wind speed and direction, areas of exposed surfaces, and size distributions of sediments exposed to the wind.

Armoring by Water and Hydraulic Sorting

Armoring by water is similar to armoring by wind. If the supply of sediment to a reach of a river is

checked—by the construction of a reservoir, for example—the clear water will scour the finer sediments from the bed until a layer of nonmoving particles forms that protects the underlying sediments from further erosion. The process is well described by Harrison (1950), and Shen and Lu (1983) presented methods for estimating approximately the size distribution of the resulting armor layer. In a river where there are no modifications to the incoming sediment load, there still may be reaches that are armored or paved with coarse immobile particles over which the incoming sediment moves. This armoring comes about usually in one of two ways. The more common process is where a steep tributary subject to infrequent floods dumps into a river a large quantity of sediments composed of particles coarser than anything that can be moved by existing flows. This sediment load commonly is the agent responsible for rapids and riffles in mountain streams. Another common process is where a stream cuts into old terraces deposited by the larger flows of ancient rivers and containing material too coarse to be moved by present flows. As the material is exposed, it simply paves the bed and the incoming sediment moves over it.

Neither of these processes applies generally to the Río Orinoco, although there are reaches downstream of Cabruta where the river is cutting into a formation that contains some medium to coarse gravel that probably cannot be transported by existing flows. More likely, though, if lag deposits or armoring occur, they are the result of local hydraulic sorting.

Hydraulic sorting downstream of obstructions is common in any river. This was discussed in connection with the rock outcrops along the right bank near Isla Chimborazo (fig. 20*A*), and at Las Culatas (fig. 27*A*). At those places, the sorting likely was dominated by the process of material settling out of suspension. What concerns us here is a different kind of hydraulic sorting—that which occurs in more or less unobstructed channels conveying variable inflows of water and sediment.

An example of lag deposits resulting from the action of the flow was investigated during March 1983, at an exposed bar near the gage of the Río Orinoco at Trapichote, just downstream of the confluence of the Río Ventuari and Río Orinoco (see fig. 7). The bar extended about 200 m across the channel near the center of the river and was 500–600 m long. The surface of the bar was covered uniformly with coarse sand and fine gravel (fig. 60*A*). Notice the difference in appearance between this surface layer and wind armor in figure 53*A*. Figure 60*B* is a view across the bar towards the right bank. The holes in the surface are attributed by local observors to sting- rays, so they were dug through the armor layer while the bar was under water. The size distributions of the surface layer and the underlying sediments are shown in figure 61.

There is fairly convincing evidence that the surface lag deposit was formed by water rather than wind. First, this location is far enough upriver that the trade winds are not very strong. There were no wind ripples, no gradients of surface particle size along the bar, and no evidence of strong wind action over the surface of the bar. Second, the surface layer was several grain diameters thick, and its appearance (fig. 60*A*) was quite different from the appearance of the wind armor (fig. 53*A*). Finally, the size distribution of the layer (fig. 61) is not at all similar to the distribution of the wind armor (fig. 54).

The hydraulic conditions over the bar during high flows are not known, but some rough approximations can be made. The water-surface drop though the rapids at Santa Bárbara is reported to be 34 cm/km (U.S. Army Corps of Engineers, 1943). Downstream of the confluence of Río Orinoco and Río Ventuari it probably is about one-half of that, say a slope of 0.0002. If the slope is approximately constant, the shear velocity varies with depth as shown in figure 62. Shown also on the figure are the largest size suspended and largest size moving as bed load from figure 40. At depths of 2–3 m, all sizes found in the bed (fig. 61) can be moved; particles as large as 0.4 mm, which represent about 20 percent by weight, can be moved in suspension. At depths of 1 m, particles coarser than about 2.5 mm would be immobile, nothing coarser than 0.25 mm would be suspended, and there would be a coarsening of the bed layer as armoring commenced. At 0.3 m depth, nothing coarser than 1 mm can be moved and only 3 percent (fig. 61) of the bed material (finer than 0.16 mm) could be suspended. Probably, then, the lag deposit forms during falling stages when depths are between about 1 to 0.3 m.

The mechanisms leading to the development of lag deposits under unsteady-flow conditions cannot now be specified; however, they are probably similar to the ones for equilibrium-flow conditions over a poorly sorted bed in a recirculating flume observed by Parker and others (1982). The material transported was the same composition as the bulk underlying bed, but because the finer part of the material moves in suspension at a greater velocity than the coarser bed material, the moving bed layer, which is several grain diameters thick, is considerably coarser than the underlying mixture. How this coarser bed layer could be preserved as the flow decreases is not clear, unless in some way the upstream supply of coarser suspended sediments is depleted so the

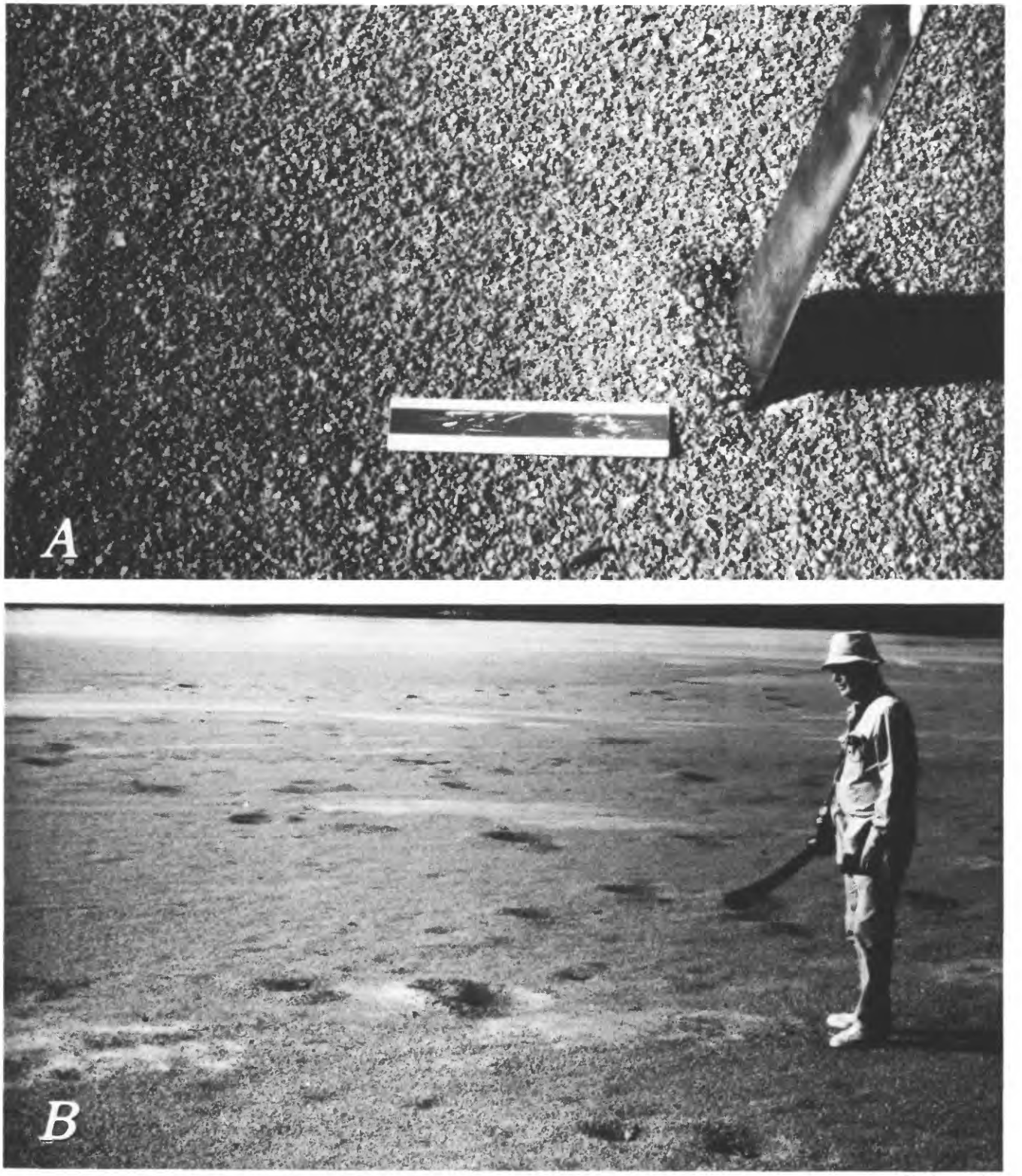

Figure 60. The bar at Trapichote. *A*, Close-up view of the armor surface; scale is 15 cm long. *B*, View across the bar. The holes are made by sting-rays.

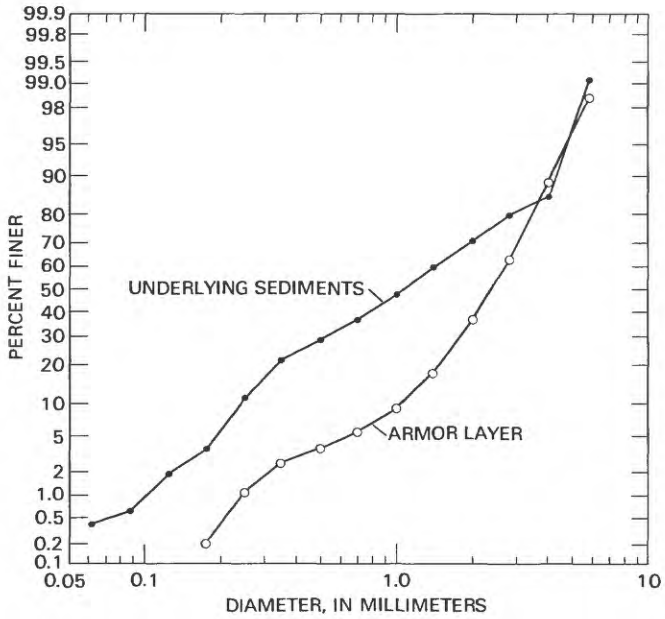

Figure 61. Size distributions of the armor layer and underlying sediments of the bar at Trapichote.

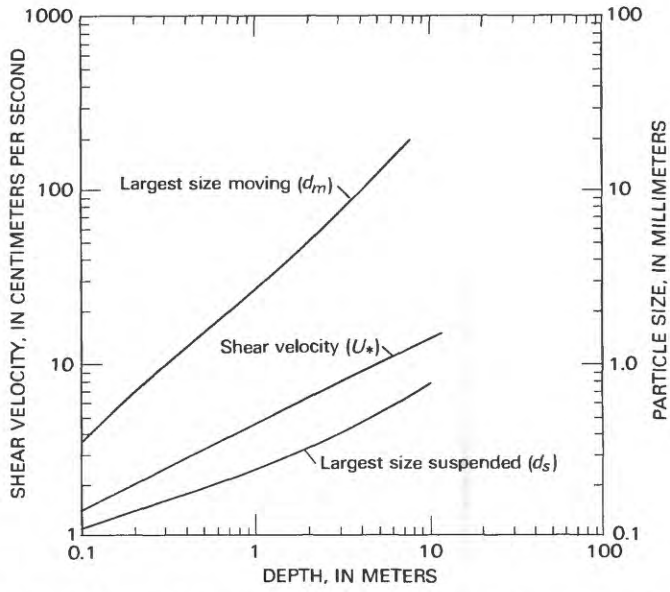

Figure 62. Relation between depth and the largest particle moved in suspension and at the bed, Río Orinoco at Trapichote.

finer components of the load run ahead of the coarser. On the bar at Trapichote, the bed layer contains about 90 percent coarse sand and fine gravel compared with 50 percent for the underlying sediments, so approximatley 40 percent by weight of the finer sediments are depleted. If the suspended sediments move almost at the mean flow velocity, this depletion could occur fairly rapidly once the upstream supply is reduced.

SUMMARY AND CONCLUSIONS

During low flow of March 1982, a reconnaissance study was made along a reach of the Río Orinoco between Puerto Ayacucho and Ciudad Bolívar. Bed-material samples were collected at more than 70 locations, suspended-sediment samples were taken at 10 locations, and the sand waves and large bars exposed in the channel were measured and mapped at 4 locations. Soundings were made over these same bars during rising flows in June and falling flows in November. These same sites, as well as others, were occupied during March 1983. This report summarizes the size distributions of bed sediments, the concentrations of suspended-sediment samples, and the lengths and heights of the sand waves. Observations on wind processes also are reported.

The main conclusions of the study are as follows:

1. The bed of the Río Orinoco in the reach betwen Puerto Ayacucho and Ciudad Bolívar is controlled at a number of locations by rapids and bedrock outcrops of the Guayana Shield. Between controls, there are long alluvial reaches in which the bed is composed mostly of sand with small quantities of fine gravel. The particle sizes vary widely along the channel and across the channel at any section. There is no systematic decrease in median diamter or sorting coefficient in the downstream direction.

2. Suspended-sediment concentrations during March 1982, were low; about 20mg/L upstream of Río Apure and 30–40 mg/L downstream. The Río Cinaruco contained 15 mg/L suspended sediment and the Río Meta contained 106 mg/L.

3. A new definition of wash load is proposed. It is the size material that can be suspended as soon as its motion at the bed is initiated. For the Río Orinoco, this is material finer than 0.1 mm.

4. Approximate relations are developed between water discharge and the largest size particle that can be suspended and largest size that can be moved at the bed for a typical wide and narrow section near Musinacio. Relations between bed-material discharge and water discharge are developed for the same two sections (fig. 50) using the Engelund-Hansen transport function and a new definition for effective bed diameter, equation 26.

The estimated annual bed-sediment discharge, about 30×10^6 Mg/y, agrees well with independent estimates made by Pérez-Godoy (1982) using the modified Einstein method.

5. During the dry season, 35 percent or more of the river bed is exposed, mostly in the form of large bars. The bars are composed of sand waves averaging at various locations along the river from 60 to 100 m long and from 2 to 3 m high. Statistics of the lengths and heights are given for several locations.

6. Strong trade winds blow upriver during the dry season, and these winds transport substantial quantities of sands and finer sediments. If the bars contain very coarse sands and fine gravel, their surfaces become armored with a lag deposit. If they do not contain gravel, like the point bar at Cabruta, the sand-wave crests are drastically eroded.

7. The lower limit for the fraction of the bed that needs to be covered by nonmoving particles to prevent further erosion is derived, and the fraction and lower size of the armor are shown to be functions only of wind speed.

REFERENCES CITED

Bagnold, R.A., 1941, The physics of blown sands and desert dunes: London, Methuen & Co. Ltd., 265 p.

Brownlie, W.R., 1981, Prediction of flow depth and sediment discharge in open channels: California Institute of Technology Report KH–R–43A, 232 p.

Chiu, C.L., and Hsiung, D.E., 1981, Secondary flow, shear stress and sediment transport: American Society of Civil Engineers Proceedings, v. 107, no. HY 7, p. 879–898.

Chiu, C.L., and Lin, F.G., 1983, Computation of 3–D flow and shear in open channels: American Society of Civil Engineers Proceedings, v. 109, no. HY 11, p. 1424–1440.

Chiu, C.L., Nordin, C.F., Jr., and Hu, Wei De, 1983, A model for mathematically modeling and computation of hydraulic processes in river bend: American Society of Civil Engineers Specialty Conference, Hydraulics Division, New Orleans, 14 p.

Dawdy, D.R., 1961, Depth-discharge relations of alluvial streams—Discontinuous rating curves: U.S. Geological Survey Water-Supply Paper 1498–C, 16 p.

Einstein, H.A., Anderson, A.G., and Johnson, J.W., 1940, A distinction between bed-load and suspended load in natural streams: American Geophysical Union Transactions, p. 628–633.

Engelund, Frank, and Fredsφe, Jorgen, 1976, A sediment transport model for straight alluvial channels: Nordic Hydrology, v. 7, no. 5, p. 293–306.

Engelund, Frank, and Hansen, Eggert, 1967, A monograph on sediment transport in alluvial streams: Copenhagen, Teknisk Forlag, 62 p.

Federal Inter-Agency Sedimentation Project, 1957, A study of methods used in measurement and analysis of sediment loads in streams—Some fundamentals of particle size analysis: Report 12, Washington, U.S. Government Printing Office, 55 p.

_____ 1963, A study of methods used in measurement and analysis of sediment loads in streams—Determination of fluvial sediment discharge: Report 14, Washington, U.S. Government Printing Office, 151 p.

Guy, H.P.,1969, Laboratory theory and methods for sediment analysis: U.S. Geological Survey Techniques of Water-Resources Investigations, book 5, chap. C1, 55 p.

Harrison, A.S., 1950, Report on special investigation of bed sediment segregation in a degrading bed: University of California Institute of Engineering Research, series 33, issue 1, 205 p.

Hsu, S.A., 1973, Computing eolian sand transport from shear velocity measurements: Journal of Geology, v. 8, p. 739–743.

Lane, E.W., and Eden, E.W., 1940, Sand waves in the lower Mississippi River: Journal Western Society Engineers, v. 45, p. 281–291.

Lane, E.W., and Kalinske, A.A., 1939, The relation of suspended to bed material in rivers: American Geophysical Union Transactions, p. 637–641.

Lumley, J.L., and Panofsky, H.A., 1964, The structure of atmospheric turbulence: New York, Interscience Publishers, 239 p.

Maegley, W.J., 1976, Saltation and Martian sandstorms: Reviews of Geophysics and Space Physics, v. 14, no. 1, p. 135–142.

McKee, E.D., 1989, Sedimentary structures and textures of Río Orinoco channel sands, Venezuela and Colombia: U.S. Geological Survey Water-Supply Paper 2326–B, 23 p.

Meade, R.H., Nordin, C.F., Jr., Pérez-Hernández, David, Mejía B., Abel, and Pérez-Godoy, J.M., 1983, Sediment and water discharge in Río Orinoco, Venezuela and Colombia, in Proceedings of the Second International Symposium on River Sedimentation, Nanjing: Beijing, Water Resource and Electric Power Press, p. 1134–1144.

Meyer-Peter, E., and Muller, R., 1948, Formulas for bed-load transport: International Association for Hydraulic Structures Research Proceedings, Stockholm, Annex 2, p. 39–64.

Middleton, G.V., 1976, Hydraulic interpretation of sand size distributions: Journal of Geology, v. 84, p. 405–426.

Miller, M.C., and Komar, P.D., 1977, The development of sediment threshold curves for unusual environments (Mars) and for inadequately studied materials (foram sands): Sedimentology, v. 24, no. 5, p. 709–721.

Nordin, C.F., Jr., Cranston, C.C., and Mejía B., Abel, 1983, New technology for measuring water and suspended-sediment discharge of large rivers, in Proceedings of the Second International Symposium on River Sedimentation, Nanjing: Beijing, Water Resources and Electric Power Press, p. 1145–1158.

Nordin, C.F., Jr., and Meade, R.H., 1985, The Amazon and the Orinoco, in McGraw-Hill yearbook of science and technology, 1986: New York, New York, p. 385–390.

Nordin, C.F., Jr., Meade, R.H., Cranston, C.C., and Curtis, W.F., 1983, Data from sediment studies of the Río Orinoco, Venezuela, August 15–25, 1982: U.S. Geological Survey Open-File Report 83–679, 25 p.

Nordin, C.F., Jr., Meade, R.H., Curtis, W.F., Bósio, N.J., and Landim, P.M.B., 1980, Size distribution of Amazon River bed sediment: Nature, v. 286, p. 52–53.

Parker, Gary, Sundararajan, Dhamotharan, and Stefan, Heinz, 1982, Model experiments on mobile paved gravel bed streams: Water Resources Research, v. 19, no. 5, p. 1395–1408.

Pérez-Godoy, J.M., 1982, Revisión de la información limnimétrica, batimétrica y modelos matemáticos así como de los datos hidrológicos existentes del Río Orinoco: Caracas, Ministerio del Ambiente y de los Recursos Naturales Renovables, 101 p.

_____ 1984, Aprovechamiento hidroeléctrico del Río Orinoco, estudio de la mechánica fluvial del río y su interrelación con los aprovechamientos hidroeléctricos: Caracas, Ministerio del Ambiente y de los Recursos Naturales Renovables, 273 p.

Rathbun, R.E., and Guy, H.P., 1967, Measurement of hydraulic and sediment transport variables in a small recirculating flume: Water Resources Research, v. 3, no. 1, p. 107–122.

Reineck, H.E., and Singh, I.B., 1975, Depositional sedimentary environments: Berlin, Springer-Verlag, 439 p.

Roosevelt, A.C., 1980, Parmana-Prehistoric maize and manioc subsistence along the Amazon and Orinoco: New York, Academic Press, 320 p.

Sagan, Carl, and Bagnold, R.A., 1975, Fluid transport on Earth and aeolian transport on Mars: Icarus, v. 26, p. 209–218.

Seddon, J.A., 1900, River hydraulics: American Society of Civil Engineers Transactions, v. 18, p. 179–229.

Sharp, R.P., 1963, Wind ripples: Journal of Geology, v. 71, no. 5, p. 617–636.

Shen, H.W., and Lu, J.Y., 1983, Development and prediction of bed armoring: American Society of Civil Engineers Proceedings, v. 109, no. 4, p. 611–622.

Shields, A., 1936, Anwendung der Ähnlichkeitsmechanic und des Turbulenzforschung auf die Geschiebsbewegung: Mitteilungen der Pruess, Versuchsanst. f. Wasserbau und Schiffbau, Berlin, Heft 25. *See also* translation by W.O. Ott and J.C. van Uchelen, California Institute of Technology, Hydrodynamics Laboratory Publication 167, 36 p.

Simons, D.B., Richardson, E.V., and Nordin, C.F., Jr., 1965, Sedimentary structures generated by flow in alluvial channels: Society of Economoic Paleontologists and Mineralogists Special Publication 12, p. 34–52.

Sola, Oswaldo de, 1982a, Caracterización geológica del Río Orinoco, tramo Cabruta-Ciudad Bolívar [abs.], *in* Seminario, Estudios para el aprovechamiento del eje fluvial Orinoco-Apure: Caracas, Ministerio del Ambiente y de los Recursos Naturales Renovables, p. 23–28.

_____ 1982b, Surficial geology of the Río Orinoco flood plain: Caracas, Ministerio del Ambiente y de los Recursos Naturales Renovables, scale 1:400,000, 5 sheets.

Sundborg, Åke, 1956, The river Klaralven, a study of fluvial processes: Geografiska Annaler, v. 38, no. 2, p. 127–316.

Tricart, J., 1974, Existence de périodes sèches au Quaternaire en Amazonie et dans les régions voisines: Revue de Géomorphologie Dynamique, v. 23, p. 145–158.

U.S. Army Corps of Engineers, 1943, Report on Orinoco-Casiquiare-Negro waterway, Venezuela-Colombia-Brasil: South Atlantic District, Atlanta, Georgia, 313 p.

White, B.R., 1979, Soil transport by winds on Mars: Journal of Geophysical Research, v. 84, no. B8, p. 4643–4651.

Williams, G.P., 1964, Some aspects of the eolian saltation load: Sedimentology, v. 3, no. 4, p. 257–287.

_____ 1983, Improper use of regression equations in earth sciences: Geology, v. 11, p. 195–197.

Yalin, M.S., 1977, Mechanics of sediment transport, 2d ed.: New York, Pergamon Press, 298 p.

Yalin, M.S., and Karahan, Emi, 1979, Inception of sediment transport: American Society of Civil Engineers Proceedings, v. 105, no. HY 11, p. 1433–1443.

Yang, C.T., and Stall, J.B., 1976, Applicability of unit stream power equation: American Society of Civil Engineers Proceedings, v. 102, no. HY 5, p. 559–568.

☆U.S. GOVERNMENT PRINTING OFFICE: 1989-673-047/86100

The Dunes at Punta Brava

SAND WAVES, BARS, AND WIND-BLOWN SANDS
OF THE RIO ORINOCO, VENEZUELA AND COLOMBIA